論文 / 著書情報
Article / Book Information

題目(和文)	
Title(English)	Elucidation of the dehydration mechanism of drug crystals using crystal structure and kinetic analysis
著者(和文)	溝口亮
Author(English)	Ryo Mizoguchi
出典(和文)	学位:博士(理学), 学位授与機関:東京工業大学, 報告番号:甲第11012号, 授与年月日:2018年12月31日, 学位の種別:課程博士, 審査員:植草 秀裕,江口 正,小松 隆之,豊田 真司,腰原 伸也
Citation(English)	Degree:Doctor (Science), Conferring organization: Tokyo Institute of Technology, Report number:甲第11012号, Conferred date:2018/12/31, Degree Type:Course doctor, Examiner:,,,,
学位種別(和文)	博士論文
Type(English)	Doctoral Thesis

2017 Doctoral Dissertation

Elucidation of the dehydration mechanism of drug crystals using crystal structure and kinetic analysis

Ryo Mizoguchi

Department of Chemistry and Materials Science,
Tokyo Institute of Technology

Acknowledgement

I would like to sincerely thank my academic supervisor Associate Professor Hidehiro Uekusa for his enthusiasm, encouragement and continued support. Working with him over the past few years has been both a privilege and an absolute pleasure. Dr. Akiko Sekine and the colleagues of research groups are thanked for their endless assistance.

I would like to do appreciate Astellas pharma. Inc. members. Dr. Hisashi Mimura and Dr. Yutaka Hirakura gave me the opportunity to study and understood spending time for my research. I appreciate Mr. Noritaka Hamada and Mr. Katsuhiko Gato for their cooperation about experiments at SPring-8, thermal transition experiments and important and suggestive comments and discussion . I also appreciate Dr. Yukihito Sugano for his assistance about X-ray crystal structure analysis and deep discussion. The colleagues of Analytical Research Labs. are also thanked for their assistance and understanding.

Finally, I would like to give a huge thanks to my wife and children for their superb love, guidance and encouragement.

December 2017
Ryo Mizoguchi

Chapter 1
General Introduction

1.1. General Introduction of Drug discovery

1.1.1. Trend of drug discovery

Development of drugs - from candidate selection through preclinical and clinical studies to approval - is a long and slow process which incurs considerable cost.[1] Today, the probability that a compound newly entering development will eventually be launched as a new drug is decreasing, while the cost of development continues to increase. Strategies to overcome the decreasing probability of launching new products are therefore urgently required.[2] In addition, since the number of drug discovery target itself is also decreasing, the race of drug discovery becomes cutthroat.

Factors which affect the decreasing probability of launching a new drug relate to drug efficacy, toxicity, metabolic profile and marketability, among others. The demand against safety by the authority such as Food and Drug Administration (FDA), European Medicines Agency (EMA) and Pharmaceutical and Medical Devices Agency (PMDA) is crucially strict. Pharmaceutical companies continuously make an effort to develop the new drug candidates.

1.1.2. Importance of physicochemical properties

The physicochemical properties of drug candidates are key to some of these factors.[3] Drug candidates that are discovered using high-throughput screening (HTS) methods tend to exhibit high lipophilicity and low solubility against water.[4] In general, high-throughput screening methods is carried out using the dimethylsulfoxide (DMSO) solutions of compounds. The trend of the promising candidates becomes quite different from the era when in vivo studies were the main tools to select the candidates.

Low solubility in particular can make it difficult to attain good oral absorption and to develop intravenous formulations; therefore, low solubility of a drug candidate can strongly impede drug discovery.[5] As an example, the development of ritonavir is well-known case in which solid state properties affected drug discovery. Ritonavir is one of the anti-AIDS drugs which are HIV protease inhibitors (Fig. 1-1). After launch, crystal form I of ritonavir could not be synthesized because of the presence of crystal form II, which was the more thermodynamically stable form.[6] This more thermodynamically stable form had

lower solubility than metastable forms, so the exposure level in blood at which the drug exerted its pharmacological effect could not be achieved. As a result, ritonavir had to be removed from the market, and additional clinical studies were needed. The case of ritonavir indicates that solubility is one of the most important parameters for drug development and low solubility of a drug candidate can strongly impede drug discovery.

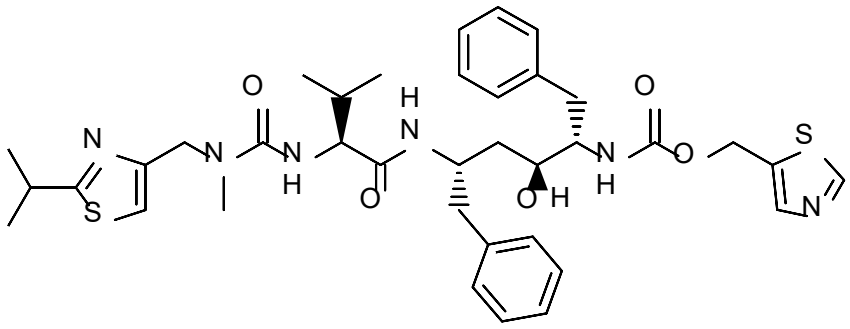

Fig. 1-1 Chemical structure of ritonavir

1.1.3. Stability requested by authorities

Apart from solubility, the stability of a candidate drug also affects drug discovery.[7, 8] A drug that is unstable and must be stored under special conditions such as refrigeration and drying is highly likely to have decreased market competitiveness. Moreover, from the view point of safety, safety of degradation products must be ensured by toxicity study or another rationale. Stability data and toxicological data are defined in ICH guidelines (The International Council for Harmonisation of Technical Requirements for Pharmaceuticals for Human Use)[9] for New Drug Application (NDA). In ICH Q series, harmonisation achievements in the Quality area include pivotal milestones such as the conduct of stability, defining relevant thresholds for impurities testing and a more flexible approach to pharmaceutical quality. In ICH Q1A (R2),[10] stability testing of new drug substances and products are written. Since, in general, stability data for 3 years is needed for NDA, evaluation of the stability of drug candidate forms is extremely important in early drug discovery stages.[11]

However, as it is generally difficult to find sufficient time to evaluate stability for long periods in the early discovery stages, accelerated stability studies should be conducted.[12] In ICH Q1A(R2), accelerated stability studies are also mentioned. Accelerated stability studies are based on the assumption that degradation reactions are followed by the Arrhenius rule. The Arrhenius rule is understood as the rule of the temperature dependence of reaction rates. If the activation energy of the reaction is assumed, result of short period study at the higher temperature is available to predict that of the longer period studies at the lower temperature. Such studies are useful for predicting the tendency of degradation in chemical reactions,[13] but are not particularly effective for

predicting physical stability such as changes in crystal form.[14] If physical changes occur at room temperature, the drug form should be carefully evaluated.[15]

1.2. Solid state evaluation

As you can see the case of ritonavir, physicochemical properties strongly depends on the solid states of drug candidates. If the solid state changed, it is highly probable that physicochemical properties would also change. In other words, to control the physicochemical properties is possible by changing the solid state of a drug candidate, so solid state evaluation is much important in drug discovery.

Solid states observed in drugs are shown in Fig. 1-2. Observed forms can be classified into two parts. One is single-component and another is multi-component forms.

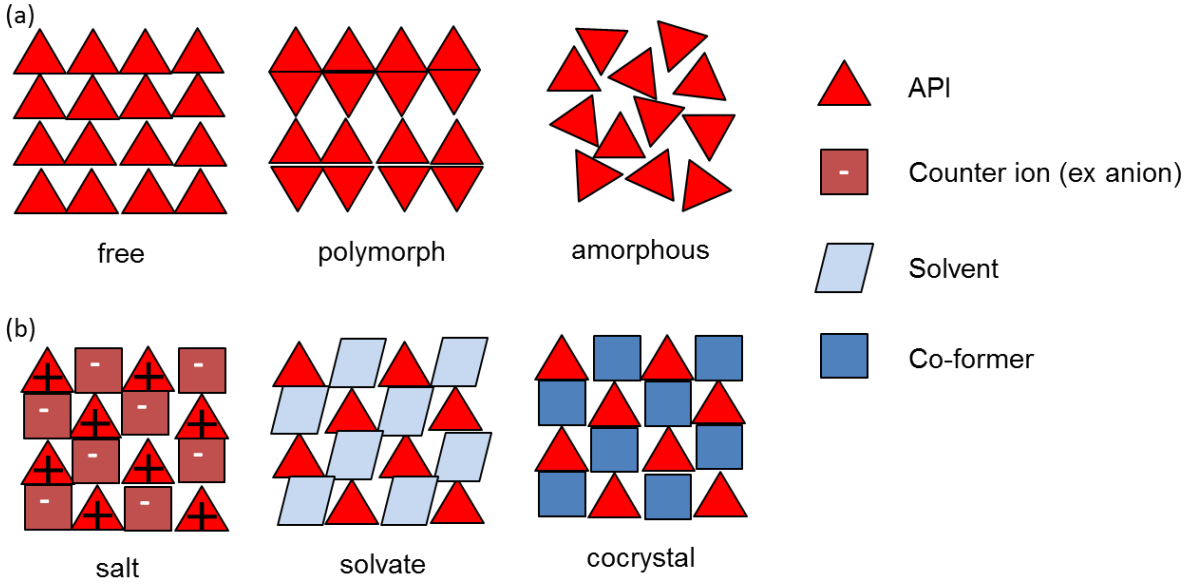

Fig. 1-2 Schematic representation of solid forms observed in drugs. (a) single-component forms, (b) multi-component forms

Single-component state consists of only an active pharmaceutical ingredient (API) which shows the pharmacological effect. In the single-component state, API is crystallized or not crystallized, that is, amorphous state. In crystallized API, polymorphism is often observed. Polymorph forms generally show the different crystal packing patterns, and each polymorph shows the different physicochemical properties (e.g. solubility[16]) such as ritonavir.[6] Since API is the complicated chemical structure, most APIs show polymorphism.[17] It is important to control the polymorphs in terms of regulation of physicochemical properties.[18]

Amorphous state does not form the crystal state. Amorphous state is sometimes used for the improvement of solubility since the amorphous state is the high energy state.[19, 20] But, physical and chemical stability of amorphous state should be paid attention to. In comparison with the crystallized form, amorphous state shows the lower stability, so amorphous state is not available for degradable APIs. Moreover, physical stability should be carefully treated. In general, because it is difficult to predict the stability that keeps the amorphous state without the crystallization for the long storage condition mentioned at previous section.

Multi-component states consist of an API and co-formers. Salts are formed between the charged API and co-formers with the ionic interaction. Cocrystals are done between the neutral API and co-formers with non-ionic interactions, such as the hydrogen bonds and van der Waals interactions. Solvates are also formed with the non-ionic interactions. In general, the definition of solvates is that co-formers are solvents at room temperature. On the other hand, definition of cocrystal is that co-formers are solids at room temperature. In drug discovery, the most proper forms should be selected from these possible forms. Especially, salt formation is considered to be effective for the improvement of solubility. Since low solubility candidates are discovered with HTS, salt formation is general process for pharmaceutical companies.

In early drug discovery stage, solid state evaluation has to be done using the limited amount of candidate, so a kind of evaluation items are also limited.[21, 22] In general, solid state evaluation is carried out the following items (in Fig. 1-3); (1) solid state is the crystal or amorphous state, (2) melting temperature, (3) solubility and dissolution, (4) hygroscopicity, and (5) physical and chemical stability.

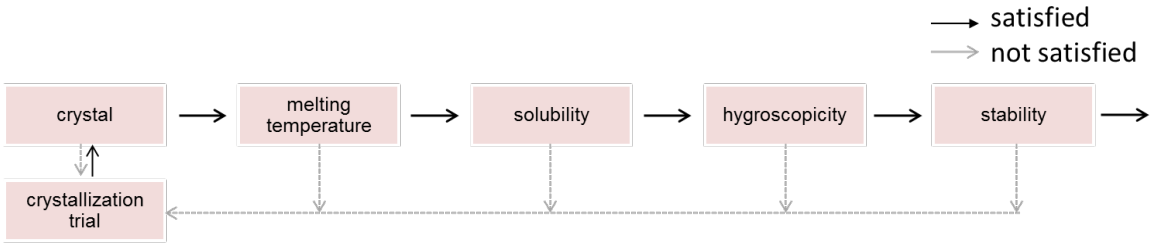

Fig. 1-3 Schematic image of the evaluation flow of solid state in early drug discovery stage.

Since the amorphous state generally shows the lower stability, it is difficult to select as a development solid form. In other words, solid state evaluation begins by obtaining crystalline materials. If the melting temperature is quite low, for example, below 80 ºC,[22] the materials may be melted in some manufacturing processes and under some storage conditions. Melted materials may show the

lower stability and it is difficult to handle, so they should be avoided selecting such the candidates having solid state. Some estimation technologies of melting point is established, but the robustness is limited.[23, 24] It is necessary to confirm with experimental.

Improvement of solubility is one of the main purpose of solid state evaluation. The value of solubility should be evaluated at salt formations or other states for enhancement of solubility. A lot of evaluation systems for solubility have been reported. The main purpose of solubility enhancement is to improve the oral absorbability, so at these evaluation systems, artificial gastrointestinal solutions are used for solubility evaluation. Traditional artificial gastrointestinal solutions are pH controlled buffers. pH 1.2 buffer is used for the mimic of gastric fluid and pH 6.8 on is done for the mimic of intestinal fluid. With the purpose to simulate the solubility and dissolution of API in the gastrointestinal tract several media simulating gastric and intestinal fluids have been developed.[25-27]

Hygroscopicity is the solid state property of water absorption or desorption under the various relative humidity (RH) conditions. Hygroscopicity is generally evaluated by monitoring the weight change at various RHs. Since it is easy to handle materials which show no hygroscopicity, those are preferable for API solid form.

Evaluation of stability is conducted with the accelerated stability studies because it is not enough time to evaluate the long term stability study in early drug discovery stage mentioned previously. In particular, general conditions of the accelerated stability study are at 40 ºC for a few months, at 70 ºC for 2 weeks.[22] Duration and temperature depend on the target stability profile. After the storage, physical stability is evaluated with powder X-ray diffraction (XRD), thermal analysis, spectroscopic methods and microscope. In addition, chemical stability is also evaluated with high-performance liquid chromatography (HPLC) and HPLC with mass spectrometry.

Higher solubility, lower hygroscopicity and higher stability are main purpose of solid state evaluation described before.

1.2.1. Salts screening

Physicochemical properties correspond to the solid state and changing the solid state affects the physicochemical properties. For the purpose of improvement of physicochemical properties, it is useful to change the solid state.

Salt optimization and salt screening are general, useful and powerful tools to improve the physicochemical properties by changing the solid state.[28, 29] For example, hygroscopicity improvement of ethambutol dihydrochloride salt was reported.[30] In this paper, an oxalate showed no deliquescence because the

packing efficiency of an oxalate crystal was improved than that of hydrochloride and penetration of water was inhibited.

Some well-established screening systems are widely used for drug discovery. These screening systems aim for exhaustive discovery of salts formation with target API using 96 well plates.[31, 32] Parallel crystallization is conducted with various counter ions and solvents in these systems. Plate designs are arbitrarily able to be chosen. In general, salt screening with a 96 well plate can crystallize the only small amount of each salt, therefore, promising salt candidates will be scaled up for the further characterizations. Finally, the best salt will be selected. As estimated, approximately 50% of all drugs available for medicinal use are marketed as salts.[33] Hydrochloride salt and sodium salt are conventional salts and are often seen in case of basic API and acidic API, respectively.[34] Toxicity is not concerned in using both salts because chloride anion and sodium cation abundantly exist in human body. Salt screening process became more general and kinds of acids and bases became large. Rare salts might be observed in future.

1.2.2. Hydrate

At previous sections, optimization of the solid states is carried out for the improvement of physicochemical properties. Changing the solid state can cause the change of physicochemical properties despite the change was expected or not (Fig.1-4).

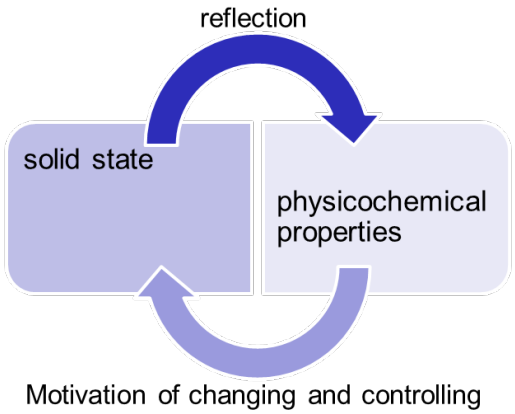

Fig. 1-4 Schematic representation of the relationship between the solid state and physicochemical properties.

In the manufacturing process or at the storage condition, the unexpected changing of the solid state is sometimes faced. Moreover, physicochemical properties will also change and the changed properties are unpredictable. Sudden appearance of ritonavir form II was typical case of unexpected changing (see section 1.1.2), and unpredictable decreasing of solubility affected the drug

development.[6] Changing of solid state should be taken careful attention.

Hydrate is often observed as a drug substance form.[35] The hydrate is seen mostly in such unexpected cases. In the drying process which is necessary for both drug substance and drug product, dehydration reaction may occur because of low RH and high temperature. In the granulation process for drug product and under high humidity storage condition, hydration may also occur. It is particularly important to evaluate stability for hydrate forms because physical changes in hydrates occur due to changes in humidity.[36, 37]

For example, FK041 which was developed as an antibacterial drug (in Fig. 1-5) forms a clathrate hydrate, revealing continuous changes in the amount of water due to humidity. The chemical stability of FK041 hydrate is strongly dependent on the amount of water.[38] Degradation of FK041 hydrate Dehydration became severe in case of more than trihydrate, so humidity control is necessary for controling the amount of hydrated water to keep the stability. As you can see . dehydrate and hydration cause changes in the physicochemical properties of compounds, which can significantly affect drug discovery.

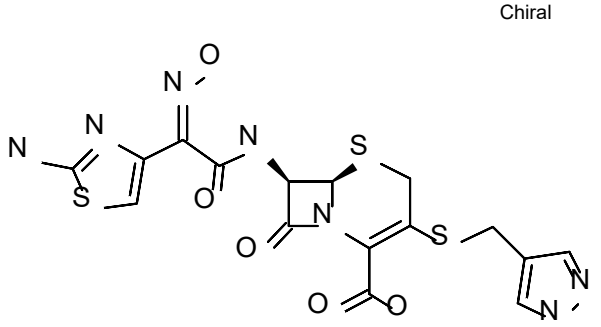

Fig. 1-5 Chemical structure of FK041

1.3. Utilization of crystal structure analysis for elucidation of dehydration mechanism

It is crucial to evaluate the physicochemical properties of both hydrates and anhydrates and to understand the mechanism of physical transition between hydrates and anhydrates.[39-43] If both forms can be isolated, a few tests for evaluation of physicochemical properties will be able to be conducted. Moreover, we have already reported that crystal structure analysis is powerful tool to understand the mechanism of dehydration and hydration reaction.[44] By comparison with crystal structures before and after dehydration or hydration process, change of interactions, movements of molecular, driving forces of transition etc. can be discussed

It is often difficult to not only assess the physicochemical properties of anhydrates, but also to analyze the crystal structure of anhydrates obtained after dehydration because they are unstable at room temperature and relative humidity.

In some cases, dehydrate reactions have been traced by single crystal transitions[45, 46]; however, the maintenance of single crystals is not always easy, particularly when large changes to the crystal structure occur, which is the case for dehydration reactions. In these cases, crystal structure analysis using powder X-ray diffraction is a powerful and useful method for analyzing the unstable crystal form.[39, 43 47-51]

For instance, we have already reported the dehydration mechanism of lisinopril dihydrate using the crystal structures (in Fig.1-6).[52] Crystal structures of the dihydrate, monohydrate, and anhydrate phases of lisinopril were determined with powder X-ray diffraction data. The mechanistic aspects of the two-step dehydration of the dihydrate phase of lisinopril were clearly established from crystal structures. In particular, the mechanism of the two-step dehydration via the metastable intermediate phase of the pharmaceutical hydrates was clearly revealed by the crystal structures.

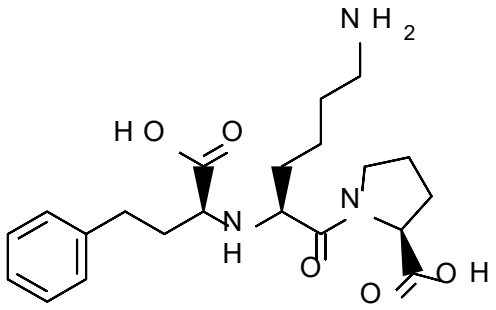

Fig. 1-6 Chemical structure of lisinopril

Recently, crystal structure analysis using powder X-ray patterns has become more widely used in many indexing programs, the introduction of initial structure with direct space methods and Rietveld refinement.[53, 54] As powder is relatively stable during the transition phase compared with single crystals, this method is appropriate for analyzing unstable forms such as dehydration products.

1.4. Kinetic analysis

Although the comparison with crystal structures is powerful tool for the mechanism discussion, unfortunately, crystal structure is not always obtained because a single crystal is not able to be obtained and the crystallinity is not enough to adapt the crystal structure analysis with powder X-ray pattern. Moreover, there are some cases in which the target material forms amorphous state. Furthermore, it is difficult to consider the transition state of reactions

because the crystal structure represents the static situation. Kinetic analysis is considered to be effective for such cases.

Kinetic analysis is based on the ability to accurately monitor the reaction conversion over time. Kinetic analysis is available for liquid state and solid state reactions. Monitoring is carried out with many analytical tools such as chromatographic method,[55] spectroscopy, X-ray diffraction,[56, 57] thermal analysis,[58] nuclear magnetic resonance (NMR)[59, 60] and so on. To succeed the kinetic analyses gives us the kinetic constant, the reaction model and the activation energy. If the kinetic constant and the activation energy are available, estimation of reaction progress can be done and half-life can be calculated.[56] Half-life is the one of the most useful parameters for estimation of the stability of drug. Therefore, kinetic analysis is powerful tool for drug discovery.

In kinetic analysis of solid state reaction, thermal analysis is useful technology. A lot of methods have been reported for the kinetic study with the thermal analysis such as thermal gravimetric analysis (TGA) and differential scanning calorimetry (DSC). Model fitting method has been widely used for kinetic analysis.[61-63] Dehydration or hydration reaction can be deeply understood and kinetics approach is suitable for understanding the transition state and mechanism of dehydration reaction.[64-66] Generally speaking, the solid state reaction has the large variability, so experimental condition should be carefully considered.[67]

1.5. Purpose of research

As previously mentioned, evaluation of solid state properties is important for drug development, therefore, transition of solid state should be understood because the solid state represents these properties. We have the powerful tools for elucidating the mechanism. These are the crystal structure analysis and the kinetic analysis. In chapter 2, I will show the promising results of the crystal structure analysis for the elucidation of the dehydration mechanism using ondansetron hydrochloride dihydrate as a model compound. In chapter 3, I will show the important results of the kinetic analysis using ondansetron hydrochloride dihydrate as a model compound. In addition, I will also conclude that the combination of the crystal structure analysis and the kinetics analysis is useful for understanding the dehydration mechanism. In chapter 4, the utilization of the combination method is proved by another compound (ozagrel hydrochloride hydrate). In chapter 5, I will show the results of salt changing of ondansetron to control the physicochemical properties. I will discuss the foresight of the rational salt optimization process using the combination of the crystal structure analysis and the kinetic analysis.

In summary, elucidation of the dehydration mechanism of drug crystals is

purposed using the combination of crystal structure analysis and kinetic analysis. There are only a few reports about the utilization of these combination studies,[41a, 43] and there are few reports that evaluated the drug hydrate using these studies.[68] It will be proposed that the combination study is powerful tool for drug discovery.

Chapter 2

Form transition of ondansetron HCl dihydrate

2.1. General information of ondansetron

Ondansetron hydrochloride dihydrate, known as Zofran, was developed by GSK and launched in the USA in 1991. Ondansetron is a competitive serotonin type 3 receptor antagonist which is effective in the treatment of nausea and vomiting caused by cytotoxic chemotherapy drugs.[68] Although patents of ondansetron have already expired, Zofran was a blockbuster drug with peak annual sales of more than one US$ billion.

While the crystal structure of ondansetron hydrochloride dihydrate has been reported (CSD refcode: YILGAB[69]), the temperature of dehydration and crystal transition after dehydration have not.[69-71]

2.2. Purpose of this chapter

The purpose of this chapter was to understand the mechanism of dehydration/hydration by comparing the crystal structures of active pharmaceutical hydrates. Ondansetron hydrochloride dihydrate was used as a model compound (Fig. 2-1). This research aimed to fill in the gaps in knowledge concerning the mechanism underlying the transition of dihydrates.

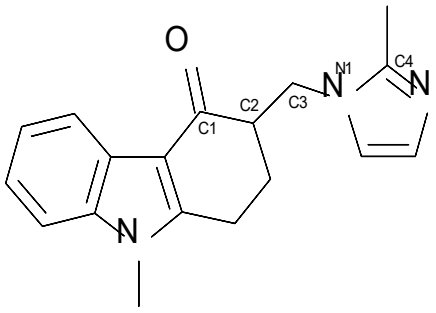

Fig. 2-1 Chemical structure of ondansetron. Torsion angle φ1 is formed by C1-C2-C3-N1 and φ2 is by C2-C3-N1-C4.

2.3. Materials and methods

2.3.1. Materials

Ondansetron hydrochloride dihydrate was purchased from Sigma Aldrich (St. Louis, MO, USA). Characterization was performed using samples pulverized with an agate mortar.

2.3.2. Heating

Samples were heated in a Fine Oven DF42 (Yamato Science, Tokyo, Japan).

2.3.3. Powder X-ray diffraction (PXRD)

PXRD analysis was performed on a TTR II (Rigaku, Tokyo, Japan) and used Cu Kα radiation at 1.54184 Å at a voltage of 50 kV and current of 300 mA. Data were collected at a scan rate of 4 º/min over a 2θ range of 2.5 º to 40 º.

2.3.4. X-Ray differential scanning calorimetry (DSC)

Simultaneous measurement of powder X-ray diffraction data and DSC data was carried out on a SmartLab system (Rigaku) using Cu Kα radiation at 1.54184 Å at a voltage of 45 kV and current of 200 mA, with a DSC attachment and a D/Tex Ultra as a detector. Samples were weighed (1.5–2.5 mg) in aluminum pans and analyzed at a heating rate of 2 °C/min using a similar empty pan as a reference. X-ray diffraction data were collected at a scan rate of 20 °/min over a 2θ range of 10 ° to 25 °.

2.3.5. Thermal analysis: Differential scanning calorimetry

Thermal analysis was performed using a TA Q20 DSC instrument that included a refrigerated cooling system (TA Instruments, New Castle, DE, USA). Temperature calibration was carried out using the indium metal standard supplied with the instrument. Samples were weighed (about 3 mg) in aluminum pans and analyzed from 25 °C to 300 °C at heating rates of 10 °C/min using a similar empty pan as a reference. An inert atmosphere was maintained in the calorimeter by purging with nitrogen gas at a flow rate of 50 mL/min.

2.3.6. Thermal analysis: Thermogravimetric analysis (TGA)

TGA was performed using a TA Q50 TGA instrument (TA Instruments). Approximately 4 mg of sample was loaded into a platinum pan and heated to 300°C at a rate of 10 °C/min. Measurements were carried out under nitrogen purge at a flow rate of 100 mL/min. Temperature calibration was carried out using standard nickel.

To identify the intermediate, a sample was heated in jump mode to 45, 50, and 55 °C, and kept at each temperature for 60, 40, and 20 min, respectively. Measurements were carried out under a nitrogen purge at a flow rate of 50 mL/min (sample purge gas only flowed).

2.3.7. Water vapor sorption and desorption studies

Dynamic vapor sorption experiments were performed on a VTI SGA 100. Samples (about 10 mg) were studied over a selected humidity range (from 5−50 %relative humidity (RH) to 5−95 %RH) at each temperature (25-50 °C). For each humidity step, the equilibration was set to dm/dt 0.03 %/min on a 5-min time frame (maximum hold time 180 min).

2.3.8. SPring-8

The powder samples were enclosed in a 0.3 mm Lindemann glass capillary. X-ray powder diffraction data were collected at SPring-8 BL19B2[72], which is equipped with a high-resolution type Debye–Scherrer camera and a curved imaging-plate detector. The wavelength was set at 1.0000 Å. It took one minute to set each temperature, which was maintained for 4 minute to ensure equilibrium was reached before measurements were taken. Data were collected for 5 minutes. During data collection, the sample was maintained at the set temperature and rotated at 1 r/min to reduce potential preferential orientation effects.

2.3.9. Structure determination using powder X-ray patterns

Crystal structures of both the hemihydrate and anhydrate were determined from the PXRD patterns obtained at SPring-8. Crystal structure analysis was carried out in the Powder Solve module of Materials Studio (BIOVIA).

After selecting the peaks set, indexing was conducted in the XCELL module[73] to introduce the unit cell and appropriate space group. The unit cell was refined by Pawley refinement and optimized.

The initial chemical structures of ondansetron and the water molecules were

introduced using the Forcite module with COMPASS II[74] as a force field. The initial crystal structure was introduced by the POWDER SOLVE module[75] using the simulated-annealing approach and optimized by Rietveld refinement. Pareto optimization, a Rietveld refinement method that considers the energy of the structure calculated by a force field,[76] was carried out at the final optimization step.

2.4. Results and Discussion

2.4.1. Phase transition

Thermal analysis was carried out to confirm the crystal phase transitions of ondansetron hydrochloride dihydrate with heating. The results of the thermal analysis are shown in Fig. 2-2.

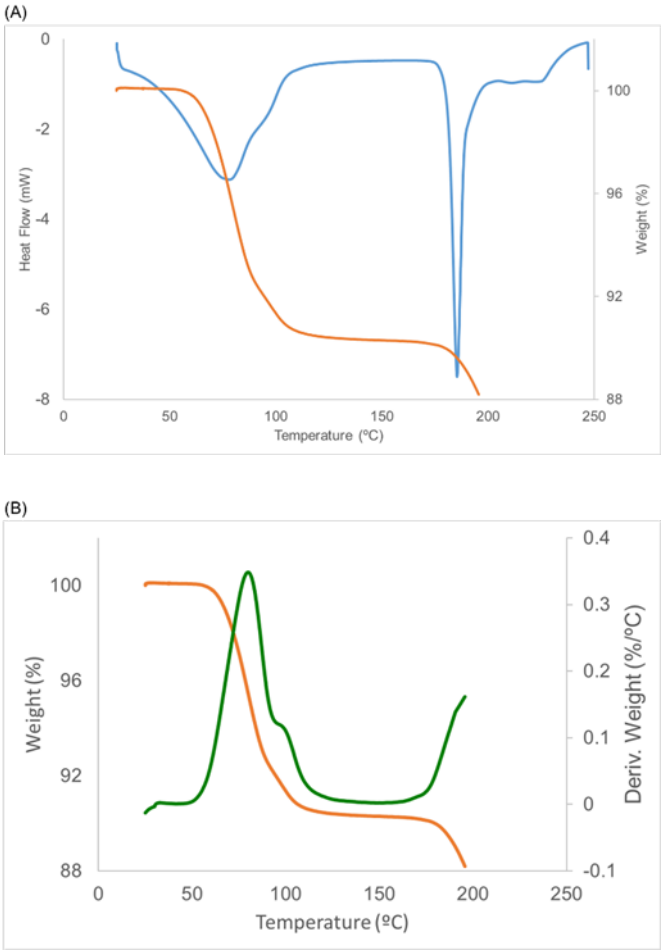

Fig. 2-2 (A) Thermal behavior of ondansetron hydrochloride dihydrate. Blue line indicates the differential scanning calorimetry curve, orange line indicates the thermogravimetric (TG) curve. (B) The TG curve (orange) was overwritten by the derivation of the TG (green).

An endothermic peak with decreasing weight was observed near room temperature. The weight change (%) was about 10%. As the theoretical value for the dehydration of a dihydrate is 9.85%, this findings indicated that the endothermic peak occurring between room temperature and about 120 ºC was the result of the dehydration of a dihydrate. After this dehydration, the melting point of hydrochloride was observed at an initial temperature of around 180 ºC. As shown in Fig. 2-2(B), the derivation curve of the TGA was not smooth and showed two peaks, indicating that dehydration of ondansetron hydrochloride dihydrate was not a simple or one-step dehydration reaction.

In next step, an anhydrate of ondansetron hydrochloride was tried to be isolated to further elucidate the physicochemical properties of the compound. The time course data of the PXRD results after heating at 100 ºC for 30 minutes are shown in Fig 2-3.

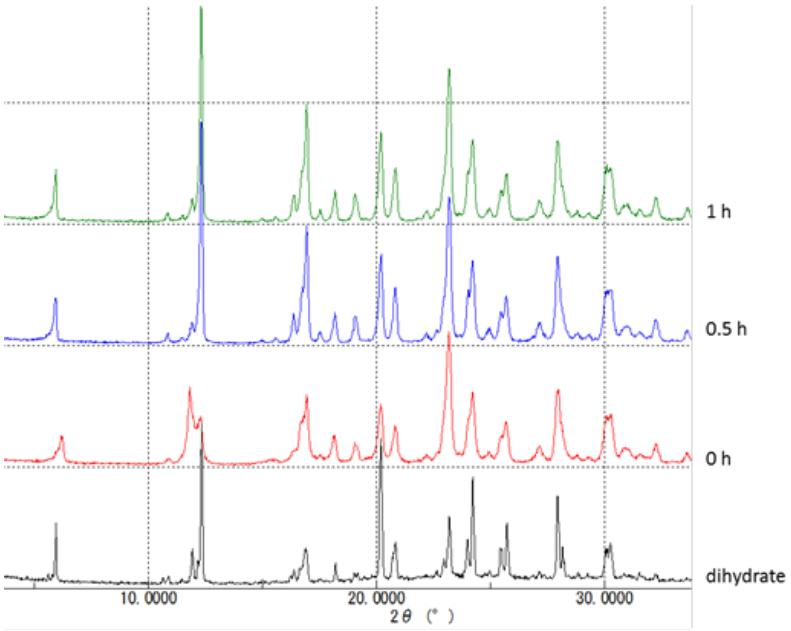

Fig. 2-3 Reversibility after heating confirmed with X-ray diffraction patterns: dihydrate as a reference (black), 0 h (red), 0.5 h (blue), 1 h (green) after heating at 100 ºC.

The X-ray pattern differed slightly in the 0 hour sample (Fig. 2-3, red pattern) after heating compared to that before heating (Fig.2-3, black pattern). The XRD patterns became similar to those of initial patterns after 0.5 and 1 hour (Fig. 2-3; blue and green patterns, respectively). These results suggest that the anhydrate was easily transformed back into its initial dihydrate form after heating and relocation to a room temperature environment for X-Ray measurement. It was therefore concluded that isolation of an anhydrate of ondansetron hydrochloride

was difficult and that it would be impossible to experimentally evaluate the physicochemical properties of such an anhydrate. It was further concluded that elucidating the crystal form transition would require elucidation of the mechanism by crystal structure analysis.

To determine the crystal form after heating, XRD measurements with heating was conducted (Fig. 2-4). Interestingly, a two-stage change was observed in the XRD pattern with heating. At around 45 ºC, XRD patterns were greatly changed and, at around 70 ºC, only a minute change was observed, compared to that before heating. This change correlated with the TGA derivation curve (Fig. 2-2(B)). To our knowledge, this is the first observation of the existence of an intermediate in the dehydration of ondansetron hydrochloride. Observation of the dehydration of two water molecules at more than 70 ºC (Fig. 2-2(A)) suggested the existence of an anhydrate.

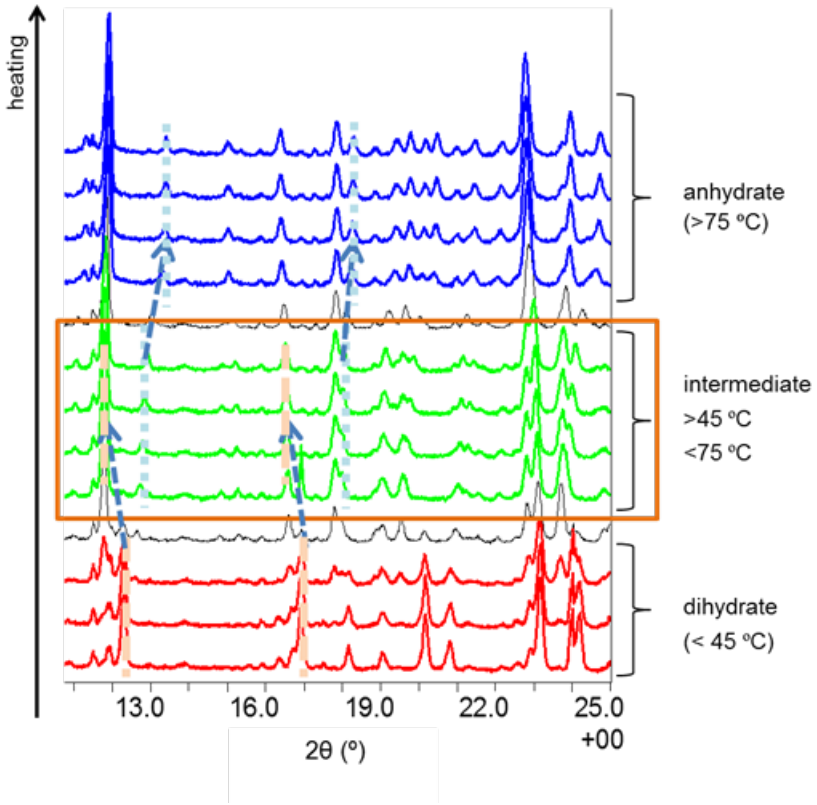

Fig. 2-4 Variable temperature X-ray diffraction by XRD-DSC measurement. Patterns of: dihydrate (red), intermediate (green), anhydrate (blue). Arrows and pale broken lines shows the change of characteristic peak positions.

The stoichiometry of the hydrate was determined using TGA to confirm the identity of the intermediate present between 45 ºC and 70 ºC. The results of the TGA are shown in Fig. 2-5. Time course data of weight (%) were obtained under

three temperatures (45 ºC, 50 ºC, and 55 ºC). A consistent decrease in weight (%) was observed under the three temperature conditions, at which the intermediate should be stable. Thermal analysis results may indicate whether or not the intermediate or a mixture of dihydrate and anhydrate was formed. However, the continuous change in X-ray patterns in XRD with heating did not support the presence of a mixture of the crystal forms. The amount of decrease corresponded to 1.5 water molecules, leading to conclude that the intermediate was a hemihydrate.

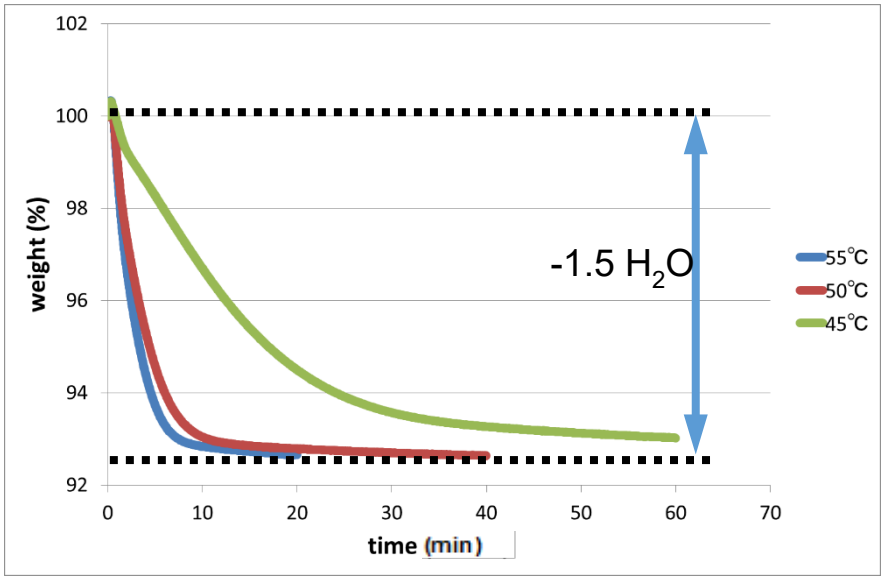

Fig. 2-5 Identification of the intermediate using a thermogravimetric analysis. Changes in weight (%) at different temperatures: 45 ºC (green), 50 ºC (red), 55 ºC (blue).

2.4.2. Crystal structure analysis

Because both the intermediate (hemihydrate) and an anhydrate were unstable at room temperature, crystal structure analysis with PXRD was carried out with heating. PXRD at 95 ºC was used for crystal structure analysis of the hemihydrate and at 140 ºC was used for the anhydrate. In the crystal structure analysis of the hemihydrate, the occupancy of water molecules was fixed at 0.5; and the value was not optimized through Rietveld refinement. Crystal structure analyses with PXRD were successful.

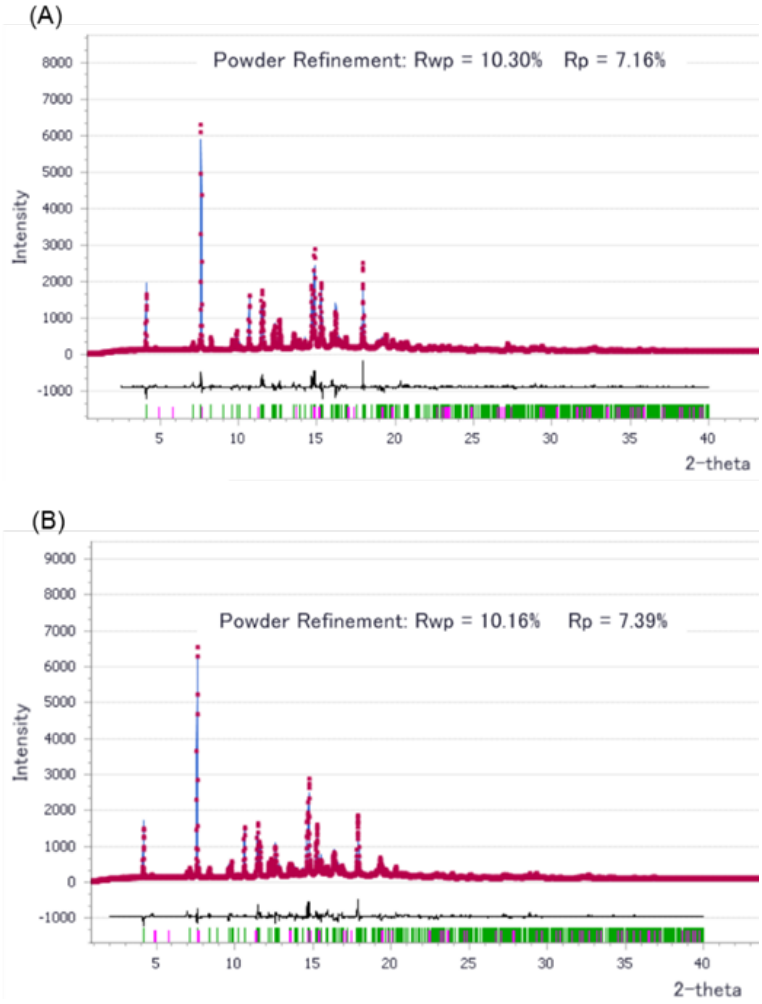

Fig. 2-6 Final Rietveld refinement for ondansetron (A) hemihydrate (at 95 ºC) and (B) anhydrate (at 140 ºC). Red dots: measured data points; blue line: calculated pattern; black line: difference profile; green ticks: calculated peak positions; pink ticks: systematic absence markers.

The lattice parameters in each phase are shown in Table 2-1. The space group was not changed at $P2_1/c$ during the whole dehydration process. During transition from the dihydrate to the hemihydrate, a beta angle change (100 º to 115 º) and decrease in volume were observed. In contrast, the transition from the hemihydrate to anhydrate did not result in any extreme changes in lattice parameters.

Table 2-1 Crystal data for ondansetron hydrochloride hydrates

	Dihydrate[69]	Hemihydrate	Anhydrate
Molecular formula	$C_{18}H_{20}N_3OCl.2H_2O$	$C_{18}H_{20}N_3OCl.0.5H_2O$	$C_{18}H_{20}N_3OCl$
Sample type	Single crystal	Powder	Powder
Crystal system	Monoclinic	Monoclinic	Monoclinic
Space group	$P2_1/c$	$P2_1/c$	$P2_1/c$
a (Å)	15.082(3)	15.375(2)	15.084(4)
b (Å)	9.741(3)	9.907(1)	9.898(2)
c (Å)	12.734(3)	12.719(2)	12.913(3)
β (º)	100.83(1)	114.508(1)	114.717(2)
V (Å^3)	1837.5(8)	1762.8(4)	1751.1(7)
R-Factor (%)	7	-	-
R_p (%)	-	7.16	7.39
R_{wp} (%)	-	10.30	10.16

Projection views of the b axis are shown in Fig. 2-7(A). Two layers were commonly observed in the crystal structures of the three phases. One layer was occupied by the ondansetron structures, and the other by waters and chloride anions; that is, the crystal structure consisted of hydrophobic and hydrophilic layers, respectively. The layer around the ondansetron structure (hydrophobic layer) was maintained in all three structures, and did not change throughout the crystal phase transition, indicating that the dynamic crystal transition took place in the hydrophilic layer.

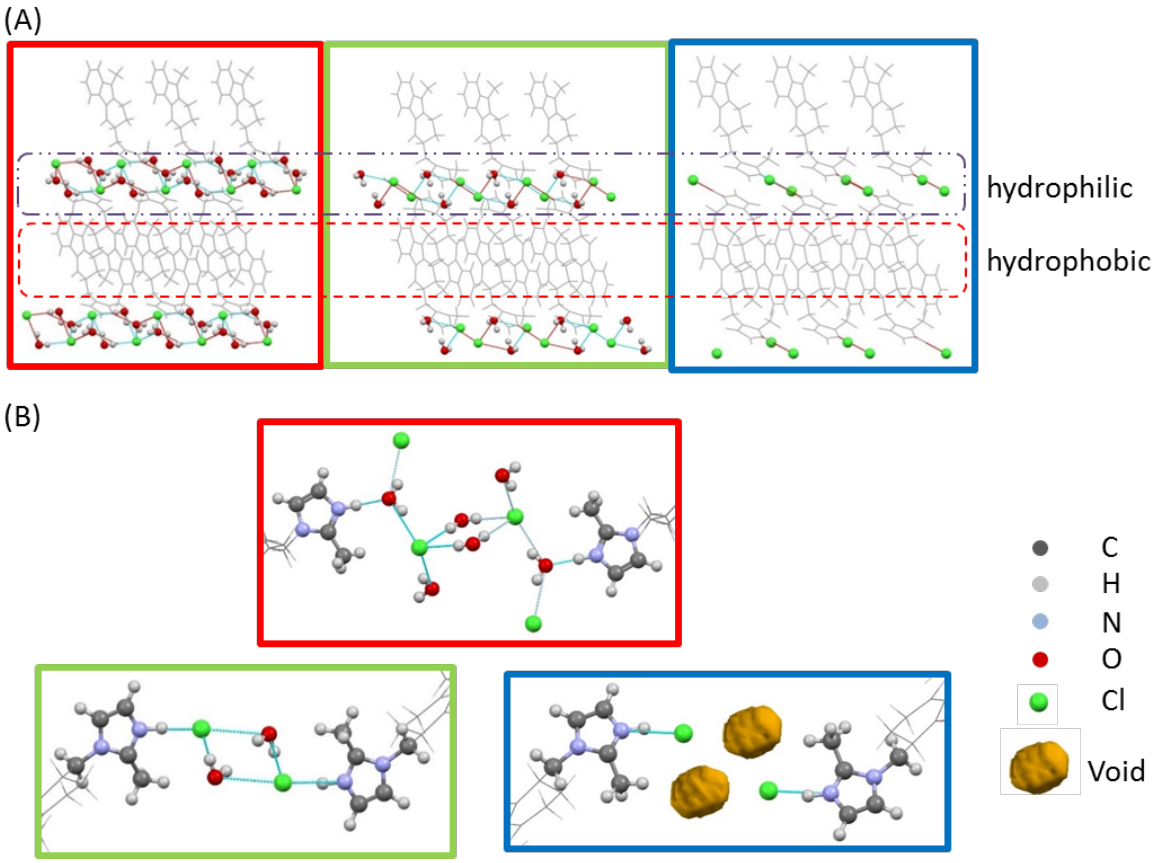

Fig. 2-7 Comparison of crystal forms observed throughout the crystal transition. (A) Hydrophobic and hydrophilic layers are indicated by the regions enclosed by the dotted lines. (B) Hydrogen bond networks. Red square: dehydrate; green square: hemihydrate; blue square: anhydrate.

I focused on the network of hydrogen bonds and observed interactions between an imidazole cation and a water molecule and between water molecules and chloride anions in the dihydrate structure (Fig. 2-7(B)). In the first dehydration reaction, a water molecule that interacted with an imidazole cation was removed, and half of a water molecule, which interacted with chloride anions, was also removed. In the second dehydration reaction, a water molecule that interacted with a chloride anion was removed and the space left by the water in the crystal structure was left as a void structure. The size of this void was 6.1 Å. It can be considered that the presence of this void may be the underlying reason for the instability of the anhydrate and its rapid transformation back to the hydrate form.

The distance between the chloride anions was reduced in the transition (dihydrate: 5.228 Å, hemihydrate: 4.917 Å, anhydrate: 4.755 Å). In the first dehydration reaction, the change was about 0.31 Å, indicating that a water

molecule that was present between the chloride anions was also dehydrated and the intermediate was not a monohydrate. In the second dehydration reaction, the change was about 0.16 Å, which was half that resulting from the first dehydration. We hypothesized that the size of this change was due to a repulsion force between the chloride anions, which resulted in the formation of the void.

The space left by the dehydration of a water molecule in the first dehydration reaction was filled by the translation of imidazole rings. A stacking of the imidazole rings occurred after the translation. In contrast, in the second dehydration reaction, the structure around the imidazole rings was not changed (Fig. 2-8).

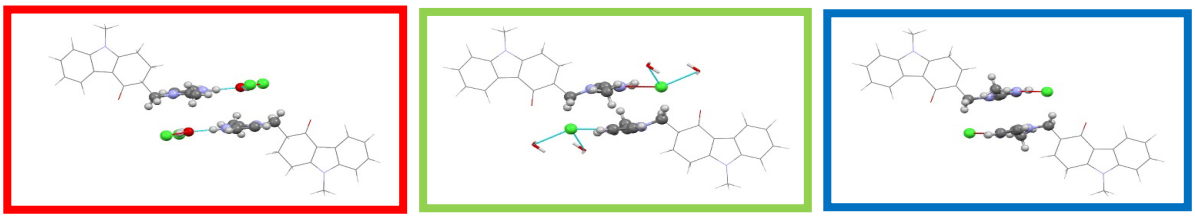

Fig. 2-8 Comparison of the crystal forms around the imidazole rings in the dihydrate (red square), hemihydrate (green square) and anhydrate (blue square) forms.

The monomer structure of ondansetron remained present and unchanged throughout the two stage transitions. An overlay of the ondansetron molecule across the stages is shown in Fig. 2-9. The torsion angle φ1 changed from 179 º to -171 º and φ2 from 109 º to 111 º. The imidazole position slightly changed to maintain interactions such as those between hydrogen bonds, the ionic interaction and the stacking interaction.

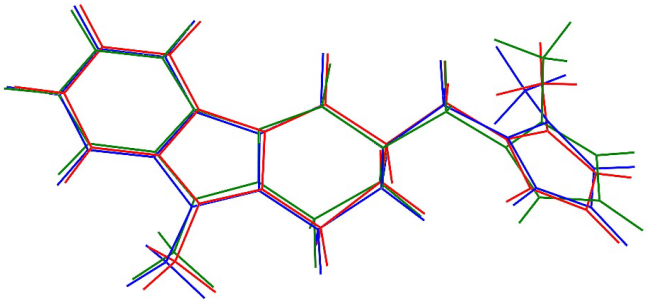

Fig. 2-9 Overlay of the molecular structures of ondansetron in each crystal form: dihydrate (red), hemihydrate (green), anhydrate (blue).

The dimer structure formed between the tricyclic rings of ondansetron was also maintained across all crystal phases. The distance between the rings was about 3.6 Å, allowing the π-π stacking interaction to be maintained (Fig. 2-10). In addition, CH-π interaction was also observed, and the distance was about 2.6 Å. It can be considered that this interaction contributed to the stabilization of the crystal structure and made it possible for the anhydrate to rapidly transform back to the dihydrate in the solid state.

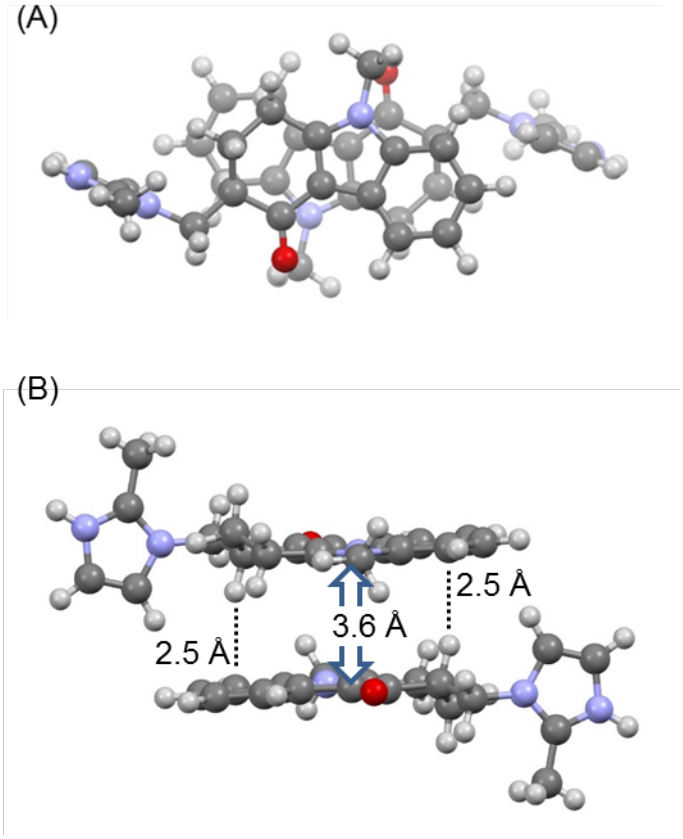

Fig. 2-10 Stacking interaction between the tricyclic parts of ondansetron. (A) Top view, (B) side view. Dotted lines indicated the CH–π interaction.

The temperature at which the hemihydrate existed differed between the experiments in Figs. 2-4 and 2-6. This was due to the use of different experimental conditions: whereas an open pan was used for the experiments in Fig. 2-4, a capillary of 0.3 mmΦ was used for the experiments in Fig. 2-6. The pressure was higher under the capillary condition than the open pan condition. Because dehydration reactions are strongly dependent on pressure, the increased pressure delayed the dehydration reaction under the capillary condition.

The order of the dehydrating water molecules was examined. Crystal structure

analysis indicated that the water molecule located between the two chloride ions was maintained in the first dehydration reaction. However, there are no direct experimental data to confirm which water molecule was dehydrated in this first dehydration reaction between the one water molecule that interacted with an imidazole or the 0.5 water molecule located between the chloride anions. If both of these dehydration reactions occurred simultaneously, the energy loss caused by each dehydration should be almost same. Dehydration of the water molecule that interacted with imidazole was compensated with the formation of a new ionic bond between an imidazole cation and chloride anion. A repulsion force should exist between chloride anions due to electrostatic interactions, and may constitute the root cause of the void structure observed in the anhydrate. Although hydrogen bonds formed with water molecules are preferable to inhibit the repulsion force between chloride anions, the electron-donating capacity of chloride anions was reduced by the ionic bond between the imidazole cation and chloride anion, making it potentially difficult to maintain the monohydrate, and resulting in a hemihydrate as an intermediate.

2.4.3. Hygroscopicity

The dehydration tendency of ondansetron hydrochloride dihydrate against various levels of relative humidity (5-50% RH) at 30 ºC was evaluated (Fig. 2-11). At 5% RH, the dehydration reaction was not completed such that neither an anhydrate nor hemihydrate were formed. In the transition between the dihydrate and hemihydrate, an exchange of hydrogen bonds and translation of imidazole rings were observed, representing a relatively large degree of change. Because this transition took some time to complete, the hysteresis could be observed.

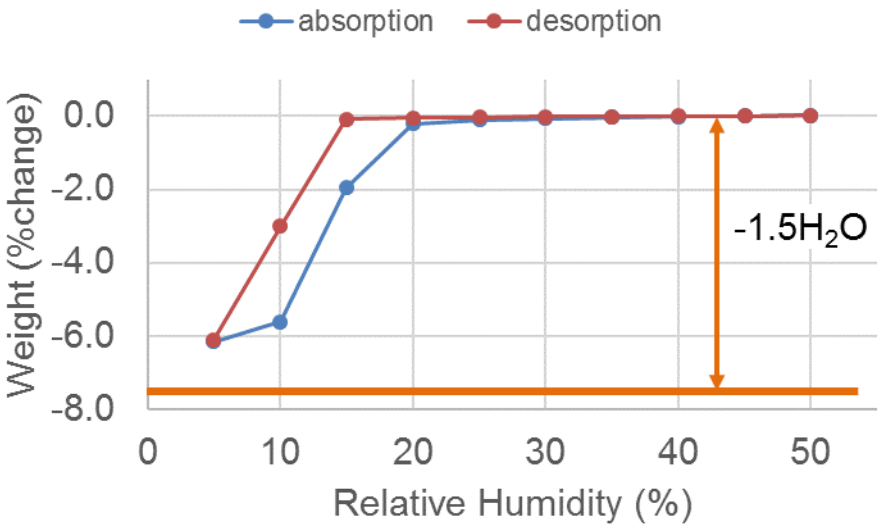

Fig. 2-11 Hygroscopicity of ondansetron hydrochloride dihydrate at 30 ºC. Orange line indicates the theoretical value when the hemihydrate is produced.

The dependency of hygroscopicity on relative humidity and temperature is shown in Fig. 2-12.

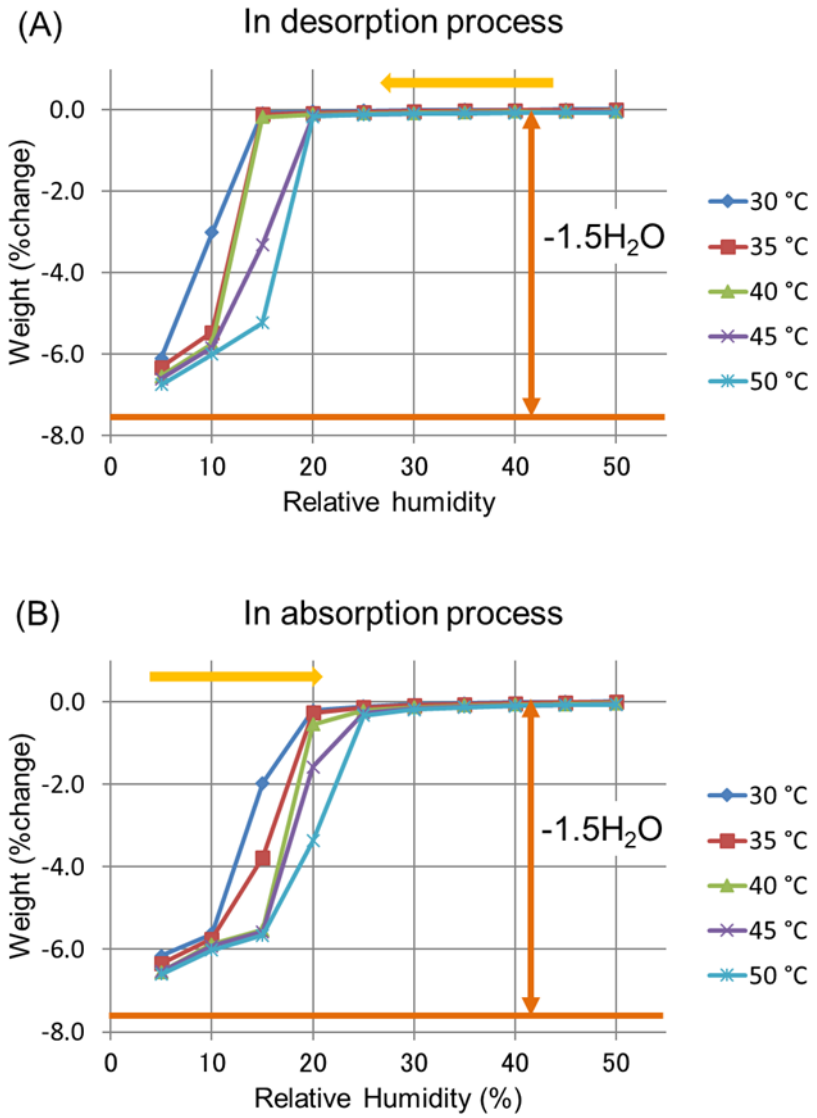

Fig. 2-12 The temperature dependence of hygroscopicity in the (A) desorption process (from 50 to 5% RH) and (B) absorption process (from 5 to 50% RH). The arrows indicate the reaction direction.

No anhydrate was observed even at the higher temperature at 5% RH. The critical relative humidity (CRH) at which the transition began was higher at higher temperatures; that is, the dehydration reaction occurred more easily at higher temperatures, making a hydration reaction unlikely to occur. The phenomenon of hysteresis was observed by comparing the desorption and absorption processes. The occurrence of hysteresis did not depend on temperature because the change in the CRH (RH at the beginning of dehydration minus the RH at the beginning of hydration) was about 5-10% RH.

2.5. Short summary

Ondansetron hydrochloride dihydrate was selected as one of the model compounds for elucidating the dehydration mechanism and evaluating the relationship of between the crystal structure and physicochemical properties. Ondansetron hydcochloride dihydrate transformed into an anhydrate under heating condition. Interestingly, that dihydrate transformed into a hemihydrate as an intermediate before the transformation into an anhydrate. Both the hemihydrate and the anhydrate were unstable at room environment and these forms immediately went back into the initial dihydrate. Crystal structure analysis for two unstable forms succeeded with powder X-ray patterns. Changing of the hydrogen bonds network was observed thought these transformations although the overall structures were similar. The void structure was observed in an anhydrate, so this structure was considered to be accountable for the root cause of the instability of an anhydrate at room conditions.

In hygroscopicity tests, the hysteresis was observed. In the transition between the dihydrate and hemihydrate, an exchange of hydrogen bonds and translation of imidazole rings occurred, representing a relatively large degree of change. Because this transition took some time to complete, we were able to observe the hysteresis.

Hygroscopicity studies also mentioned that a dihydrate is possible to transform into a hemihydrate in drying condition. In consideration of the various situation of drug discovery such as the synthesis process of drug substance, the formulation process, the transportation condition and so on, the drying condition was supposed, so transformation to a hemihydrate may occur, so that both hydrate states were considered to need to be assessed the chemical stability for the risk mitigation for drug development.

The contents of this chapter have been already published on Crystal Growth & Design (Cryst. Growth Des. 2018, 18, 10, 6142-6149).

Chapter 3

ondansetron HCl kinetic analysis

3.1. General introduction

We have already evaluated a number of hydrates and found out the dehydration mechanism of those hydrates.[52] The dehydration mechanism can be discussed by comparison with crystal structures between a hydrate and an anhydrate. It is sometimes difficult to analysis crystal structure of the anhydrate obtained after dehydration of hydrate because the anhydrate is unstable under the room temperature and relative humidity. In this case, crystal structure analysis with powder X-ray patterns is useful because this method is appropriate for analyzing the unstable forms such as a dehydration product.[47-51] In previous chapter, we found out the dehydration mechanism of Ondansetron hydrochloride dihydrate (in Fig. 2-1) with crystal structure analysis with powder X-ray patterns. Ondansetron hydrochloride dihydrate transformed to an anhydrate with heating. In the transition, new intermediate was observed and identified as a hemihydrate.

Although the comparison with crystal structures is powerful tool for the mechanism discussion, it is difficult to consider the transition state of reactions because the crystal structure represents the static situation. Kinetics approach is suitable for understanding the transition state and mechanism of dehydration reaction.[64-66, 77] In this chapter, kinetics approach was carried out for the dehydration of a hydrate by using ondansetron hydrochloride dihydrate as a model compound. Moreover, the deeper understanding for the mechanism of dehydration was aimed with the combination of kinetics analysis with crystal structure analysis.

3.2. Materials and methods

3.2.1. Materials

Ondansetron hydrochloride dihydrate was purchased from Sigma Aldrich (St. Louis, MO, USA). Characterization was performed using samples pulverized with an agate mortar.

3.2.2. Kinetics study

3.2.2.1 Thermal analysis TGA Thermogravimetric Analysis

TGA was performed using a TA Q50 TGA instrument (TA Instruments, New Castle, DE, USA). Approximately 3 mg of sample was loaded into a platinum pan. Measurements were carried out under a nitrogen purge with a flow rate of 50 mL/min (sample purge gas only flowed). Temperature calibration was carried out using standard nickel.

3.2.2.2 Isoconversion methods

A sample was heated at a rate of 1, 2, 5, and 10 °C/min. Measurement at each temperature was repeated in four or five times.

3.2.2.3 Isothermal methods.

For the kinetics of first step dehydration reaction, a sample was heated at jump mode to 45, 50, 55, and 60 °C, and kept on each temperature for 60, 40, 20, 10 min, respectively. Measurement at each temperature was repeated in four or five times.

For the kinetics of second step dehydration reaction, a sample was heated at 55 °C, and kept for 20 min to transition to a hemihydrate. After the transition, a sample was heated again to 65, 70, 75, and 80 °C, and kept on each temperature for 45, 30, 20, and 15 min, respectively. Measurement at each temperature was repeated in four or five times.

3.2.2.4 Water Vapor Sorption and Desorption Studies.

Dynamic vapor sorption experiments were performed on a VTI SGA 100. Samples (about 3 mg) were studied at each temperature (30-40 °C). Instrument was set at 55 °C 5% RH for the dehydration, then temperature was changed to the target, and finally the humidity was controlled at 20% RH and the weight change of sample was traced. These steps were repeated at three times, and weight change was monitored. Each step was taken with the equilibration set to dm/dt 0.03 %/min on a 5 min time frame (with the maximum hold time of 180 min).

3.2.2.5 Calculations

Reaction ratio is α, and the changing ratio of α is described below,

$$\frac{d\alpha}{dt} = A \times e^{\frac{-E_a}{RT}} f(\alpha) \cdots (1)$$

Ea is activation energy, R is gas constant, T is temperature, A is reaction constant.

For the isoreaction rate model (ozawa method[78]), heating rate is β.

$$T = T_0 + \beta t \cdots (2)$$

T is temperature, T_0 is initial temperature, and t is time.

$$\mathrm{dT} = \beta \mathrm{dt} \cdots (3)$$

$$\mathrm{dt} = \frac{1}{\beta} dT \cdots (4)$$

In plugging in (4) for (1),

$$\frac{d\alpha}{\frac{1}{\beta} dT} = A \times e^{\frac{-E_a}{RT}} f(\alpha) \cdots (5)$$

$$\frac{d\alpha}{dT} = \frac{A}{\beta} \times e^{\frac{-E_a}{RT}} f(\alpha) \cdots (6)$$

For introducing the integral equation g(α),

$$\frac{d\alpha}{f(\alpha)} = \frac{A}{\beta} \times e^{\frac{-E_a}{RT}} dT \cdots (7)$$

$$\mathrm{g}(\alpha) = \int_0^{\alpha} \frac{d\alpha}{f(\alpha)} = \frac{A}{\beta} \int_{T_0}^{T} e^{\frac{-E_a}{RT}} dT = \frac{AE_a}{\beta R} p(x) \cdots (8)$$

$$\beta = \frac{AE_a}{Rg(\alpha)} \times p(x) \cdots (9)$$

$$\log\beta = \log\frac{AE_a}{Rg(\alpha)} + \log p(x) \cdots (10)$$

p(x) is described below,

$$\mathrm{p}(x) = \frac{e^{-x}}{x} - E_i(-x) \cdots (11)$$

$$E_i(-x) = -\int_x^{\infty} \frac{e^{-x}}{x} dx \cdots (12)$$

$$\mathrm{x} = \frac{E_a}{RT} \cdots (13)$$

In using the approximation of Doyle, if x is more than 20, p(x) can be approximated below

$$\log p(x) = -2.315 - 0.4567x \cdots (14)$$

In plugging in (14) for (10),

$$\log\beta = \log\frac{AE_\alpha}{Rg(\alpha)} - 2.315 - 0.4567\frac{E_\alpha}{RT} \cdots (15)$$

If α is constant, term of logarithm in right section of (15) is also constant. Ea is able to be introduced as a gradient on the plot of logβ against T^{-1}.

For isothermal model, (1) is rewritten,

$$\frac{d\alpha}{dt} = k\ f(\alpha) \cdots (16)$$

where k is the temperature-dependent rate constant. Integration of the rate law in (16) introduces to,

$$\int_0^\alpha \frac{1}{f(\alpha)}\ d\alpha = \int_0^t k\ dt \cdots (17)$$

$$g(\alpha) = kt \cdots (18)$$

where g(α) represents the function of the integrated part of left side in (17).

In Table 3-1, it is summarized the relationship between the various reaction models and f(α) and g(α).[64]

Table 3-1 Various reaction models of solid state and corresponding f(α) and g(α)

model	f(α)	g(α)
Sigmoid α-time		
A2 Avrami-Erofeev	$2(1-\alpha)[-\ln(1-\alpha)]^{1/2}$	$[-\ln(1-\alpha)]^{1/2}$
A3 Avrami-Erofeev	$3(1-\alpha)[-\ln(1-\alpha)]^{2/3}$	$[-\ln(1-\alpha)]^{1/3}$
A4 Avrami-Erofeev	$4(1-\alpha)[-\ln(1-\alpha)]^{3/4}$	$[-\ln(1-\alpha)]^{1/4}$
An Avrami-Erofeev	$n(1-\alpha)[-\ln(1-\alpha)]^{(n-1)/n}$	$[-\ln(1-\alpha)]^{1/n}$
B1 Prout-Tompkins	$\alpha(1-\alpha)$	$\ln[\alpha/(1-\alpha)]$
Deceleratory α-time		
Geometrical models		
R2 contracting area	$2(1-\alpha)^{1/2}$	$1-(1-\alpha)^{1/2}$
R3 contracting volume	$3(1-\alpha)^{2/3}$	$1-(1-\alpha)^{1/3}$
Diffusion models		
D1 one-dimensional	0.5α	α^2
D2 two-dimensional	$[-\ln(1-\alpha)]^{-1}$	$(1-\alpha)\ln(1-\alpha)+\alpha$
D3 three-dimensional	$1.5(1-\alpha)^{2/3}\left[1-(1-\alpha)^{1/3}\right]$	$\left[1-(1-\alpha)^{1/3}\right]^2$
D4 Ginstling-Brounshtein	$1.5\left[(1-\alpha)^{-1/3}-1\right]^{-1}$	$1-(2\alpha/3)-(1-\alpha)^{2/3}$
Reaction-order models		
F0 zero order	1	α
F1 first order	$(1-\alpha)$	$-\ln(1-\alpha)$
F2 second order	$(1-\alpha)^2$	$(1-\alpha)^{-1}-1$
F3 third order	$(1-\alpha)^3$	$0.5[(1-\alpha)^{-2}-1]$

3.3. Results and discussion

Ondansetron hydrochloride dihydrate transformed to an anhydrate by way of hemihydrate as an intermediate with heating or drying.

That two-step dehydration reaction of Ondansetron hydrochloride dihydrate was described below (1) and (2).

$$[\text{dihydrate}] \rightarrow [\text{hemihydrate}] + 1.5[H2O] \quad \cdots (1)$$

$$[\text{hemihydrate}] \rightarrow [\text{anhydrate}] + 0.5[H2O] \cdots (2)$$

In the kinetics analysis of the reaction, thermal gravimetry assay (TGA) was used. Purpose of the kinetic analysis was to obtain the activation energy (Ea) of each step of dehydration. If Ea can be obtained, reaction ratio at an arbitral temperature is estimated as long as the same reaction mechanism. Ozawa method was firstly used to obtain Ea value because this method was simple and did not need to estimate the reaction model (model free analysis).[78] In TGA, the heating rate was set at 1, 2, 5, and 10 ºC/min and reaction ratio was calculated. The relationship between the reaction rate and time was shown in Fig. 3-1.

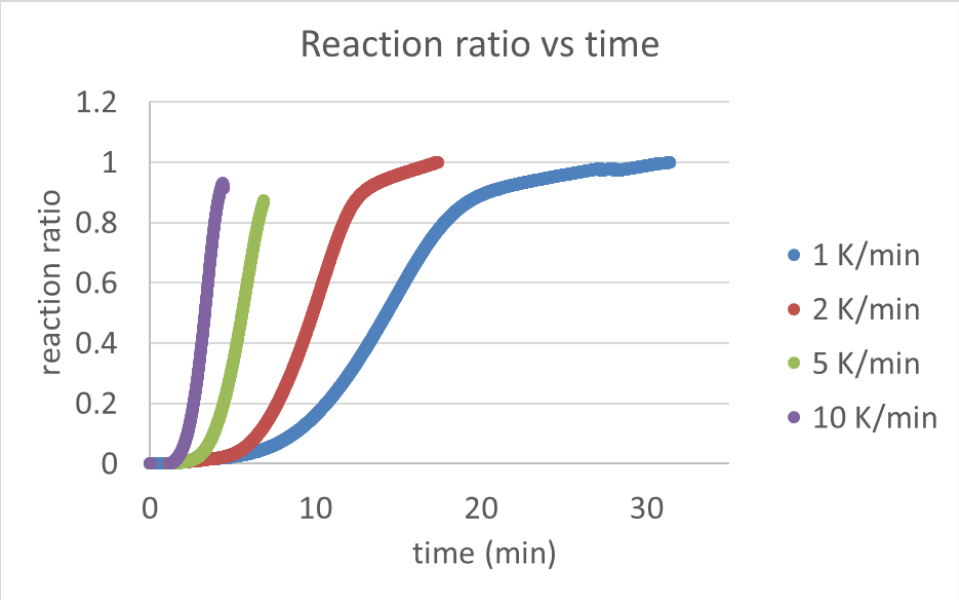

Fig. 3-1 Reaction ratio vs time at each heating rate

Ea was obtained at each reaction ratio (see calculation section). In Fig. 3-2, Ea was plotted against the reaction ratio from 0.1 to 0.8.

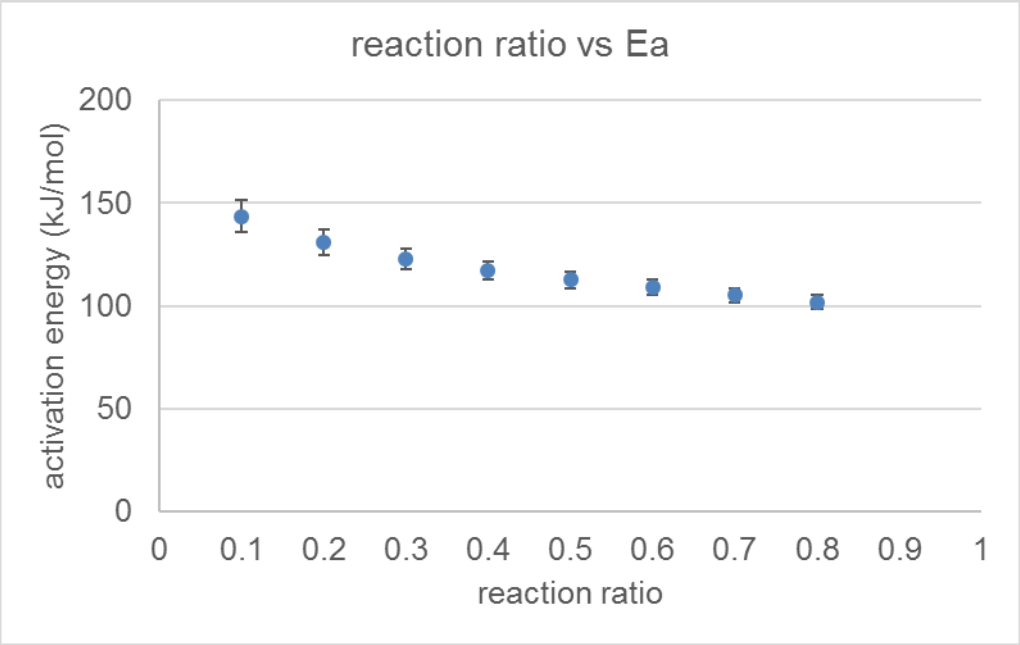

Fig. 3-2 The activation energy at each reaction rate

Ea estimated with Ozawa method was almost the same except for the early stage of the dehydration. The value of Ea at the first dehydration step was 113 ± 4 kJ/mol (at reaction rate 0.5).

It was difficult to obtain the value of Ea at the second dehydration step with Ozawa method. The dehydration reaction could not be stopped before the beginning of the second dehydrate step especially under the faster heating rate condition (i.e. 10 K/min), and two dehydration reactions may simultaneously occur. As a result, it was impossible to precisely estimate the Ea of second step with Ozawa method.

Isothermal tracing of the weight decreasing measured with TGA was conducted for the introduction of reaction model and the estimation of the activation energy (Ea). In particular, at first dehydration step, the weight decreasing was traced in jumping the temperature to 45, 50, 55, and 60 ºC from room temperature and keeping at each temperature. In Fig. 3-3, the relationship was shown between the reaction ratio (α) and temperatures. Temperature dependency was clearly observed.

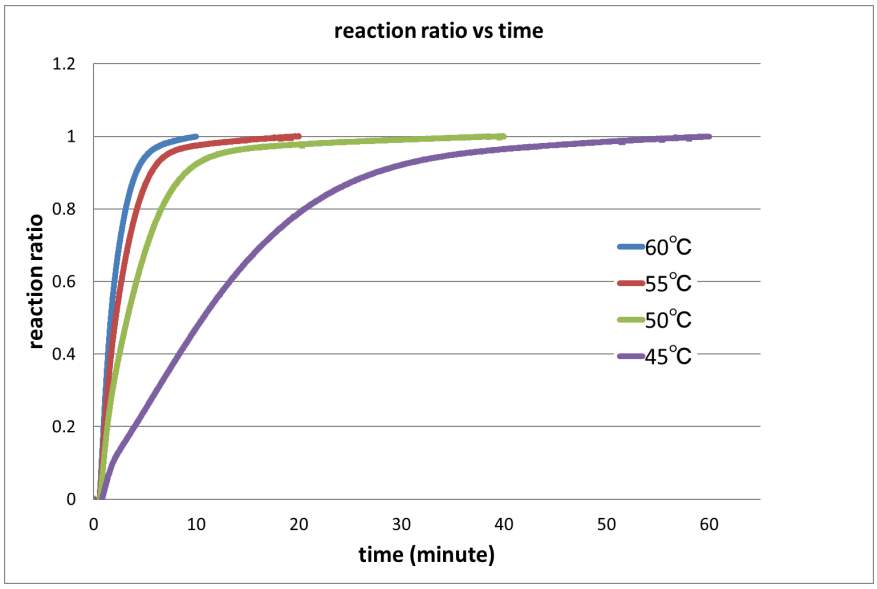

Fig. 3-3 The reaction ratio at each temperature on the first dehydration step

On the other hand, at second dehydration step, the first dehydration should be completed before the observation of the weight decreasing of second dehydration step. For this purpose, pretreatment process was assembled. Before the jumping to 65, 70, 75, and 80 ºC for measuring the second dehydration step, the first step was completed to keep the temperature at 55ºC for 15 min. By the pretreatment process two reactions did not simultaneously occur as seen in the experiment of Ozawa method. In Fig. 3-4, the relationship was shown between the reaction ratio (α) and temperatures. Temperature dependency was also clearly observed.

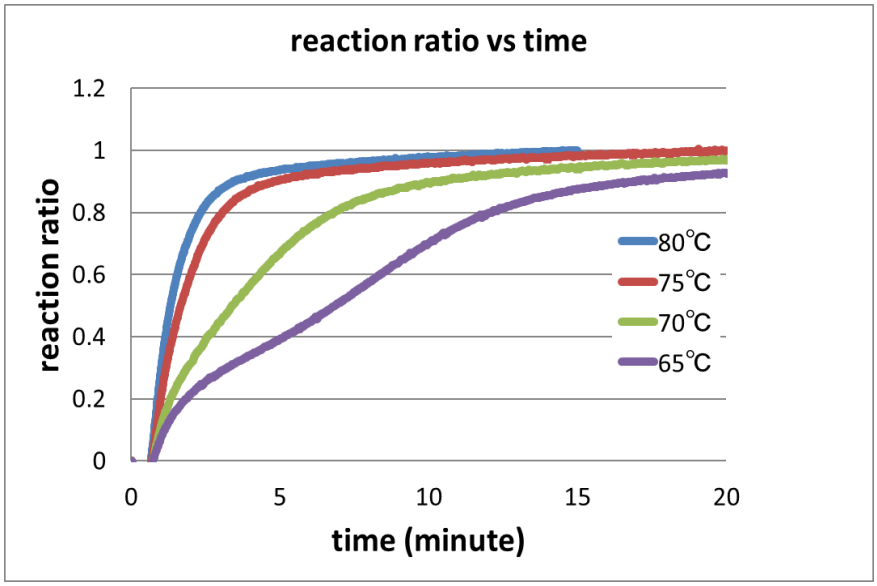

Fig. 3-4 The reaction ratio at each temperature on the second dehydration step

The most appropriate model was introduced by the fitting analysis for the various reaction models (Table 1). As a result, at first dehydration step, R3 model gave us the best fitting result. R models were known as one of the phase boundary reaction models. On the other hand, at second dehydration step, F2 model was the most appropriate. F models were not limited within the solid state reaction and the formal models for describing the general reactions. Fitting data was shown in appendix section.

The activation energies of first (Ea^{1st}) and second (Ea^{2nd}) steps were estimated as 114 ± 7 and 104 ± 6 kJ/mol, respectively. Arrhenius plots were shown in Fig. 3-5. Ea value of each reaction was almost the same, and Ea of first step was slightly larger than that of second step.

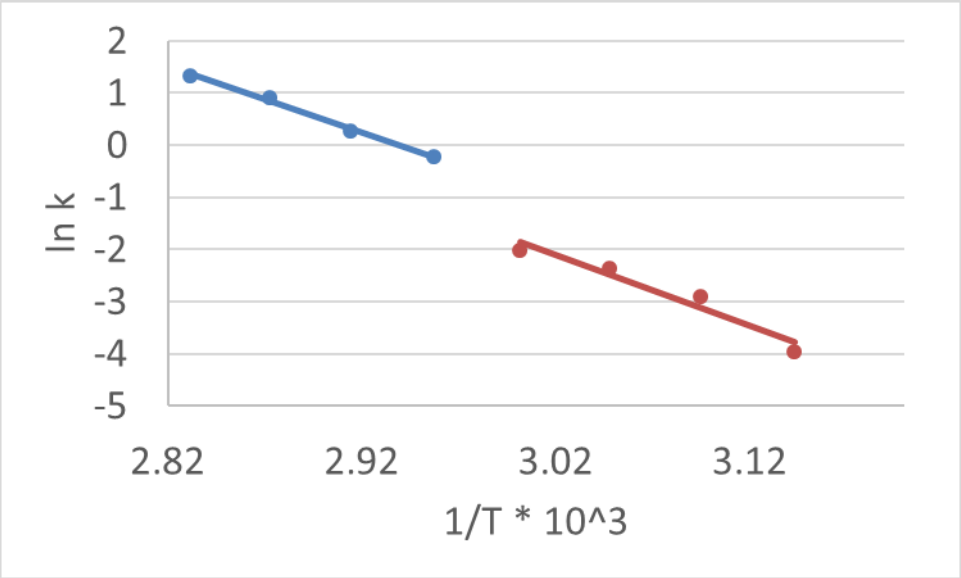

Fig. 3-5 Arrhenius plots for the two dehydration reactions. (a) Red line indicated the first reaction, (b) blue line indicated the second reaction.

In comparison with the value of Ea, values of Ea^{1st} estimated with ozawa method and estimated with the isothermal method were 113 ± 4 and 114 ± 7 kJ/mol, respectively. No large discrepancy indicated the validity of both methods for the estimation of Ea and the introduced reaction model.

Ea^{1st} was slightly larger than Ea^{2nd}. At the first dehydration, three hydrogen bonds were cleaved to remove the water molecule. On the other hand, at the second step, two hydrogen bonds were done. The order of the number of cleaved hydrogen bonds and Ea were not controversial, and it was possible to qualitatively explain in comparison with the crystal structures (Fig. 3-6).

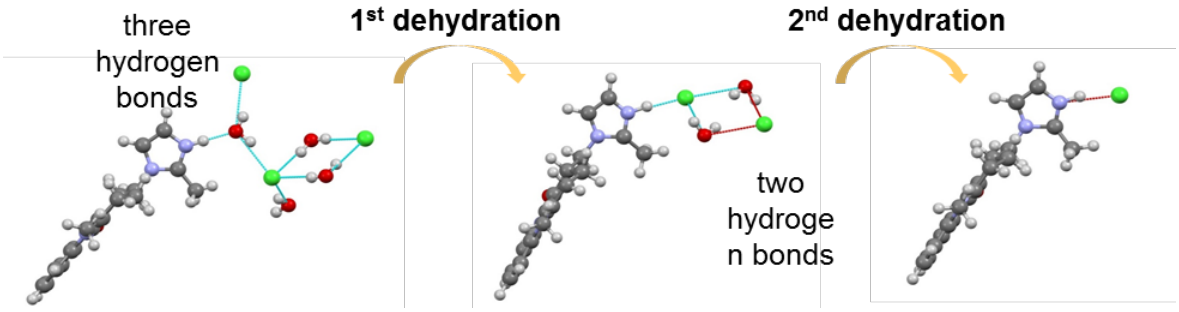

Fig. 3-6 The number of hydrogen bonds in each dehydration step

Although the hydrogen bonds should be one of the main factors to establish the crystal structure, in those dehydration steps, it was difficult to quantitatively discuss the difference of values of Ea because the difference was too small to be explained by the number of hydrogen bonds. Other factors should be contributed on the dehydration such as stacking interaction, van der Waals interaction and ionic interaction. Moreover, it has to be mentioned the larger variability of an analytical method because of solid state reaction.

Introduced reaction models were different from the first (R3 model) and second step (F2 model). The first step was the dehydration from a dihydrate to a hemihydrate. In this step, not only the rearrangement of the hydrogen bonds but also translation movement of an imidazole ring should cooperatively occur as many reactions of solid state was also cooperatively. On the other hand, at the second dehydration in which a hemihydrate transformed to an anhydrate, the crystal structure was nearly unchanged and the space of water molecule was kept as a void. It could be considered to introduce the F2 model which was not specific model for the solid reaction for the second step because there were little change of the solid state and water molecules acted like adsorption controlled by the pressure.

In taking into consideration with the experimental condition, TGA was carried out under the dry N_2 gas flow, so the relative humidity was almost equivalent to 0%. As a result, the dehydration reaction should be accelerated in comparison with room environment. It should be considered that the dehydration reaction became slow at a normal environment. The rate constants of reaction would depend on the environment although the value of activation energy was independent from the reaction environment..

Reverse reaction in which a hemihydrate transforms back into a dihydrate was focused at the next step. At this reverse reaction of ondansetron, a water molecule will insert between an imidazole cation and a chloride anion, that is, the ionic bond will be cleaved by the water molecule. It is interested in the result of kinetic analysis. TGA is not appropriate for the kinetic analysis of the reverse

reaction because not only temperature but also humidity should be controlled and it is difficult to control the humidity by TGA because of using drying N_2 gas. Therefore, an alternative evaluation method was established with the dynamic vapor sorption system (VTI instrument).

In particular, in the VTI instrument, a sample will be set at 25 ºC 60% RH and a hemihydrate will be prepared at 55 ºC 5% RH. After then, the temperature will be decreased by the target temperature with keeping the humidity at 5% RH. Finally, weight changing will be monitored at 20% RH.

In Fig. 3-7(A), time course of reaction rate regarding weight change at various temperatures was shown. Temperature dependency was clearly observed. As a result of kinetic analysis, the reaction model was able to be estimated as R3 with isothermal fitting analysis. Arrhenius plot was shown in Fig. 3-7(B). The activation energy of reverse reaction (Ea^{rev}) was calculated as 61 ± 7 kJ/mol and this value was approximately half of the value of forward reaction (Ea^{1st}: 114 ± 7 kJ/mol). This result supported that a dihydrate was more stable than a hemihydrate at a normal environment.

(A)

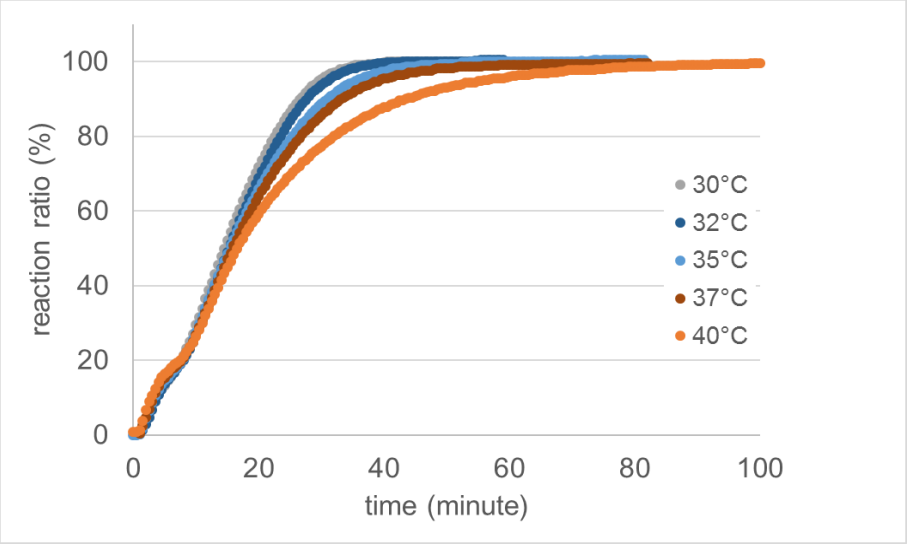

(B)

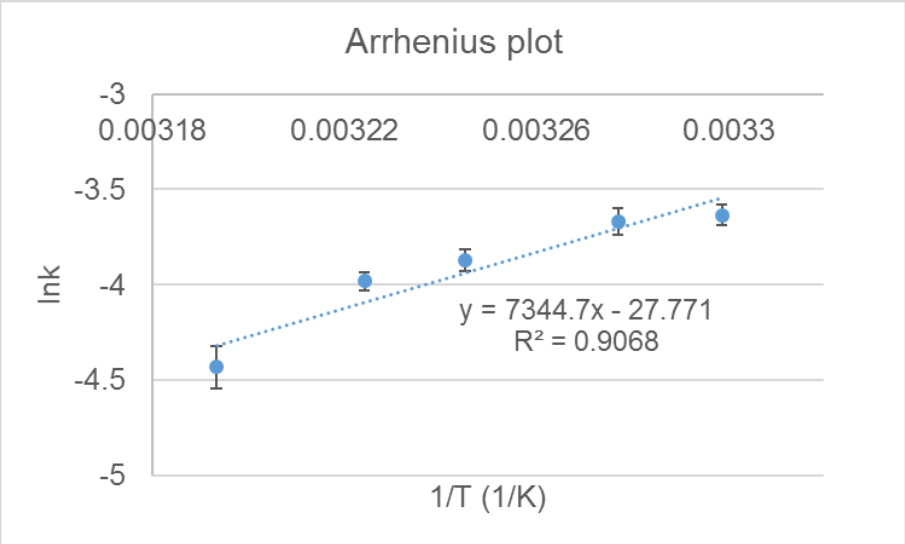

Fig. 3-7 (A) The reaction ratio at each temperature on the reverse hydration at 20% RH and (B) Arrhenius plots for the hydration reaction.

At the dehydration reaction, Ea^{1st} and Ea^{2nd} were almost the same but Ea^{1st} was slightly larger than Ea^{2nd}. At the hydration reaction, Ea^{rev} considerably decreased. The schematic energy diagram was shown in Fig. 3-8. It was considered that dehydration reaction products (hemihydrate and anhydrate) were the higher energy state and were less stable. The energy diagram also supported that a dihydrate of ondansetron hydrochloride was more stable.

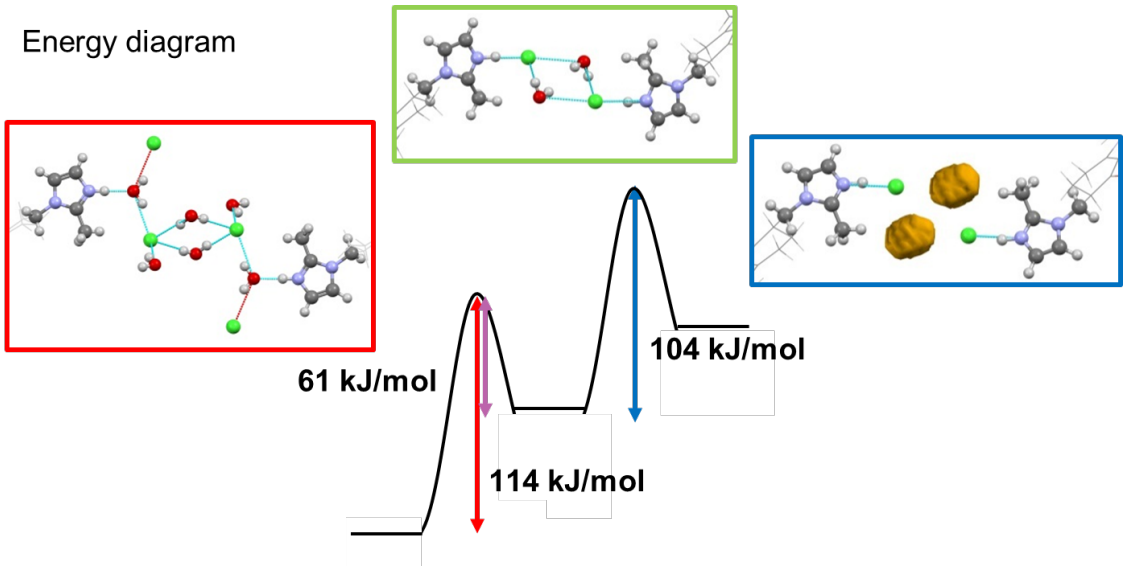

Fig. 3-8 The schematic energy diagram of the dehydration of ondansetron hydrochloride dihydrate

3.4. Short summary

Kinetic analysis was carried out about the dehydration reactions of ondansetron HCl dihydrate and consideration of mechanism was discussed.

Two kinds of analyses which were the isothermal method and the isoreaction ratio method (Ozawa method) were conducted for the dehydration reaction of ondansetron hydrochloride dihydrate. These values of the first dehydration reaction (Ea^{1st}) estimated with two methods were almost equivalent. Generally speaking, large variability was sometimes observed at the solid state reaction, so it should be carefully dealt with the results. From the view point of variability, it is important that the different methods gave us the equivalent values of Ea.

Ondansetron hydrochloride dehydrate showed two-step dehydration. Ea value of each step was almost the same, and Ea^{1st} (114 ± 7 kJ/mol) was slightly larger than Ea^{2nd} (104 ± 6 kJ/mol). The order of the number of cleaved hydrogen bonds and Ea was not controversial, and it was possible to qualitatively explain in comparison with the crystal structures (Fig. 3-6). The Ea^{rev} was calculated as 61 ± 7 kJ/mol and was approximately half of the value of forward reaction (Ea^{1st}: 114 kJ/mol). This result supported that a dihydrate is more stable than a hemihydrate at a normal environment.

In the consideration of mechanism, results of kinetic analysis and crystal structure analysis were not controversial. As a result, the combined usage of kinetic analysis and crystal structure is powerful tool for the mechanistic consideration of dehydration.

3.5. Appendix

Fitting plots for the first dehydration reaction were shown in Fig. 3-9.

(a) (b)

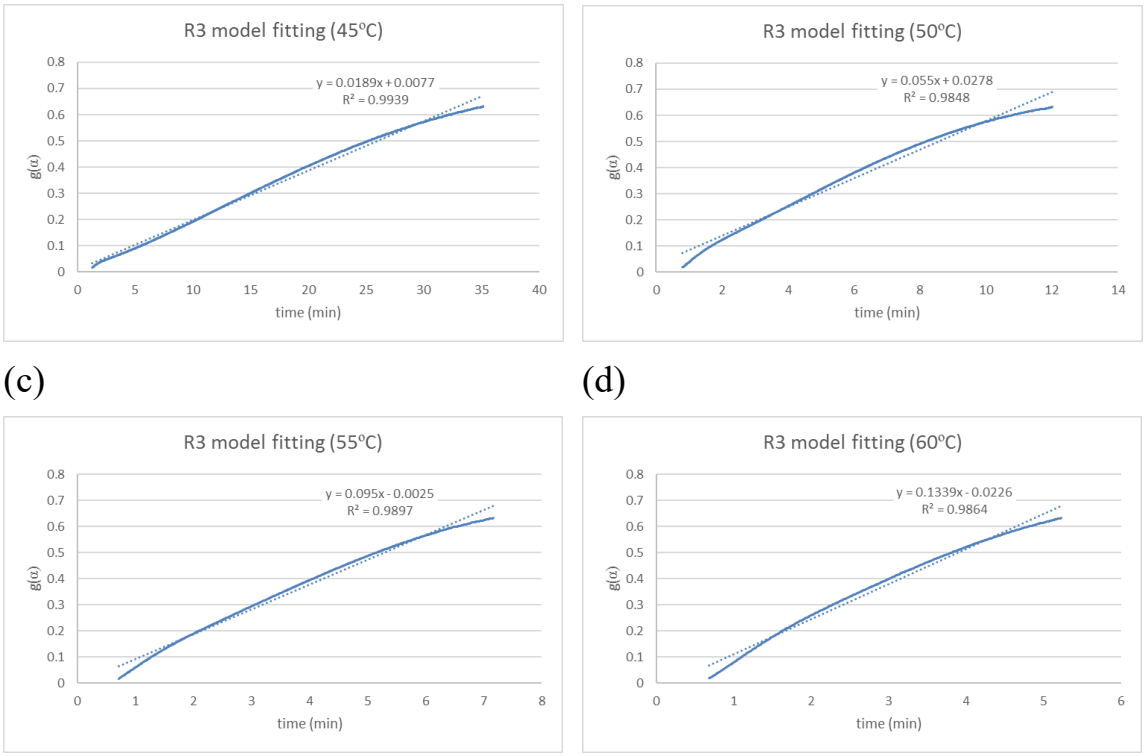

(c) (d)

Fig. 3-9 Fitting plots for the reaction model introduction at the first dehydration reaction, (a) at 45 ºC, (b) at 50 ºC, (c) at 55 ºC, and (d) at 60 ºC.

Fitting plots for the second dehydration reaction were shown in Fig. 3-10.

(a) (b)

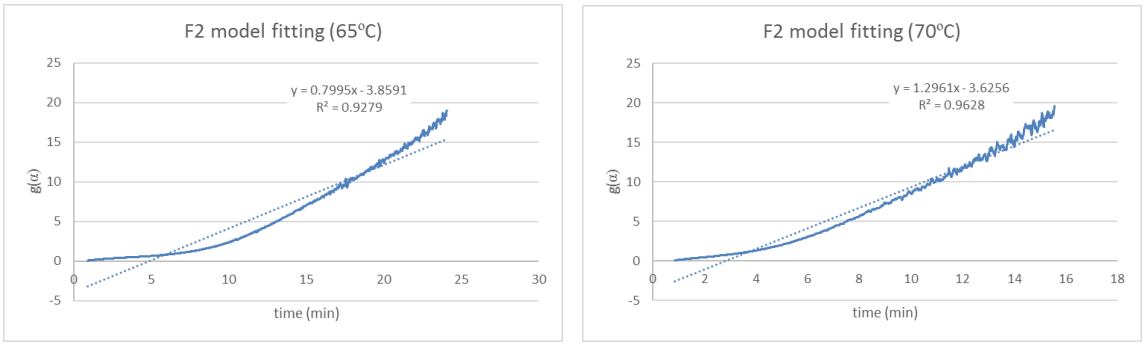

(c) (d)

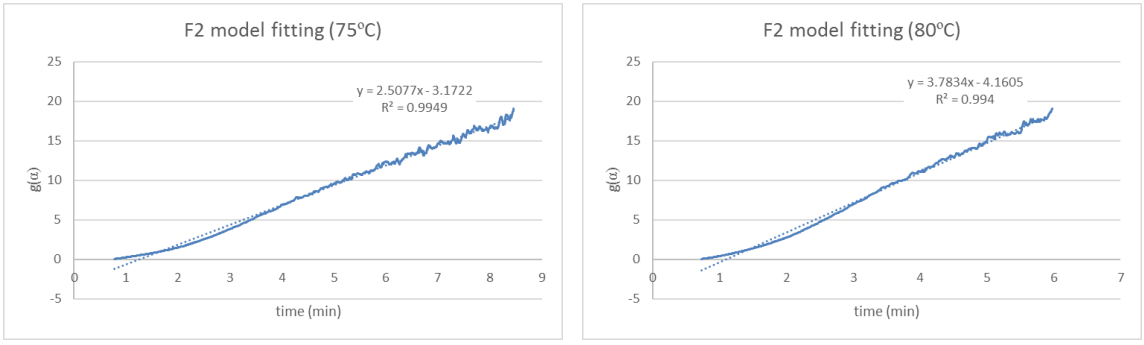

Fig. 3-10 Fitting plots for the reaction model introduction at the first dehydration reaction, (a) at 65 ºC, (b) at 70 ºC, (c) at 75 ºC, and (d) at 80 ºC.

Fitting plots for the hydration reaction were shown in Fig. 3-11.

(a)

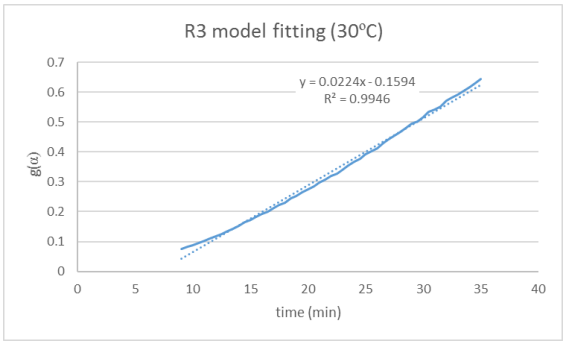

(b)

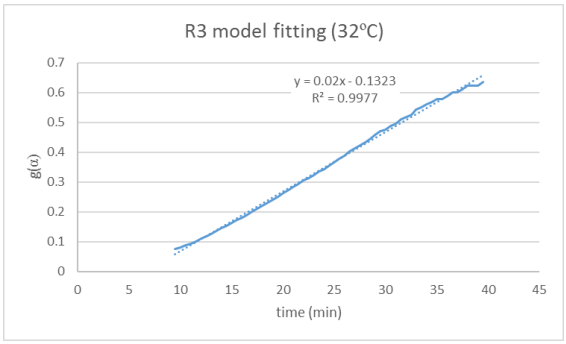

(c)

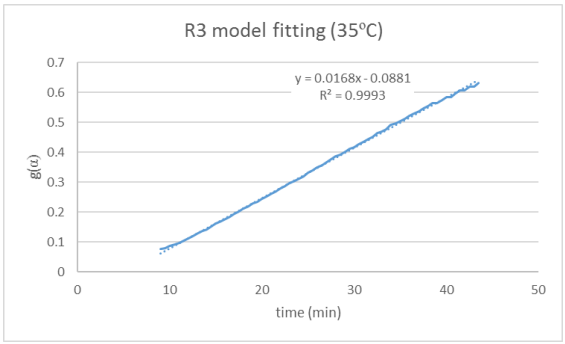

(d)

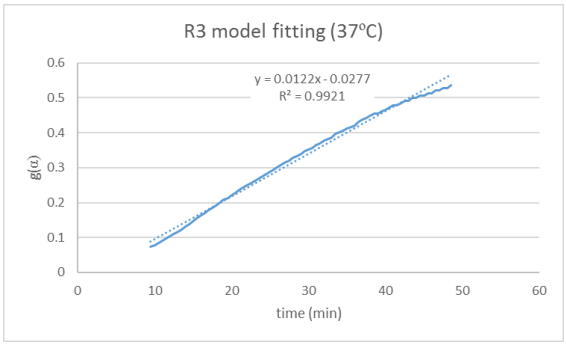

(e)

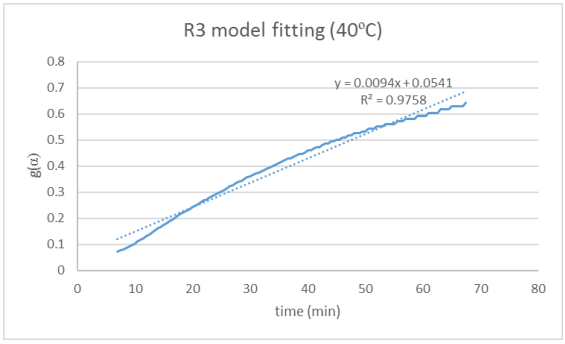

Fig. 3-11 Fitting plots for the reaction model introduction at the first dehydration reaction, (a) at 30 ºC, (b) at 32 ºC, (c) at 35 ºC, (d) at 37 ºC, and (e) at 40 ºC.

Chapter 4

Ozagrel HCl monohydrate; elucidation of dehydration reaction using crystal structure analysis and kinetic analysis

4.1. General introduction

In previous chapters, the mechanism of the dehydration of ondansetron hydrochloride dihydrate was elucidated with the combination of crystal structure analysis and kinetic analysis. In this chapter, I would like to summary the research about the dehydration mechanism of ozagrel hydrochloride hydrate and prove the effectiveness of the combination of crystal structure analysis and kinetic analysis for the elucidation of dehydration mechanism.

Chemical structure of ozagrel was shown in Fig. 4-1.

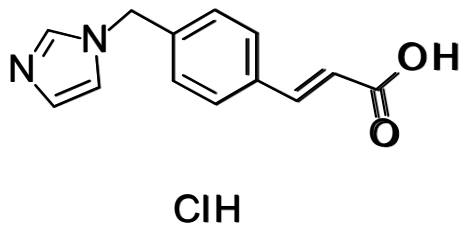

Fig. 4-1 Chemical structure of ozagrel

Ozagrel is a zwitter compound having an imidazole as a cation and a carboxylic acid as an anion part. Molecular weight is 228.25 g/mol.

Ozagrel hydrochloride has been launched as a therapeutic agent for asthma with a tablet formulation.[79] In Japan, ozagrel was on the market at 1992 named as Bega (Ono pharmaceutical co.) and Domenan (Kissei pharmaceutical co.). Moreover, ozagrel sodium has been launched as a therapeutic agent for thrombogenic disease with an intravenous formulation.

Crystal structure information of free base, fumaric acid salt hydrate and phosphate salt have been already obtained and were filed in CSD (Crystal Structure Database) as TISKAI[80] (free), WUNBIR[81] (fumarate hydrate) and XUJYEH[82] (phosphate). However, crystal structure information of ozagrel hydrochloride hydrate has never been known, and mechanism of the dehydration reaction of that hydrate has never been reported. The concrete landscape was not

well known. In this chapter, the dehydration mechanism of ozagrel hydrochloride hydrate will be elucidated with the combination of crystal structure analysis and kinetics analysis.

4.2. Materials and Methods

4.2.1. Materials

Ozagrel hydrochloride hydrate was purchased from TOKYO KASEI (Tokyo, Japan). Materials were used without any purifications.

4.2.2. Heating

Samples were heated in a Fine Oven DF42 (Yamato Science).

4.2.3. Powder X-ray diffraction (PXRD)

PXRD analysis was performed on a TTR II (Rigaku, Tokyo, Japan) and used Cu Kα radiation at 1.54184 Å at a voltage of 50 kV and current of 300 mA. Data were collected at a scan rate of 4 º/min over a 2θ range of 2.5 º to 40 º.

4.2.4. High quality powder X-ray diffraction

High quality PXRD analysis performed on a SmartLab system (Rigaku) using Cu Kα radiation at 1.54184 Å at a voltage of 45 kV and current of 200 mA, with a D/Tex Ultra as a detector for the crystal structure analysis with powder X-ray patterns. A sample was pulverized and sandwiched by the membrane.

4.2.5. Polarization microscope observation

Polarization microscope observation was performed using an ECLIPSE E600POL (Nikon, Tokyo, Japan) equipped with Nikon D300s as a camera. The small amount of a sample was suspended with a silicon oil (Kanto Kagaku) and sandwiched by a cover glass. 40 times field lens was used.

4.2.6. Thermal analysis: Differential scanning calorimetry

Thermal analysis was performed using a TA Q2000 DSC instrument that included a refrigerated cooling system (TA Instruments, New Castle, DE, USA).

Temperature calibration was carried out using the indium metal standard supplied with the instrument. Samples were weighed (about 3 mg) in aluminum pans and analyzed from 25 °C to 300 °C at heating rates of 10 °C/min using a similar empty pan as a reference. An inert atmosphere was maintained in the calorimeter by purging with nitrogen gas at a flow rate of 50 mL/min.

4.2.7. Thermal analysis: Thermogravimetric analysis (TGA)

TGA was performed using a TA Q500 TGA instrument (TA Instruments). Approximately 4 mg of sample was loaded into a platinum pan and heated to 300 °C at a rate of 10 °C/min. Measurements were carried out under nitrogen purge at a flow rate of 100 mL/min. Temperature calibration was carried out using standard nickel.

4.2.8. Water vapor sorption and desorption studies

Dynamic vapor sorption experiments were performed on a VTI SGA 100. Samples (about 10 mg) were studied over a selected humidity range (absorption process; from 5% relative humidity (RH) to 95% RH and desorption process; from 95% RH to 5% RH) at 25 °C. For each humidity step, the equilibration was set to dm/dt 0.03%/min on a 5-min time frame (maximum hold time 180 min).

4.2.9. X-Ray differential scanning calorimetry (DSC)

Simultaneous measurement of powder X-ray diffraction data and DSC data was carried out on a SmartLab system (Rigaku) using Cu Kα radiation at 1.54184 Å at a voltage of 45 kV and current of 200 mA, with a DSC attachment and a D/Tex Ultra as a detector. Samples were weighed (1.5–2.5 mg) in aluminum pans and analyzed at a heating rate of 2 °C/min using a similar empty pan as a reference. X-ray diffraction data were collected at a scan rate of 20 °/min over a 2θ range of 10 ° to 25 °.

4.2.10. SPring-8 experiments

The powder samples were enclosed in a 0.3 mmΦ Lindemann glass capillary. X-ray powder diffraction data were collected at SPring-8 BL19B2[72], which is equipped with a high-resolution type Debye–Scherrer camera and a curved imaging-plate detector. The wavelength was set at 1.0000 Å. It took one minute to set each temperature, which was maintained for 4 minute to ensure equilibrium was reached before measurements were taken. Data were collected for 5 minutes. During data collection, the sample was maintained at the set

temperature and rotated at 1 r/min to reduce potential preferential orientation effects.

4.2.11. Crystal structure analysis with powder XRD pattern

Crystal structure of a hydrate was determined from the PXRD patterns obtained at Lab instrument and crystal structure of an anhydrate was done obtained at SPring-8. Crystal structure analysis was carried out in the Powder Solve module of Materials Studio (BIOVIA).

After selecting the peaks set, indexing was conducted in the XCELL module[73] to introduce the unit cell and appropriate space group. The unit cell was refined by Pawley refinement and optimized.

The initial chemical structures of ondansetron and the water molecules were introduced using the Forcite module with COMPASS II[74] as a force field. The initial crystal structure was introduced by the POWDER SOLVE module[75] using the simulated-annealing approach and optimized by Rietveld refinement. Pareto optimization, a Rietveld refinement method that considers the energy of the structure calculated by a force field[76], was carried out at the final optimization step.

4.2.12. Kinetics study

4.2.12.1 Isoconversion methods

A sample was heated at a rate of 1, 2, 5, and 10 °C/min with TGA (Q500). Measurement at each temperature was repeated in three times.

4.2.12.2 Isothermal methods.

For the kinetic analysis of dehydration reaction, a sample was heated at jump mode to 75, 80, 85, and 90 °C, and kept on each temperature for 250, 200, 150, and 100 min with TGA (Q500), respectively. Measurement at each temperature was repeated in three times.

4.2.12.3 Calculation

See in chapter 3.

4.3. Results

4.3.1. Characterization

The solid state of ozagrel hydrochloride hydrate was evaluated. XRD pattern data and polarization microscope observation were shown in Fig. 4-2

(A)

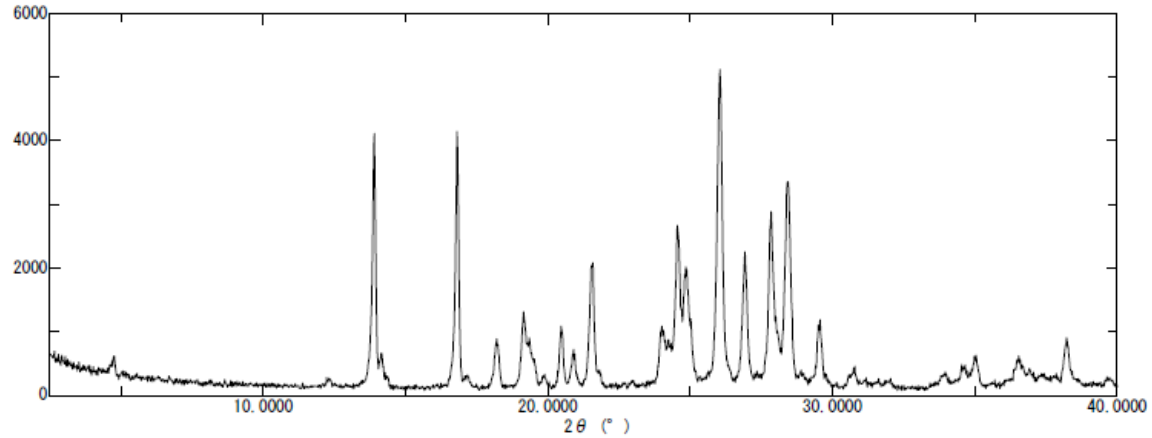

(B)

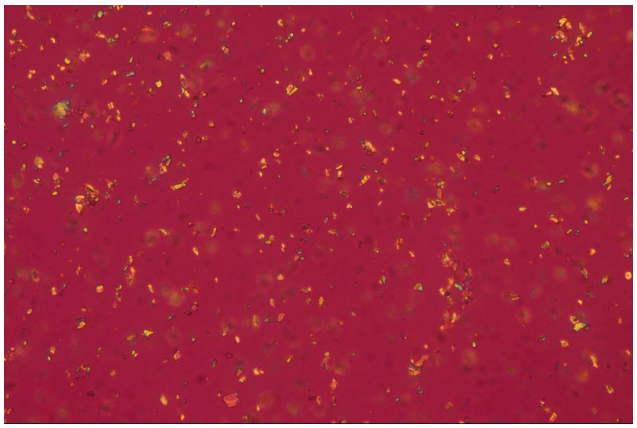

Fig. 4-2 (A) XRPD pattern of ozagrel hydrochloride hydrate, (B) polarization microscope observation.

Ozagrel hydrochloride hydrate was the crystalline powder and particle size of ozagrel hydrochloride hydrate was small, so the hydrate is the fine powder.

Hygroscopicity was evaluated for testing the stability of a monohydrate against the humidity.

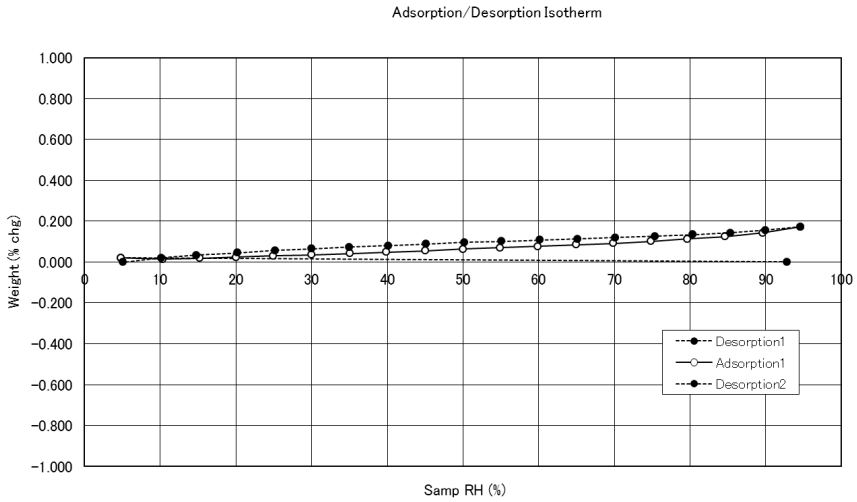

Fig. 4-3 Hygroscopicity of ozagrel hydrochloride hydrate at 25 ºC.

In Fig. 4-3, ozagrel hydrochloride hydrate was stable against the humidity since the weight change was not observed at 5-95% RH. Dehydration of a hydrate did not occur at low relative humidity condition (i.e. 5% RH).

Thermal analysis results were shown in Fig. 4-4.

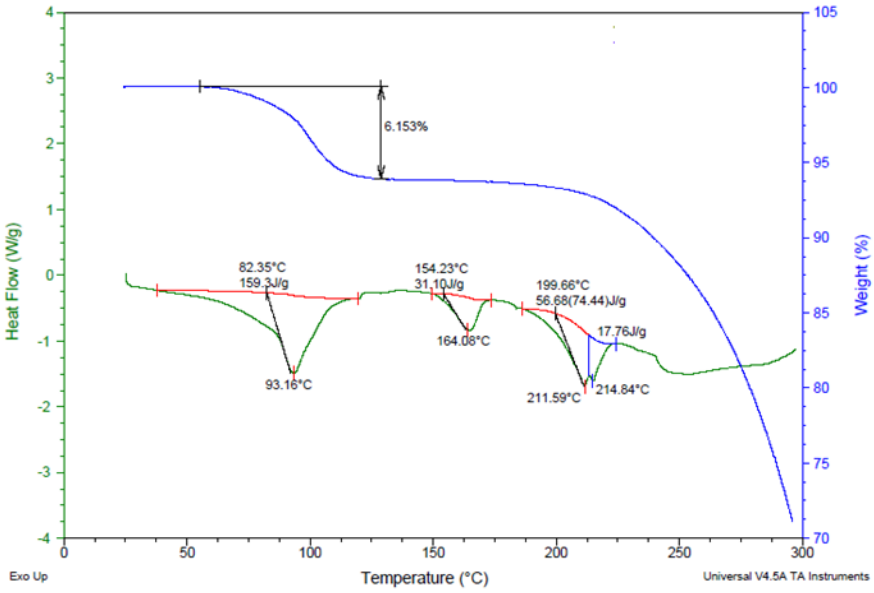

Fig. 4-4 Thermal behavior of ozagrel hydrochloride hydrate. Green line indicates the differential scanning calorimetry (DSC) curve, blue line indicates the thermogravimetric (TG) curve.

The thermal behavior seems to be complicated. The weight loss together with the endothermic peak was observed and, in addition, plural endothermic peaks were observed. The amount of weight loss was equivalent to the theoretical

value of a water molecule, so dehydration of a monohydrate was considered to be detected around 90 °C.

4.3.2. crystal structure analysis of a monohydrate

For the elucidation of dehydration mechanism, crystal structure information is necessary. However, ozagrel hydrochloride hydrate was extremely fine powder (Fig. 4-2 (B)), so it was difficult to obtain the single crystal. The structure determination with powder X-ray pattern was carried out. High quality powder X-ray pattern was obtained with a laboratory instrument (see 4.2.4).

(A)

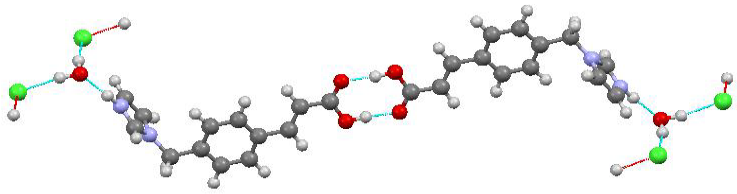

(B) (C)

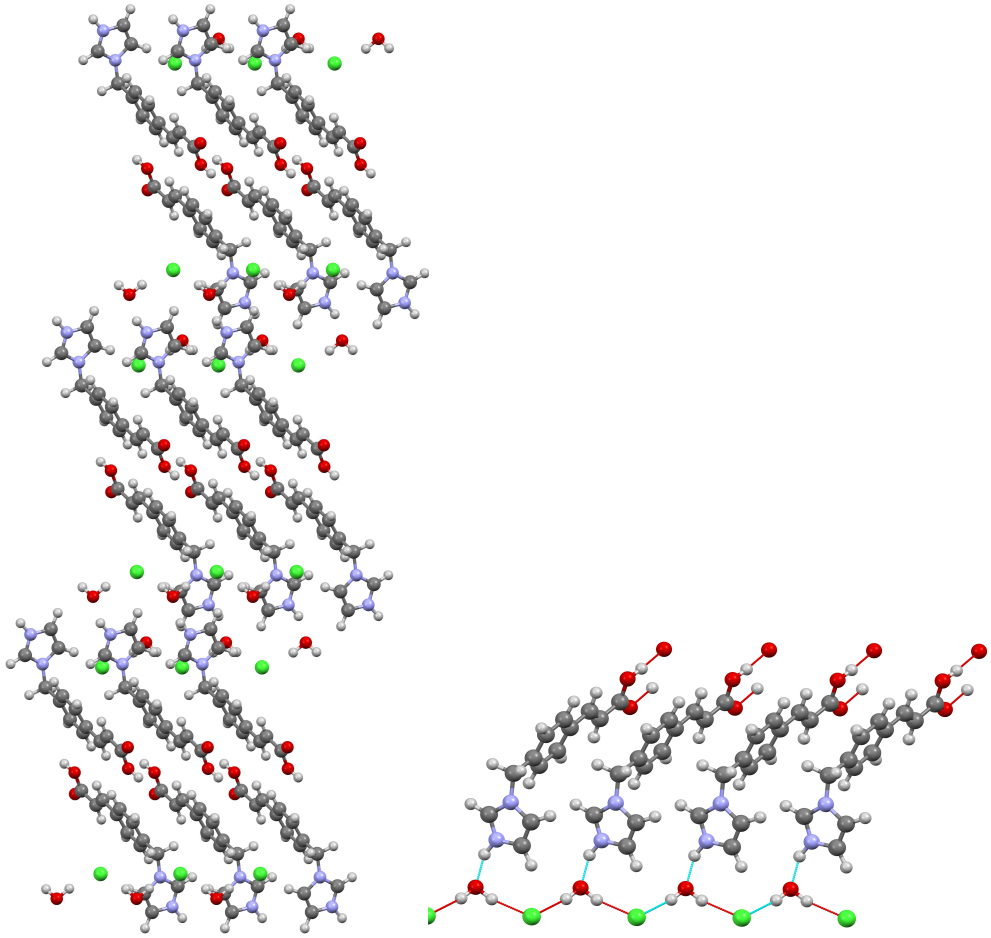

Fig. 4-5 Crystal structure of ozagrel hydrochloride hydrate. (A) the dimer structure, (B) projected figure with b axis and (C) hydrogen bonds network.

Table 4-1 Crystal data for ozagrel hydrochloride monohydrate

	monohydrate
Molecular formula	$C_{13}H_{14}N_2O_2Cl.H_2O$
Sample type	Powder
Crystal system	Triclinic
Space group	*P*-1
a (Å)	18.831(4)
b (Å)	7.533(1)
c (Å)	5.040(1)
α (º)	103.231(1)
β (º)	94.630(1)
γ (º)	98.699(1)
V (Å^3)	683.136
R_p (%)	3.05
R_{wp} (%)	4.30

Crystal structure analysis with XRD pattern obtained with a laboratory instrument was conducted and it was succeeded to be obtained the crystal structure. Ozagral is a zwitter compound having an imidazole and carboxylic acid moiety. In the crystal structure, the dimer motif formed between two carboxylic acids was observed (Fig. 4-5(A)). Hydrophobic and hydrophilic layers were observed in the crystal structure (Fig. 4-5(B)). Chain motif consisting of a water molecule and a chloride anion was also observed. Moreover, the direct interaction was not formed between an imidazole cation and a chloride anion, and that interaction was mediated by a water molecule (Fig. 4-5(C)).

4.3.3. Phase transition

It has been already mentioned that ozagrel hydrochloride hydrate showed the complicated thermal events observed in the DSC curve. Then, it was studied with XRD-DSC that each thermal event corresponded to the crystal form transition.

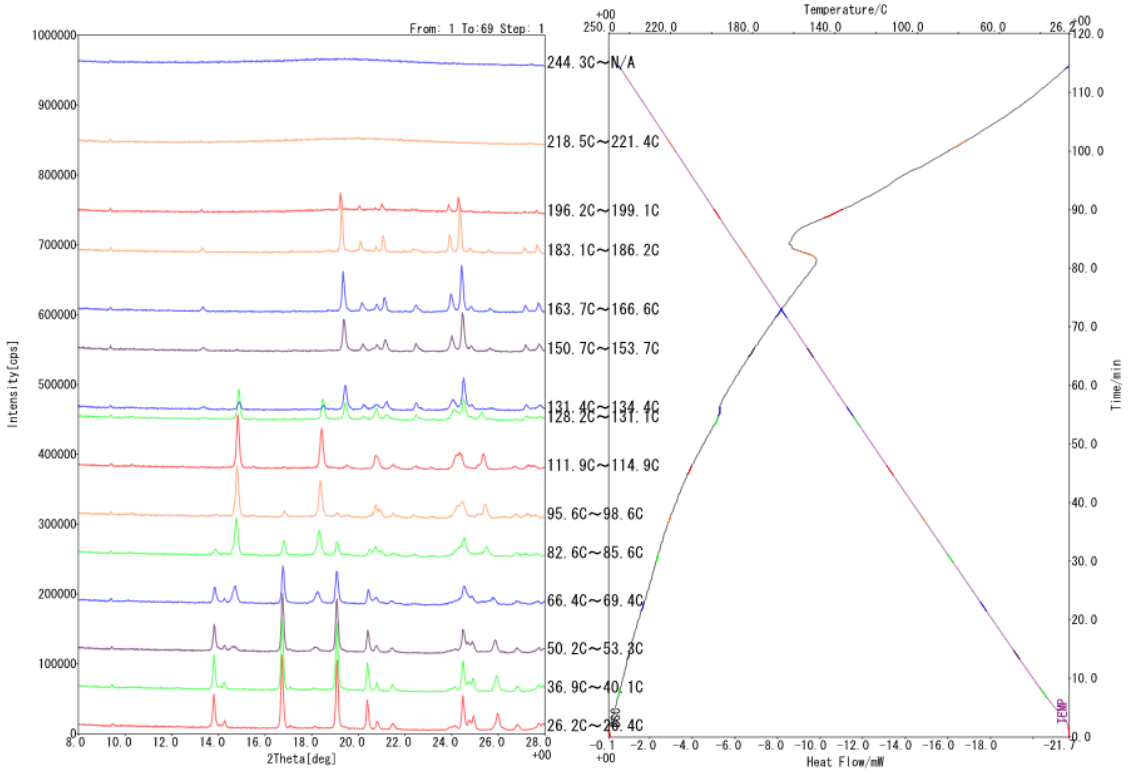

Fig. 4-6 X-ray DSC results of ozagrel hydrochloride hydrate.

In the XRD-DSC, XRD pattern was changed when the first endothermic peaks with the decrease of weight was observed, and the pattern was changed again at around 130 ºC. The temperature at which XRD pattern was changed was slightly different from that of the second endothermic peak in DSC measurement. This difference was based on the condition of analysis, so crystal form transition with the endothermic peak was considered to occur. After that, hallow pattern was observed because of the melting or the decomposition. In summary, a hydrate transformed to an anhydrate A, and transformed to an anhydrate B in the crystal form transition with heating.

Two anhydrates were discovered, and isolation of these forms was tried. In particular, time course data of XRD pattern was traced at room temperature after the heating.

Time course data of XRD pattern was shown in Fig. 4-7. after heating at 95 ºC for 30 minute.

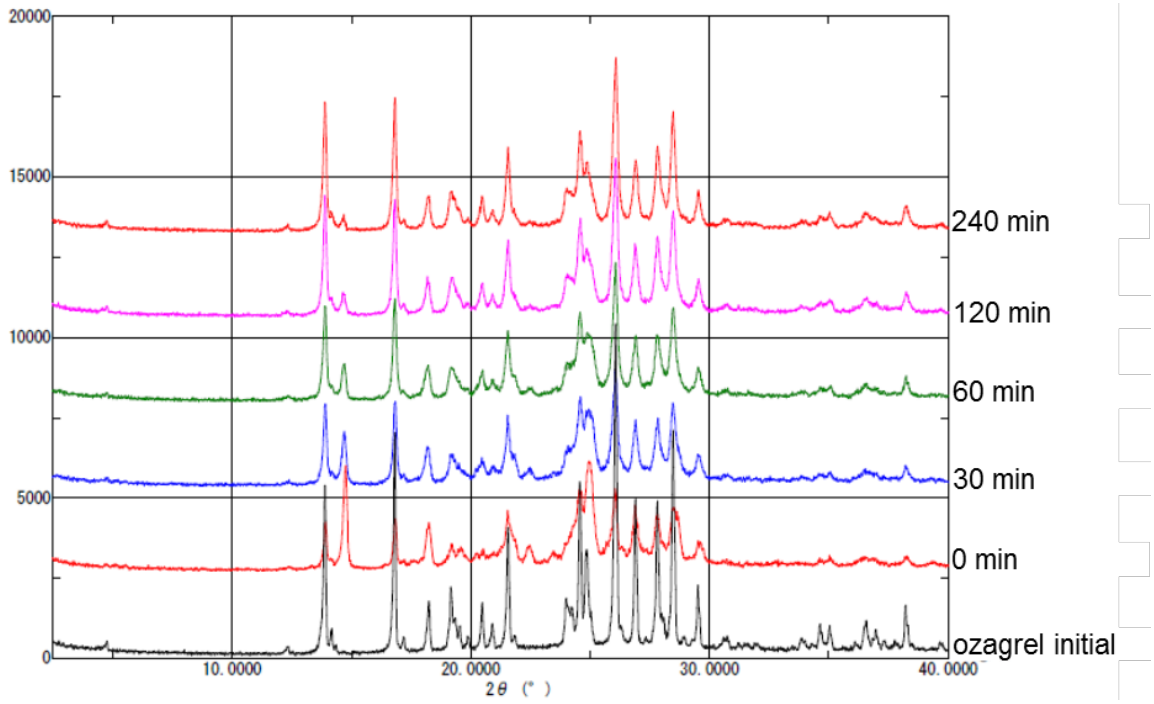

Fig. 4-7 Reversibility after heating at 95 ºC confirmed with X-ray diffraction patterns.

Although XRD pattern was changed by the heating, changed XRD pattern was diminished as time advanced. After 240 minutes for coming back to the room temperature, XRD pattern was equivalent for the initial one. In conclusion, an anhydrate A was unstable at room environment, reversible crystal form transition was confirmed.

In the next step, time course data of XRD pattern was shown in Fig. 4-8. after the heating at 150 ºC for 30 minutes.

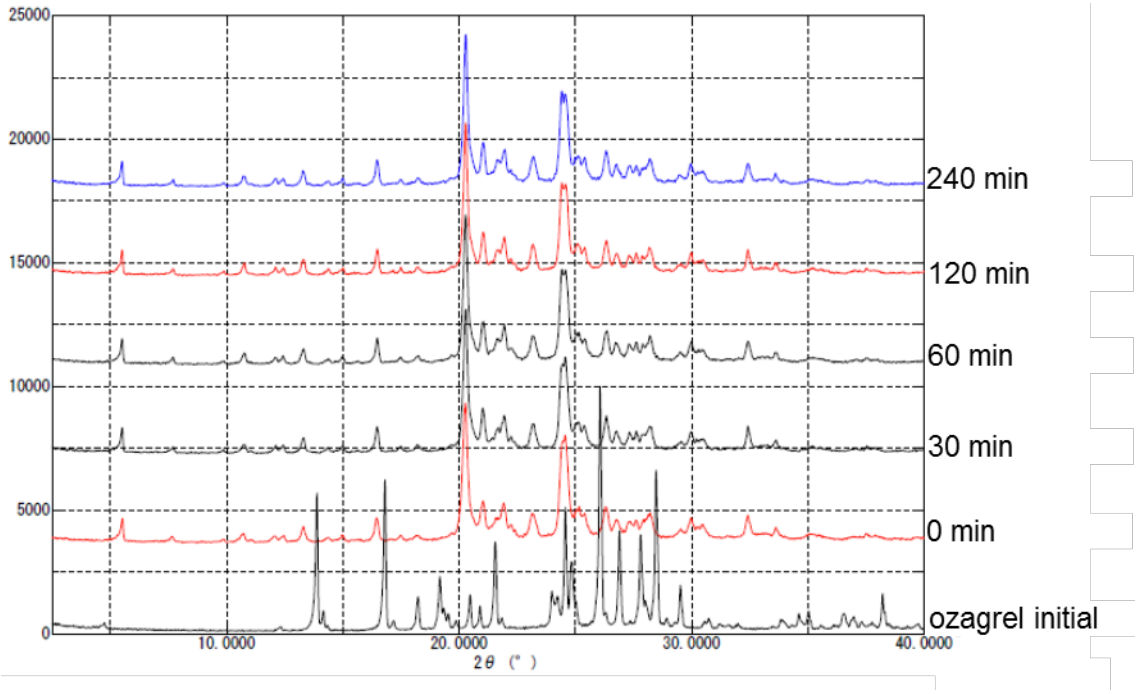

Fig. 4-8 Reversibility after heating at 95 ºC confirmed with X-ray diffraction patterns.

XRD pattern with the heating at 150 ºC was different from that of initial ozagrel and that pattern was not changed at least for 4 hours at room temperature. However, XRD pattern was different from that of result with XRD-DSC. An anhydrate C was considered to be obtained and an anhydrate B was concluded to be unstable at room condition.

Experiments of XRD with the heating was carried out at SPring-8 and crystal structure analyses were conducted with powder XRDs. The results of XRD with heating was shown.

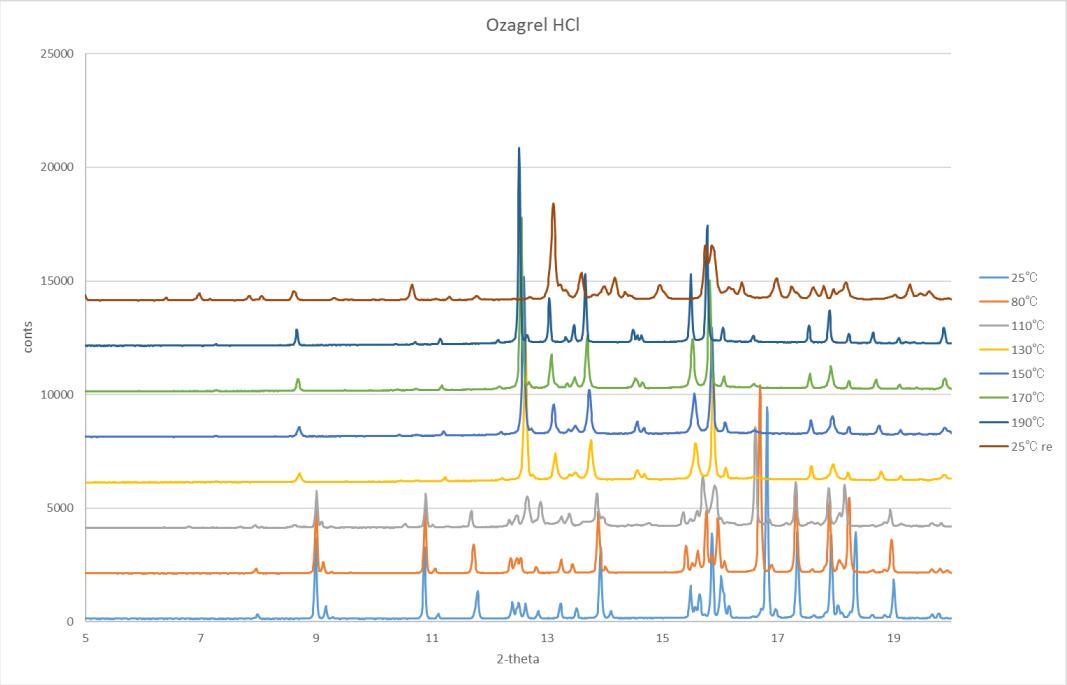

Fig. 4-9 XRD measurement with heating at SPring-8 BL19B2

In XRD with heating experiment at SPring-8, the different transition tendency was observed in comparison with the data of a lab instrument. As seen in Fig. 4-6, a monohydrate transformed to an anhydrate A, and transformed to an anhydrate B. However, in XRD with heating at SPring-8 (Fig. 4-9), the pattern of an anhydrate A was not observed and that of an anhydrate B was observed at 130 ºC. The powder samples were enclosed in a 0.3 mmΦ glass capillary at SPring-8 experiment. It was highly probable that it became the higher pressure environment in a capillary, so dehydration reaction kinetically delayed. Since crystal form transition toward an anhydrate B may be independent from the outside pressure, ozagrel hydrochloride monohydrate directly transformed to an anhydrate B in a capillary. Moreover, XRD pattern of an anhydrate C was obtained by cooling the an anhydrate B (a brawn line in Fig. 4-9).

4.3.4. Crystal structure analysis of an anhydrate B

Crystal structure analysis with powder X-ray pattern was carried out for an anhydrate B using the SPring-8 data at high temperature (130 ºC). Crystal structure information was shown in Fig. 4-10.

(A) (B)

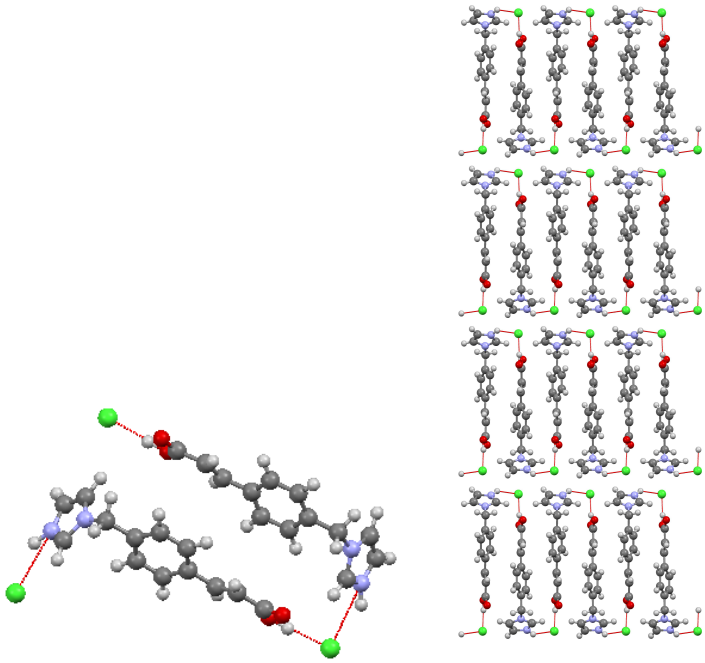

Fig. 4-10 Crystal structure analysis of an anhydrate B

Table 4-2 Crystal data for ozagrel hydrochloride anhydrate B

	anhydrate B
Molecular formula	$C_{13}H_{14}N_2O_2Cl$
Sample type	Powder
Crystal system	Orthorhombic
Space group	*Pna*2_1
a (Å)	31.670(3)
b (Å)	5.8579(8)
c (Å)	7.2574(7)
V (Å^3)	1364.4
R_p (%)	7.06
R_{wp} (%)	10.59

Although the dimer structure interacted between carboxylic acids was observed in the initial monohydrate, an anhydrate B obtained with heating did not show the dimer structure. Some specific hydrogen bonds were observed between a chloride anion and an imidazole, and between a chloride and a carboxylic acid. Hydrogen bond network of an anhydrate B was quite different from that of a hydrate. It was considered that these difference prevented an anhydrate B from transforming back to the initial a monohydrate at room temperature (Fig. 4-8).

4.3.5. Kinetic analysis

In previous section, it was concluded that a monohydrate transformed to an anhydrate A, and transformed to an anhydrate B. In this section, dehydration reaction is traced by the kinetics analysis and dehydration mechanism is elucidated.

In the kinetics analysis of the reaction, thermal gravimetry assay (TGA) was used. Ozawa method was firstly used to obtain Ea because this method was simple and did not need to estimate the reaction model (model free analysis). In TGA, the heating rate was set at 1, 2, 5, and 10 ºC/min and reaction ratio was calculated. The relationship between the reaction rate and time was shown in Fig. 4-11.

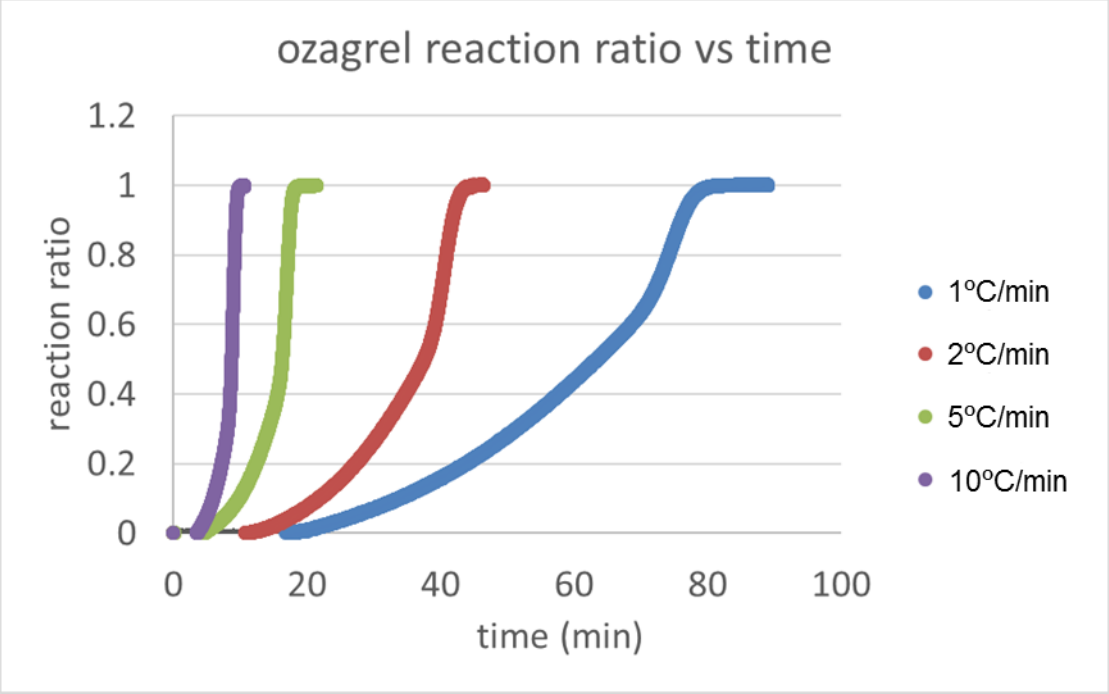

Fig. 4-11 Reaction ratio vs time at each heating rate

The reaction ratio clearly depended on the heating rate. Ea estimated with Ozawa method was plotted against in each reaction ratio (Fig. 4-12).

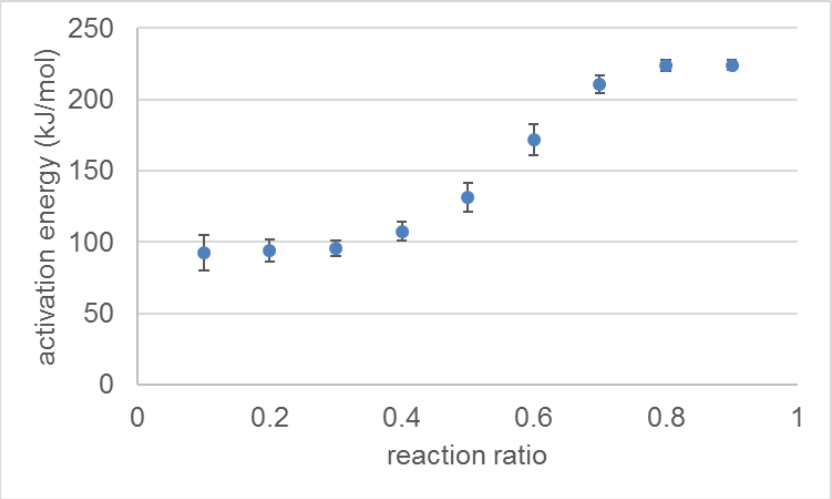

Fig. 4-12 The relationship between reaction ratio and the activation energy calculated by Ozawa method.

As it was obvious seen, the activation energy during the early part of reaction (small reaction ratio) was quite different that during the later part (big reaction ratio), and two stages of Ea were observed. These results indicated that the reaction model during the early part of reaction was different from that during later part. In other words, the reaction model at the lower temperature was different from that of the higher temperature. This assumption is proved by kinetic analysis of the isothermal reaction method. We supposed that the early part of reaction was considered at from 75 ºC to 90 ºC and the later part of reaction was considered at from 90 ºC to 105 ºC, then kinetic analysis with the isothermal method was conducted.

(A) (B)

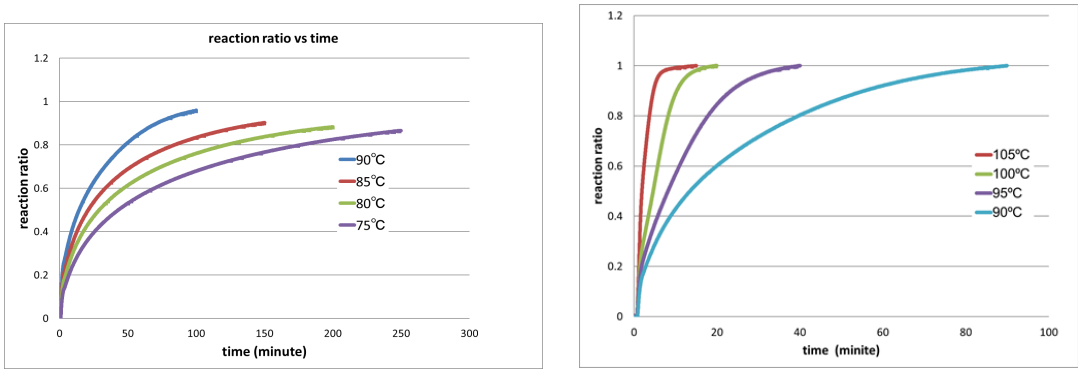

Fig. 4-13 The reaction ratio at each temperature, (A) at the lower temperature and (B) at the higher temperature.

Fitting analysis was conducted in each reaction, and Ea was estimated 95 ± 5 kJ/mol and 208 ± 2 kJ/mol with the Arrhenius plots, respectively (in Fig. 4-14). This value was quite equivalent to the results of model free analysis (in Fig. 4-12).

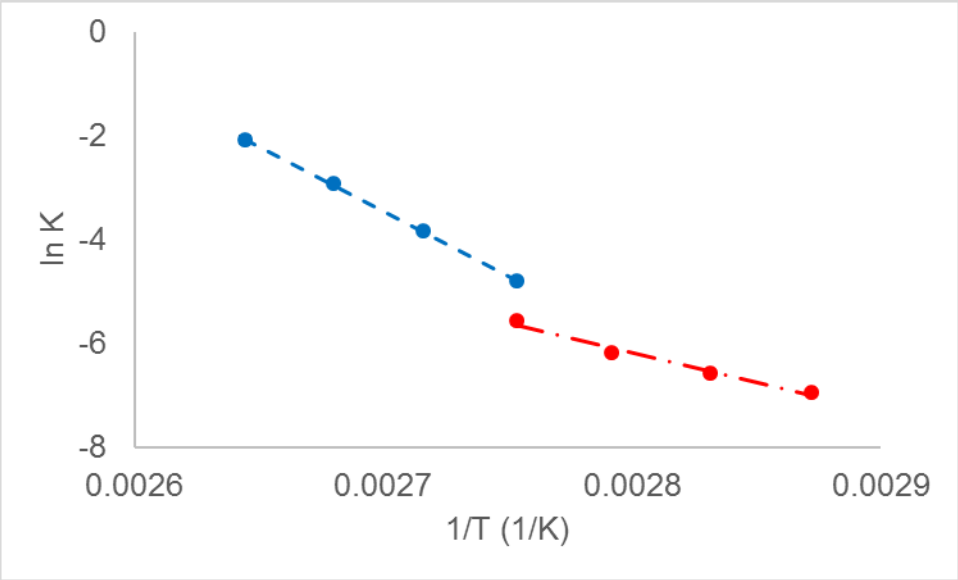

Fig. 4-14 Arrhenius plot of the dehydration reaction of ozagrel hydrochloride monohydrate.

4.4. Discussion

The results of kinetic analysis clearly showed the different activation energies (Fig. 4-14). This result indicated the dehydration reaction consisted of two-stage or the reaction mechanism was different and depended on the temperature. Since the kinetic analysis of ozagrel hydrochloride monohydrate monitored the weight decrease, the reaction is the dehydration or related with the dehydration. In this temperature, the endothermic peak together with weight loss was observed in DSC experiment and the transition into an anhydrate A was observed in XRD-DSC experiment. For the close examination of the dehydration, the derivation of TGA curve was shown in Fig. 4-15.

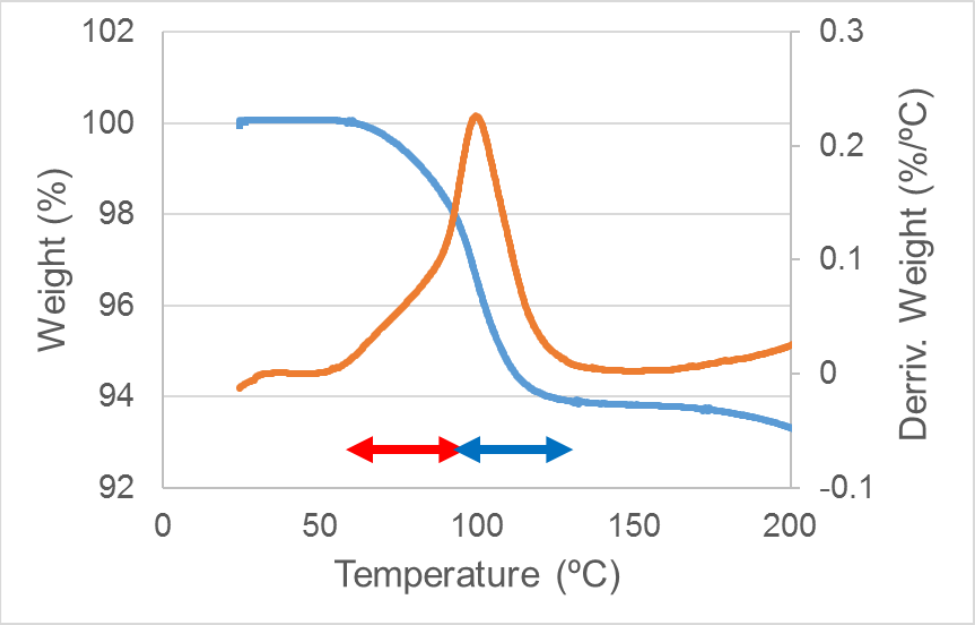

Fig. 4-15 Thermal behavior of ozagrel hydrochloride monohydrate. The TG curve (blue) was overwritten by the derivation of the TG (orange).

The derivation curve showed the different tendency depending on the temperature. Thermal analysis results indicated the dehydration mechanism of ozagrel hydrochloride monohydrate depended on temperature. In XRD study, a monohydrate transformed into an anhydrate A and next an anhydrate B. In this temperature region, only the transformation into an anhydrate A may occur. Two activation energies are considered to be represented for this transformation. Hypothesis is that the early part of reaction mainly occurs dehydration and that the late part of reaction mainly occurs crystal form transition. This hypothesis is supported by the reaction models introduced by the kinetic analysis. In the early part of reaction, D3 model was introduced. Rate determining step of D model is diffusion process. Diffusion process is considered to be related to movement of water molecule, so dehydration is dominant in the early part of reaction. On the other hand, R3 model was introduced in the late part of reaction. Rate determining step of R model is nucleation at boundary face. Nucleation of an anhydrate A could be dominant.

The crystal structure of an anhydrate A has not been obtained because the XRD pattern of an anhydrate A was not observed at SPring-8 experiment (in Fig. 4-9). In a capillary, we have a little experience which dehydration reaction delayed in cases of some hydrates. The capillary experiment may not strictly keep the high pressure environment, it is probable to trace the transition into an anhydrate form A at keeping the lower temperature (around 80ºC) for longer time during the dehydration reaction.

4.5. Short summary

In this chapter, the mechanism of dehydration of ozagrel hydrochloride monohydrate was elucidated. Crystal structure analysis of the monohydrate was succeeded using powder X-ray diffraction pattern. The monohydrate transformed into an anhydrate A, and an anhydrate A transformed into an anhydrate B with heating. Transformation reaction into an anhydrate A was evaluated with kinetic analysis. The mechanism of dehydration reaction depended on the temperature. At the lower temperature, the major driving force was the dehydration. On the other hand, at the higher temperature, the force was the crystal form change. These mechanisms were supported by the reaction models introduced by kinetic analysis. However, these mechanisms have not been supported by the crystal structure because crystal structure of an anhydrate A was not obtained. Further evaluation will be needed.

The information of crystal structure cannot be always obtained because of some reasons such as the difficulty of obtaining the single crystal, the instability of the target crystal phase, and so on. In such cases, the kinetic analysis is one of the powerful tools for the mechanism elucidation of reaction. This chapter results supported this suggestion and the utilization of the kinetic analysis. Although the kinetic analysis is useful, the mechanism elucidation with only the kinetic analysis is limited. We suggest the combination of crystal structure analysis and the kinetic analysis is the most powerful tools.

Chapter 5

Salt exchange of ondansetron

5.1. General introduction

In drug discovery, salt screening is one of the general tools for improving the physicochemical properties and obtaining the development solid form at pharmaceutical industry. It is possible for us to select the counter acids or bases as the pKa values were used as a reference and we can expect the improvement of solubility which is one of the significant issues regarding the physicochemical properties by the salt formation.

Although salt optimization is widely known in the pharmaceutical area, there are less reports about the rational design for that optimization and a lot of screening methods and conditions are empirically designed. In addition, in the early stage of drug discovery, there are a few limitations about the available drug amount and the trial period. For solving the problems, it takes about a decade to be developed the HTS salt screening system.

For the rational design, it is much necessary to store the knowledge about the structure changes by the salt changing and to progress the research which develops the relationship between the crystal structure and physicochemical properties. The crystal structures of new drug candidate are not published by the developers because of the intellectual asset. On the other hand, the research about the launched drugs is popular especially at the university, and there are a lot of papers which we can read.

In the previous chapter, the interesting dehydration reaction of ondansetron HCl dihydrate has been reported. In the drug discovery, salt optimization will be conducted and it is interesting for us to evaluate whether the rare dehydration phenomenon is succeeded to the different salts. In this chapter, the synthesis of other salts and evaluation of dehydration reaction will be elucidated. In particular, HBr salt and HI salt are synthesized and the isomorphism of crystal structures and dehydration phenomena will be evaluated.

5.2. Materials and Methods

5.2.1. Materials

Ondansetron hydrochloride dihydrate was purchased from Sigma Aldrich (St. Louis, MO, USA).

Solvents and HBr solution were purchased from Kanto Kagaku (Tokyo, Japan). HI solution was purchased from Wako Junyaku (Tokyo, Japan).

Characterization was performed using samples pulverized with an agate mortar.

5.2.2. Synthesis

Ondansetron HBr salt was synthesized described below; ondansetron HCl dihydrate was dissolved with methanol containing the equal molar of sodium hydroxide. Then, the equal molar of hydrobromide with methanol solution was added to that methanol solution including the ondansetron and the solvent was removed under dry N_2 gas. Acetone/water (9:1) was added after the drying and the sample was stirred for overnight. Obtained powder was filtered and recrystallized by ethanol/H_2O to obtain the bulk sample. In addition, single crystal was also obtained with another recrystallization condition. On the other hand, an ondansetron HBr anhydrate B was obtained by the slurry suspension with ethyl acetate or acetonitrile instead of acetone/water.

Ondansetron HI salt was synthesized described below; ondansetron HCl dihydrate was dissolved with methanol containing the equal molar of sodium hydroxide. Then, the equal molar of hydroiodide with methanol solution was added to that methanol solution including the ondansetron and the solvent was removed under dry N_2 gas. 2-propanol/water (1:1) was added and bulk samples were recrystallized. In addition, single crystal was also obtained with the recrystallization in 2-propanol/water (1:1). In addition, an ondansetron HI anhydrate B was obtained with Ethanol/water (9:1) instead of 2-propanol/water (1:1).

5.2.3. Heating

Samples were heated in a Fine Oven DF42 (Yamato Science).

5.2.4. Single crystal structure analysis

All measurements were made on a Rigaku XtaLAB P200 diffractometer with multi-layer mirror monochromated Cu-Ka radiation (l = 1.54184 Å) at 93 K and

operating in the f-w scan mode.

5.2.5. Crystal structure analysis with powder X-ray patterns

The crystal structures of both the hemihydrate and anhydrate were determined from the PXRD data measured at SPring-8 BL19B2. Crystal structure analysis was carried out using the Powder Solve module of Materials Studio (BIOVIA, Tokyo, Japan).

After selecting the peaks set, indexing was conducted in the X-CELL module [73] to introduce the unit cell and appropriate space group. The unit cell was refined by Pawley refinement and optimized.

The initial chemical structures of ondansetron and the water molecules were introduced using the Forcite module with COMPASS II[74] as a force field. The initial crystal structure was introduced by the POWDER SOLVE module[75] using the simulated-annealing approach and optimized by Rietveld refinement. Pareto optimization, a Rietveld refinement method that considers the energy of the structure calculated by a force field[76], was carried out at the final optimization step.

5.2.6. Thermal analysis: Differential scanning calorimetry (DSC)

Thermal analysis was performed using a TA Q2000 DSC instrument that included a refrigerated cooling system (TA Instruments, New Castle, DE, USA). Temperature calibration was carried out using the indium metal standard supplied with the instrument. Samples were weighed (about 3 mg) in aluminum pans and analyzed from 25 °C to 300 °C at heating rates of 10 °C/min using a similar empty pan as a reference. An inert atmosphere was maintained in the calorimeter by purging with nitrogen gas at a flow rate of 50 mL/min.

5.2.7. Thermal analysis: Thermogravimetric analysis (TGA)

TGA was performed using a TA Q500 TGA instrument (TA Instruments). Approximately 4 mg of sample was loaded into a platinum pan and heated to 300 °C at a rate of 10 °C/min. Measurements were carried out under nitrogen purge at a flow rate of 100 mL/min. Temperature calibration was carried out using standard nickel.

5.2.8. Powder X-ray diffraction (PXRD)

PXRD analysis was performed on a TTR II (Rigaku, Tokyo, Japan) and used Cu Kα radiation at 1.54184 Å at a voltage of 50 kV and current of 300 mA. Data were collected at a scan rate of 4 º/min over a 2θ range of 2.5 º to 40 º.

5.2.9. X-Ray differential scanning calorimetry (DSC)

Simultaneous measurement of powder X-ray diffraction data and DSC data was carried out on a SmartLab system (Rigaku) using Cu Kα radiation at 1.54184 Å at a voltage of 45 kV and current of 200 mA, with a DSC attachment and a D/Tex Ultra as a detector. Samples were weighed (1.5–2.5 mg) in aluminum pans and analyzed at a heating rate of 2 °C/min using a similar empty pan as a reference. X-ray diffraction data were collected at a scan rate of 20 °/min over a 2θ range of 10 ° to 25 °.

5.2.10. Water vapor sorption and desorption studies

Dynamic vapor sorption experiments were performed on VTI SGA 100 (VTI corporation, Hialeah, FL, USA). Samples (about 10 mg) were studied over a selected humidity range (absorption process; from 5% relative humidity (RH) to 95% RH and desorption process; from 95% RH to 5% RH) at 25 °C. For each humidity step, the equilibration was set to dm/dt 0.03 %/min on a 5-min time frame (maximum hold time 180 min).

5.2.11. Kinetics study

5.2.11.1 Isothermal methods.

For the kinetic analysis of dehydration reaction, a sample was heated at jump mode to arbitrary temperatures, and kept on each temperature by the end of the dehydration reaction with TGA (Q500). Measurement at each temperature was repeated in three times.

5.2.11.2 Calculation

See in chapter 3.

5.3. Results and Discussion

5.3.1. HBr salt of ondansetron (dihydrate)

The result of single crystal structure analysis is shown (in Fig. 5-1).

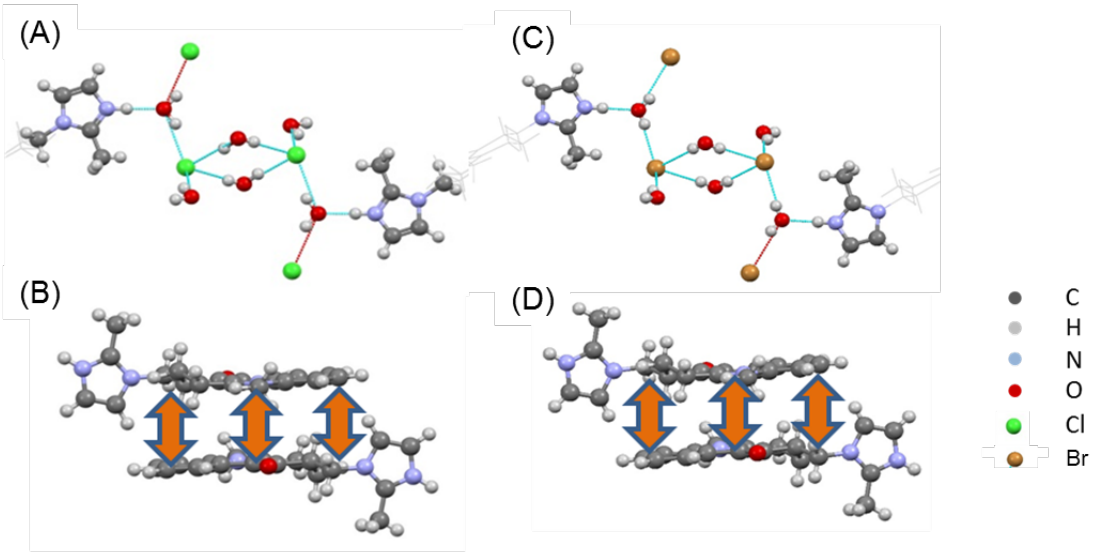

Fig. 5-1 Results of single crystal structure analysis, (A) hydrogen bonds network in HCl salt, (B) π-π stacking interaction in HCl salt, (C) hydrogen bonds network in HBr salt, (D) π-π stacking interaction in HBr salt

Table 5-1 Crystal graphic parameters of Ondansetron HCl salt and HBr salt

	HCl salt (YILGAB[69])	HBr salt
a (Å)	15.082(3)	15.19912(12)
b (Å)	9.741(3)	9.66181(8)
c (Å)	12.734(3)	12.69645(12)
β (°)	100.83(1)	100.6910(8)
Space group	$P2_1/c$	$P2_1/c$
V (Å ^{3})	1837.5(8)	1832.12(3)
Temp (K)	298	93

Ondansetron HBr was a dihydrate confirmed with single crystal structure analysis. Ondansetron HBr showed the similar pattern of ondansetron HCl. These crystals were isomorphic relationship considered by the unit cell parameters and hydrogen bond network. In particular, the water molecular directly contacted to the imidazole cation and a bromide anion was interacted to water molecules. Moreover, other water molecules existed between two bromide anions. The π-π stacking interaction and CH-π were observed between the tricyclic parts of ondansetron and were considered to stabilize the crystal structure.

Dehydration properties was studied with the crystalline powder of

ondansetron HBr. The results of thermal analysis were shown in Fig. 5-2 .

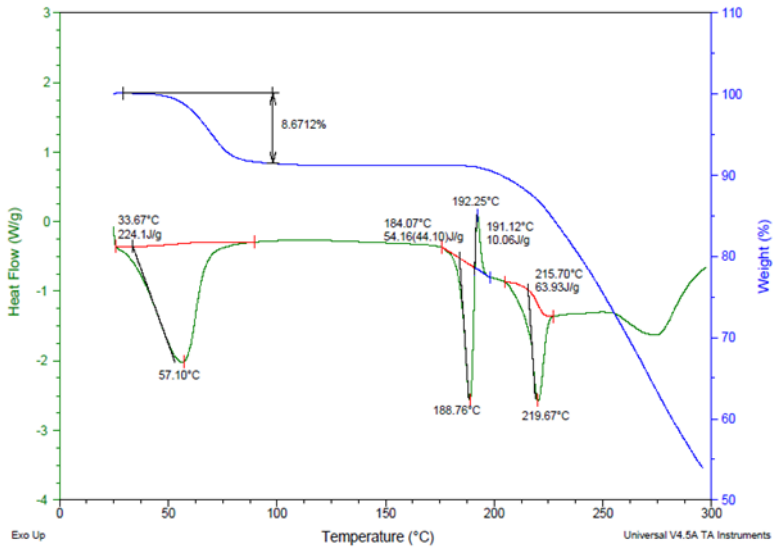

Fig. 5-2 Thermal behavior of ondansetron HBr dihydrate. Green line indicates the differential scanning calorimetry (DSC) curve, blue line indicates the thermogravimetric (TG) curve.

A broad endothermic peak associated with decreasing the weight was observed around room temperature and was considered to correspond to dehydration of water molecules. Since the amount of decreasing weight was equal to the theoretical value of the water of a dihydrate, dehydration reaction was completed and thermal behavior of an anhydrate should be observed at more than 100 °C. An endothermic peak and an exothermic peak were observed around 190 °C. These peaks indicated the melting temperature of ondansetron HBr anhydrate and crystallization of another form, respectively. Finally, an endothermic peak was observed around 220 °C. This peak indicated the melting temperature of another ondansetron HBr anhydrate.

The experiment of XRD-DSC was carried out to deeply understand the relationship of the thermal behavior and the crystal form transition.

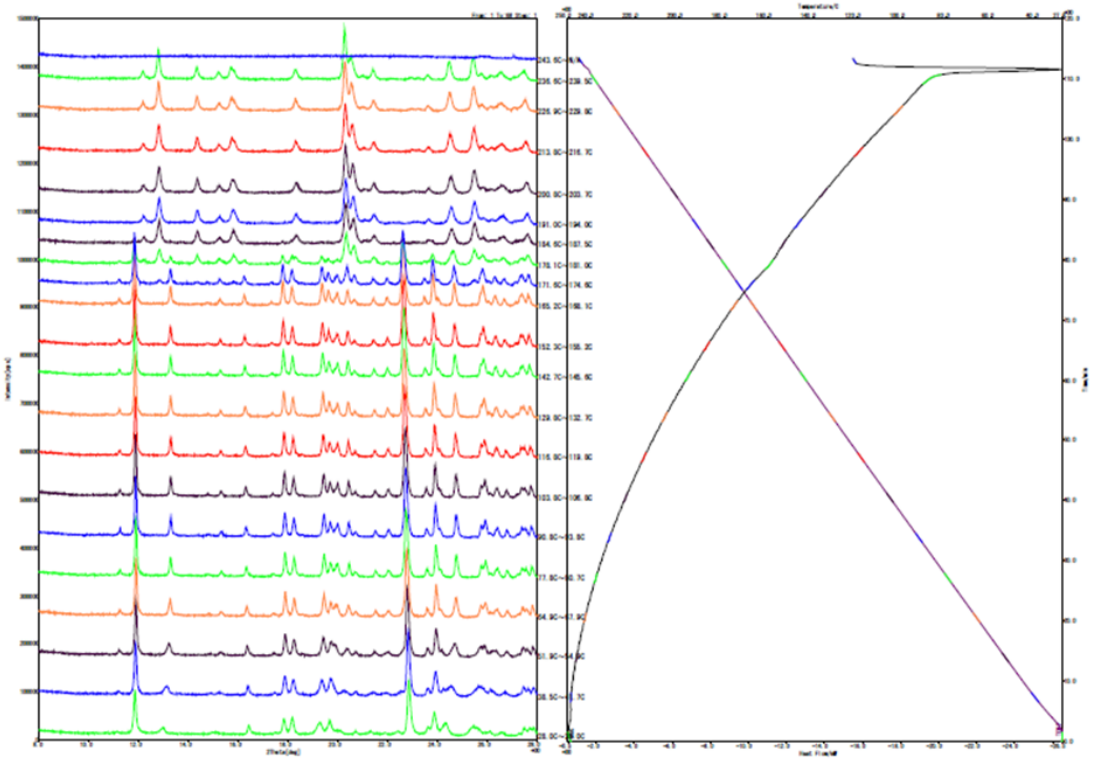

Fig. 5-3 X-ray diffraction scanning calorimetry results.

At the starting point of experiment which was carried out under the dry N_2 gas condition, transition to an anhydrate had already begun because XRD pattern was different from that of a dihydrate. In addition, transition to another crystal form occurred around 190 ºC. In summary, ondansetron HBr dihydrate transformed to an anhydrate A and did to another anhydrate B with heating.

Isolation of an anhydrate A was tested with heating. First, the dihydrate form was heated to 80 °C for 30 min to form the anhydrate A. The samples were then left at ambient conditions for varying amount of time, after which the PXRD patterns were measured.

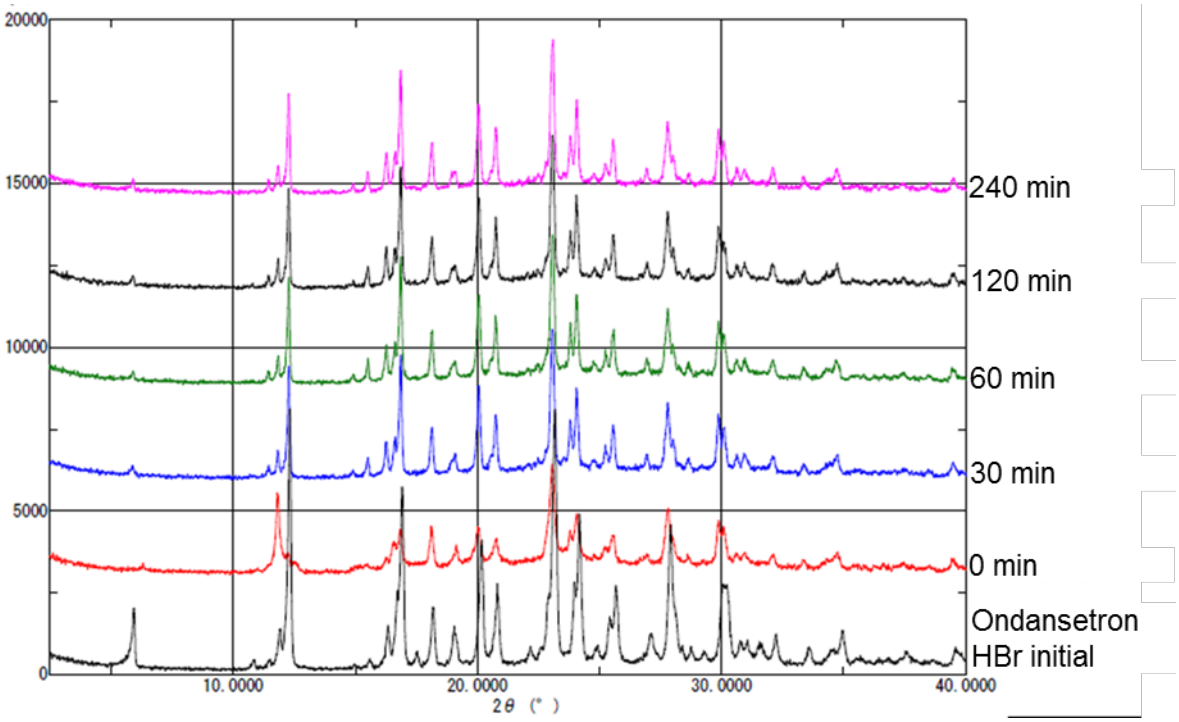

Fig. 5-4 Reversibility after heating confirmed with X-ray diffraction patterns.

As you can see in Fig. 5-4, although XRD pattern measured immediately after the heating was different from the initial pattern, the pattern went back to the initial one after the 30 minutes at room temperature. As a result, it was quite difficult to isolate an anhydrate A at room environment.

Dehydration tendency of ondansetron HBr dihydrate against the relative humidity was studied and the result was shown (Fig. 5-5).

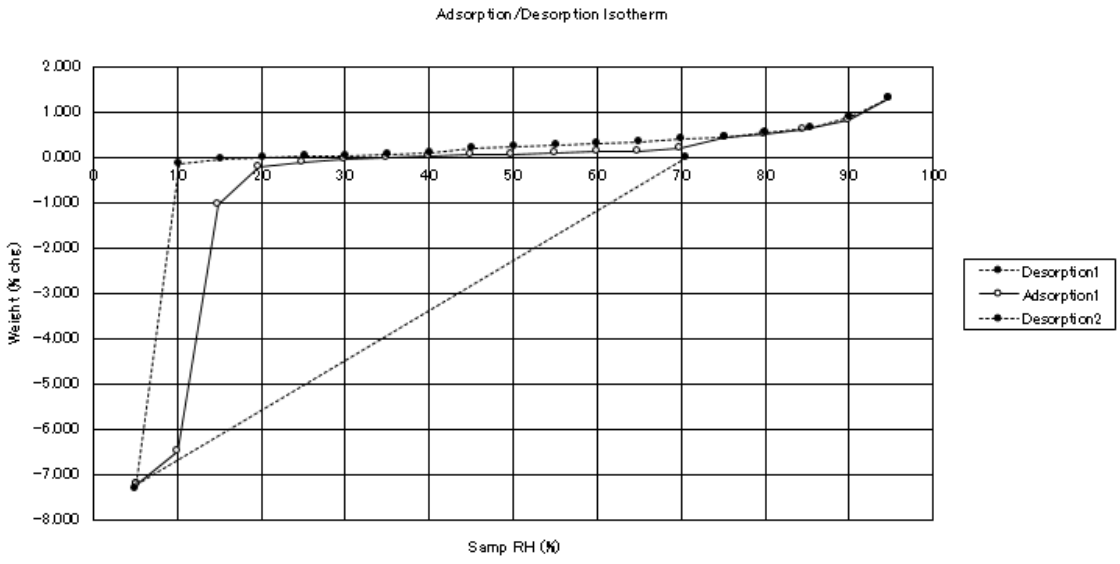

Fig. 5-5 Hygroscopicity of ondansetron hydrobromide dihydrate at 25 ºC.

In testing the weight change under from 5 to 95% RH, decrease of weight was observed around low relative humidity. In absorption process, going back to a dihydrate was observed and hydration was completed at the 20% RH. These hydroscopicity profile was not controversial that it was difficult to isolate an anhydrate at room environment.

Isomorphism was observed between ondansetron HBr dihydrate and HCl dihydrate, so HBr salt was expected to show the similar dehydration profile. In particular, it was evaluated whether an intermediate which was a hemihydrate at HCl salt was formed through the dehydration process or not. In using the thermal gravimetric assay (TGA), the existence of an intermediate was confirmed by monitoring the weight change with keeping the temperature at a few points (Fig. 5-6). The amount of weight change was equivalent for that of ondansetron HBr dihydrate (about 9%). Unexpectedly, a dihydrate of HBr salt directly transformed to an anhydrate without forming a hemihydrate as an intermediate which was formed in HCl salt in dehydrate process.

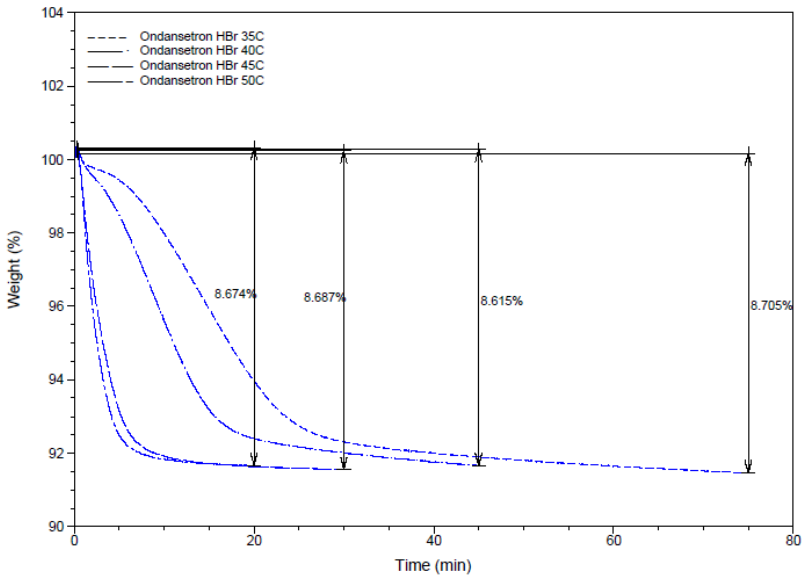

Fig. 5-6 Identification of the intermediate using a thermal gravimetry assay. Changes in weight (%) are shown from 35 ºC to 50 ºC. The amount of weight decreasing (about 9%) was equivalent to the amount of water of a dihydrate.

5.3.2. Ondansetron HBr anhydrate B

Subsequently, an anhydrate B was tried to be isolated. It was difficult to isolate the form B with heating around 200 ºC because the melting and degradation occurred and strict temperature control was considered to be needed. But, isolation was possible with slurry suspension of a dihydrate in ethyl acetate at 50 ºC. XRD pattern and thermal analysis curves were shown.

(A)

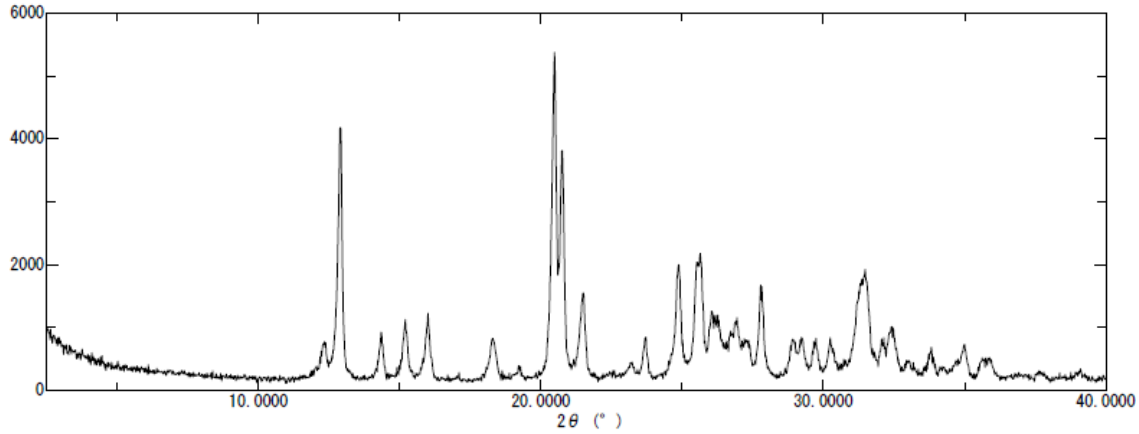

(B)

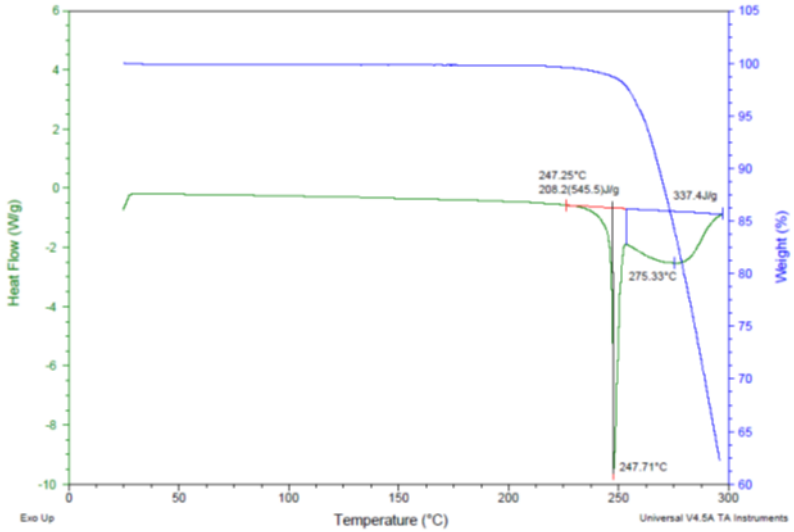

Fig. 5-7 The results of solid state analysis were shown, (A) XRPD pattern of ondansetron hydrobromide anhydrate, (B) thermal behavior of that anhydrate. Green line indicates the differential scanning calorimetry (DSC) curve, blue line indicates the thermogravimetric (TG) curve.

XRD pattern and melting temperature were similar with the previous figures (in Fig. 5-3 and 5-2, respectively), so it can be concluded that the isolated form was equivalent to the form appearing at high temperature (an anhydrate B).

For evaluating the physicochemical properties of an anhydrate B, the hygroscopicity was studied (Fig. 5-8).

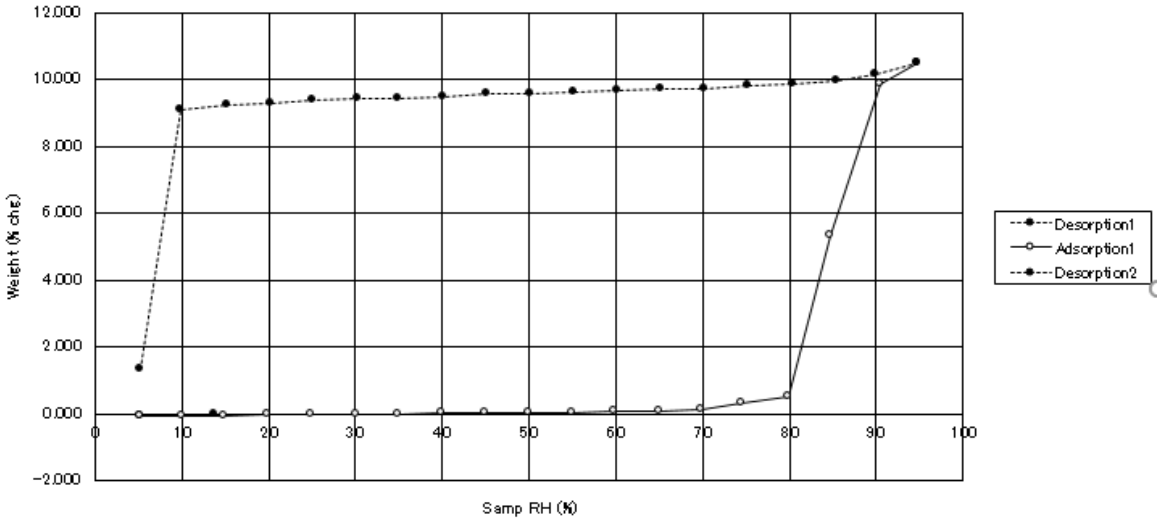

Fig. 5-8 Hygroscopicity of ondansetron HBr anhydrate B at 25 ºC.

In testing the weight change under from 5 to 95% RH, an anhydrate B absorbed the water at around 85% RH and the increase of weight which was equal to the theoretical value of a dihydrate was observed. Increased weight was kept by around 10% RH under the desorption process, and decrease of weight was observed at around 5% RH. This dehydration profile was the same manner of a dihydrate, so an anhydrate B transformed to a dihydrate at the high relative humidity.

5.3.3. Unstable an anhydrate A

To evaluate the mechanism of dehydration of ondansetron HBr dihydrate and the difference from ondansetron HCl dihydrate, crystal structure analysis with powder XRD patterns for an anhydrate A and B was carried out. For the crystal structure analysis with PXRD, experiment of XRD with heating was conducted at SPring-8 BL19B2. Results were shown in Fig. 5-9 and crystal structure analysis was executed by using the pattern at 140 ºC or 25 ºC cooling, for an anhydrate A and B, respectively.

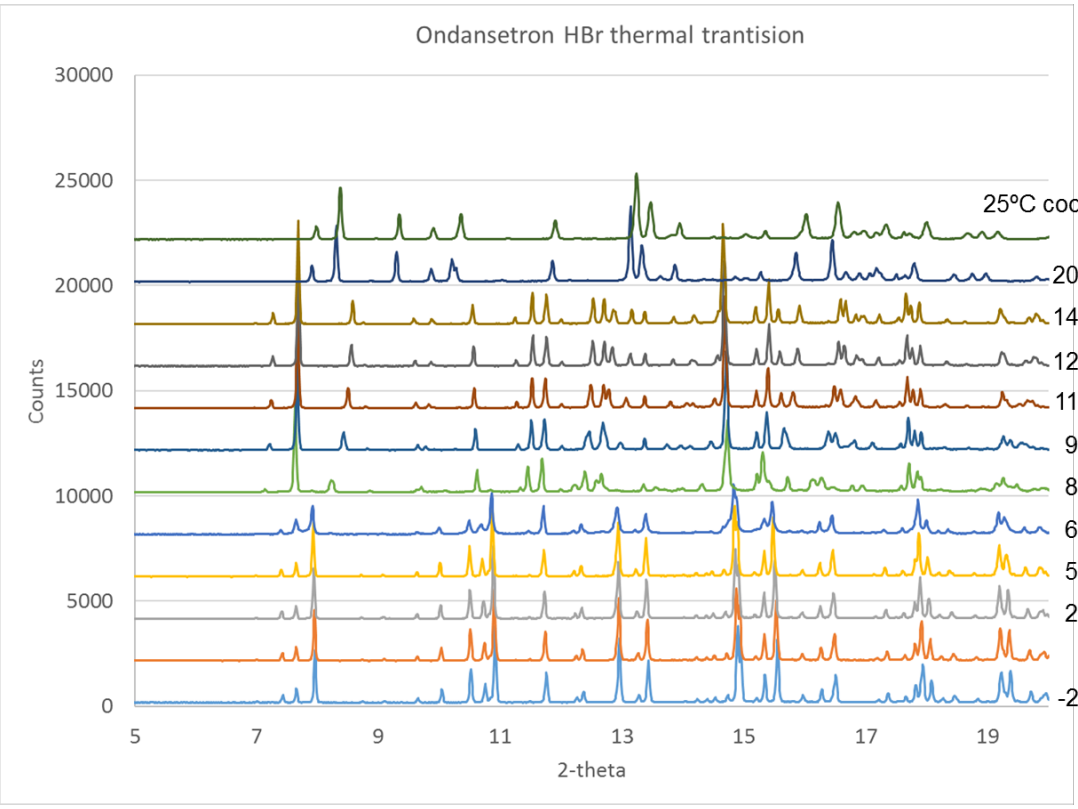

Fig. 5-9 XRD with heating measurement at SPring-8 BL19B2

As a result, crystal structures of two anhydrates were obtained. The structures of an anhydrate A and B were shown in Fig. 5-10.

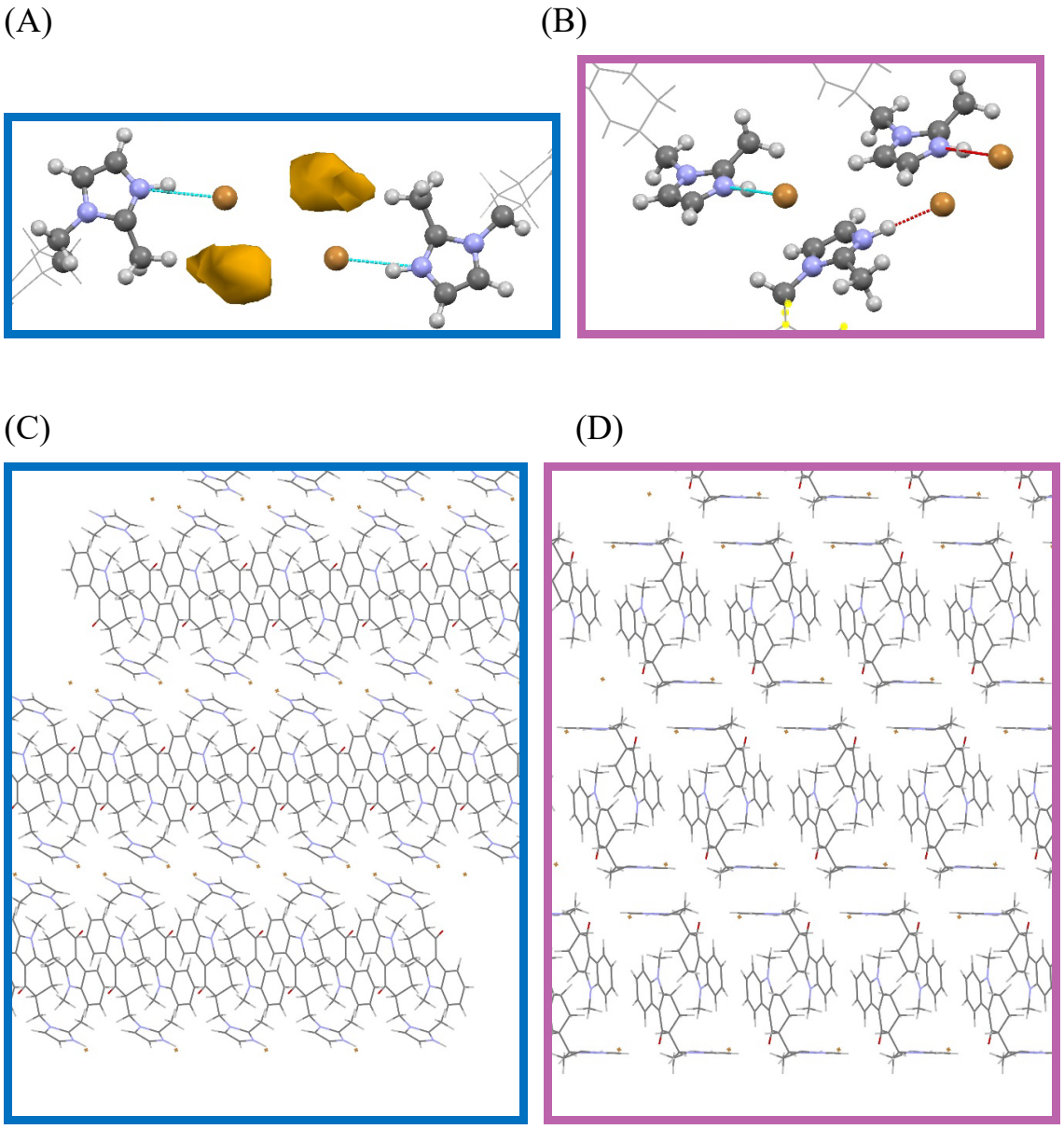

Fig. 5-10 Comparison of anhydrate crystal. Hydrogen bonds network, (A) an anhydrate A, (B) an anhydrate B. B axis projected view, (C) an anhydrate A (D) an anhydrate B.

Table 5-2 Comparison of the crystallographic parameters of ondansetron HBr salts

	Dihydrate	**Anhydrate A**	**Anhydrate B**
temp. (ºC)	-180	140	25
space group	$P2_1/c$	$P2_1/c$	$P2_1/c$
a (Å)	15.19912(12)	14.7213(23)	13.1939(22)
b (Å)	9.66181(8)	9.8124(16)	8.7052(14)
c (Å)	12.69645(12)	13.1836(21)	15.1708(26)
α (º)	90.0000	90.0000	90.0000
β (º)	100.6910(8)	114.1160(8)	104.1480(3)
γ (º)	90.0000	90.0000	90.0000
V (Å^3)	1832.12(3)	1738.17(5)	1689.6(5)
Sample	single crystal	powder	Powder

In crystal structure of an anhydrate A, the tricyclic part of ondansetron was placed anti parallel. This motif was observed in dihydrate. In a dihydrate, an imidazole cation was not directly interacted with a bromide anion and the water molecule was intercepted. On the other hand, in an anhydrate A, a cation was directly interacted with an anion because of the absence of the water molecule. The space made by the dehydration was filled by a translation of imidazole ring, and new stacking interaction between the imidazole rings was formed. These changes of interactions were similar with in the case of dehydration of HCl salt.

In an anhydrate B, the dimer structure formed by the tricyclic part was maintained, and stacking interaction between the imidazole rings was observed. The direct interaction between an imidazole cation and a bromide anion was also observed. The void structure was not observed, so an anhydrate B was considered to be relatively stable at room environment. Because an anhydrate B also transformed to a dihydrate at higher humidity condition, a dihydrate was the more stable form in case of the high water activity.

5.3.4. Kinetic analysis of ondansetron HBr dihydrate

Isothermal tracing of the weight decreasing measured with TGA was conducted for the estimation of the activation energy (Ea). In particular, the weight decreasing was observed in jumping the temperature to 35, 40, 45, and 50 ºC from room temperature and being kept at each temperature. In Fig. 5-11, the relationship was shown between the reaction ratio (α) and temperatures. Temperature dependency was clearly observed.

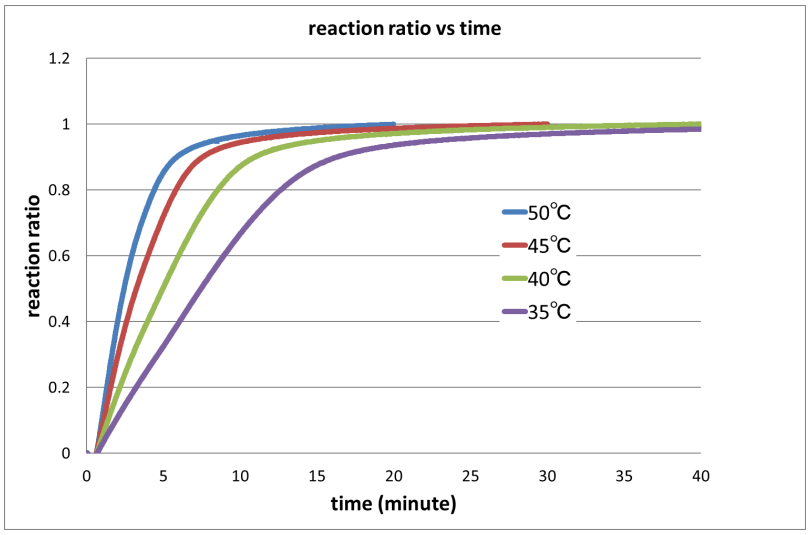

Fig. 5-11 The reaction ratio at each temperature of ondansetron HBr dihydrate.

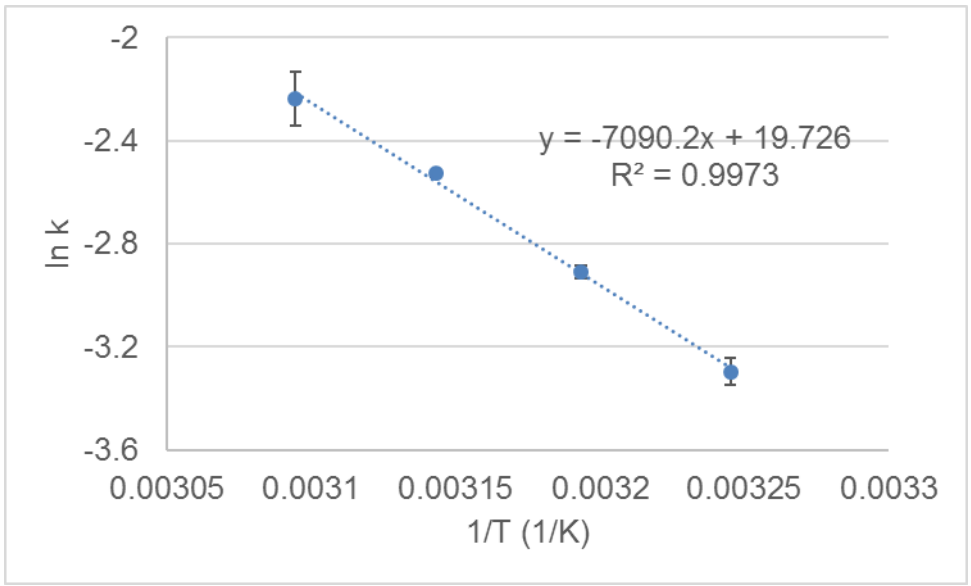

Fig. 5-12 Arrhenius plot of dehydration reaction of ondansetron HBr dihydrate

Ea was estimated as 59 ± 2 kJ/mol. This value was quite smaller than that of

ondansetron HCl dihydrate. At the same condition, the dehydration of HBr salt will easily occur in comparison with that of HCl salt. Actually, in XRD-DSC study (Fig. 5-3), transition into an anhydrate A of HBr salt has already been observed at the start point of experiment. The value of Ea of HBr salt can explain the phenomena of transition.

5.3.5. Why did not exist the intermediate of ondansetron HBr through the dehydration?

The intermediate was not observed through the dehydration of ondansetron HBr dihydrate as mentioned before. The relationship between ondansetron HCl and HBr dihydrate was considered to be isomorphism. To consider the reason, some parameters were shown in Table 5-3.

Table 5-3 Comparison of parameters of HCl and HBr salt

	HCl salt	HBr salt
distance between anions (Å)	4.755	4.767
ion radius (Å)	1.81	1.96
void volume ($Å^3$)	6.1	1.3
unit cell volume ($Å^3$)	1751	1735

Ion radius of a bromide anion is bigger than that of a chloride anion, so there is a good reason that the distance between two bromide anions was bigger. The distance should get much longer in making consideration with the difference of ion radius, so the distance between bromide anions was relatively near. As a result, void volume was quite different and unit cell volume of HBr salt was smaller than that of HCl salt. Since the void space was occupied by the water molecule in a hemihydrate, HBr salt could not maintain water molecule. This is the root cause of no intermediate of HBr salt considered with crystal structure analysis.

In Fig. 5-13, the schematic representation of energy diagram was shown.

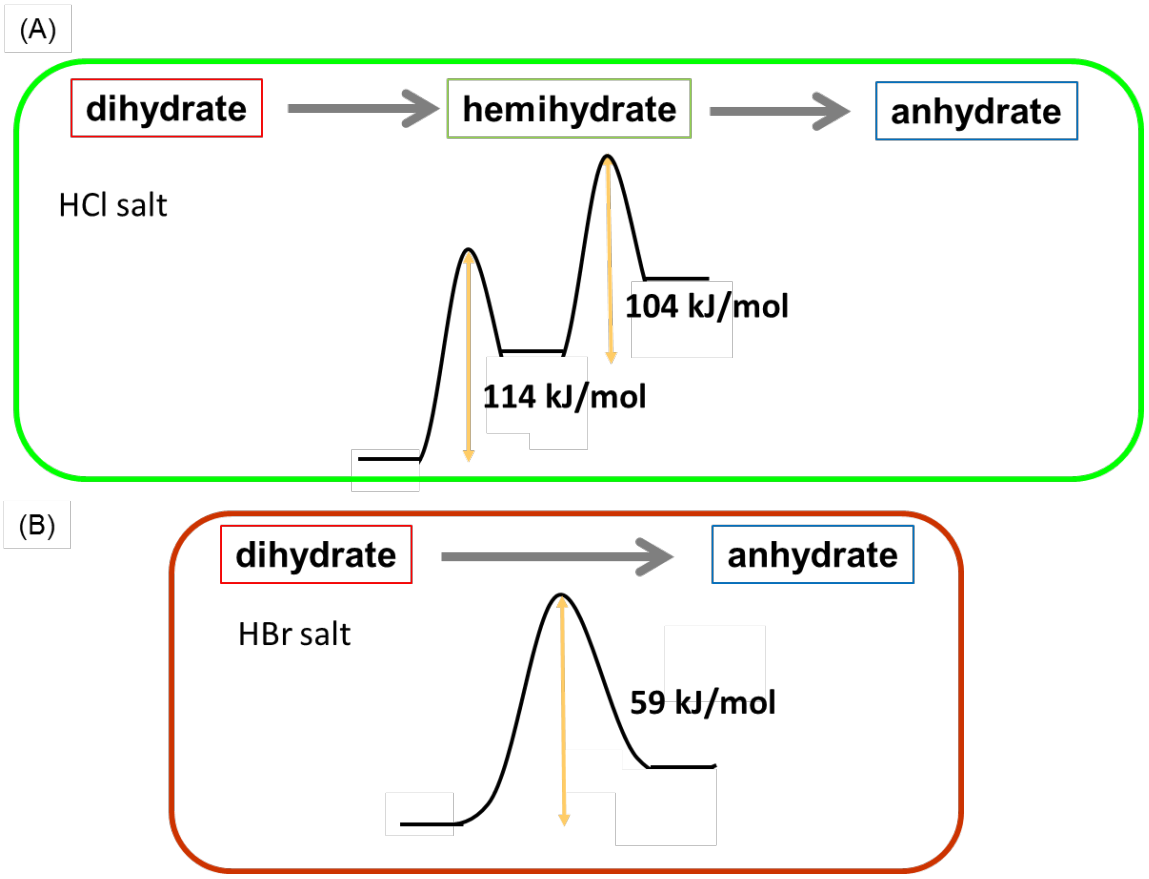

Fig. 5-13 Schematic representation of energy diagram. (A) two-stage dehydration of ondansetron HCl dihydrate, (B) single stage dehydration of ondansetron HBr dihydrate

The activation energies of HCl and HBr salt were quite different. An anhydrate of ondansetron HBr salt should be relatively stable considered by the schematic representation compared with an anhydrate and even a hemihydrate of HCl salt. This consideration is supported by the crystal structure. Packing efficiency of HBr salt may be better than that of HCl salt of an anhydrate because of the void structure and unit cell volume. The high energy barrier at which a dihydrate translates into an anhydrate of HCl salt is the root cause of the existence of intermediate.

5.4. HI salt of ondansetron

5.4.1. ondansetron HI dihydrate

In this section, results of hydroiodide salt were introduced.

The crystal structure of a dihydrate was shown in Fig. 5-14.

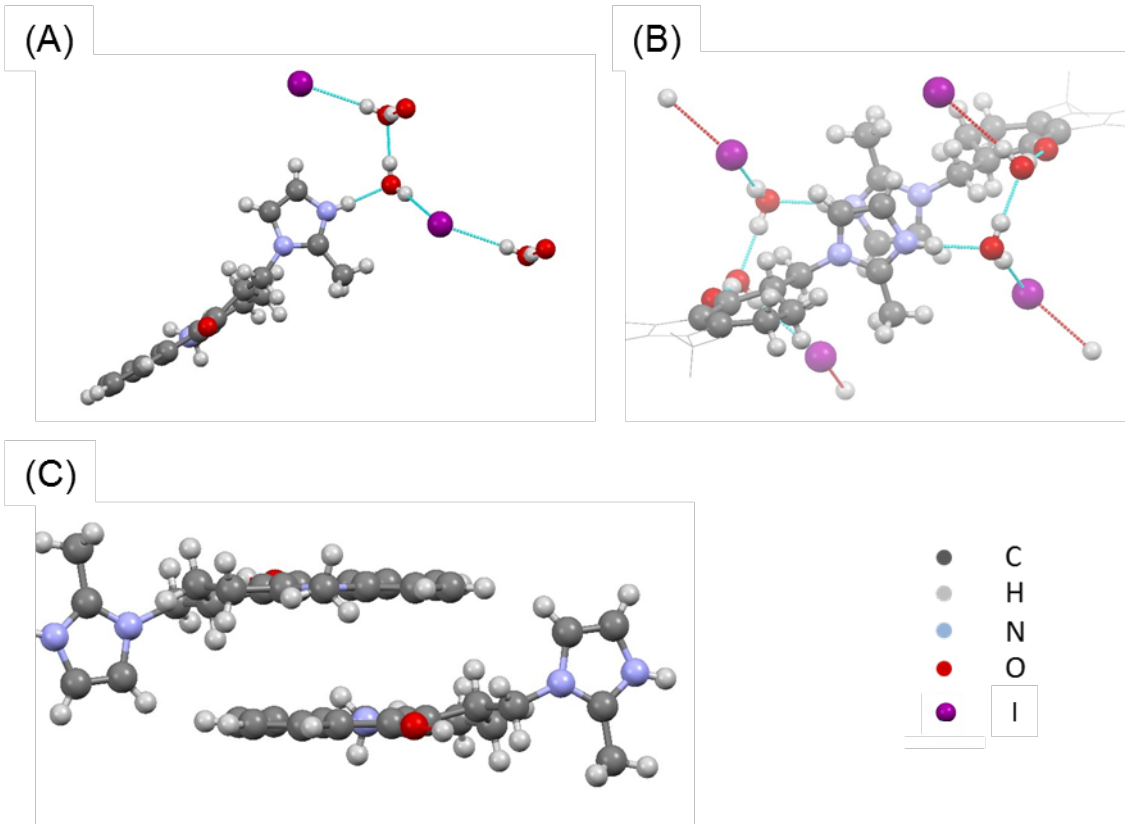

Fig. 5-14 Crystal structure of ondansetron HI dihydrate. (A) hydrogen bonds network, (B), overlapping of imidazole rings (C) tricyclic part of ondansetron

In a dihydrate structure, an imidazole cation was interacted with a water molecule and an iodide anion was not directly interacted with an imidazole cation. The diamond shape hydrogen bonds network which was formed in the crystal structures of HCl and HBr salts was not observed. A hydrogen bond was formed between the water molecules. The stacking interaction between the imidazole rings was observed in HI salt. On the other hand, the stacking interaction and CH-π interaction between the tricyclic parts were maintained.

Table 5-4 Crystallographic parameters of HCl, HBr and HI dihydrate

	HCl salt (YILGAB[69])	HI salt	HBr salt
a (Å)	15.082(3)	7.69854(14)	15.19912(12)
b (Å)	9.741(3)	8.42520(15)	9.66181(8)
c (Å)	12.734(3)	15.6102(3)	12.69645(12)
α (º)	90	90.2705(14)	90
β (º)	100.83(1)	96.0841(15)	100.6910(8)
γ (º)	90	107.9273(17)	90
Space group	$P2_1/c$	*P*-1	$P2_1/c$
Volume (Å^3)	1837.48(8)	957.17(3)	1832.12(3)
Temp (K)	298	100	100

In comparison with unit cell parameters, although the isomorphism relationship between the HCl salt and HBr salt was observed, HI salt was not isomorphism since the unit cell of HI salt was quite different such that the space group was *P*-1.

5.4.2. solid state evaluation of ondansetron HI dihydrate

Results of powder X-ray patterns and thermal analysis were shown in Fig. 5-15 to study the physicochemical properties of dihydrate.

(A)

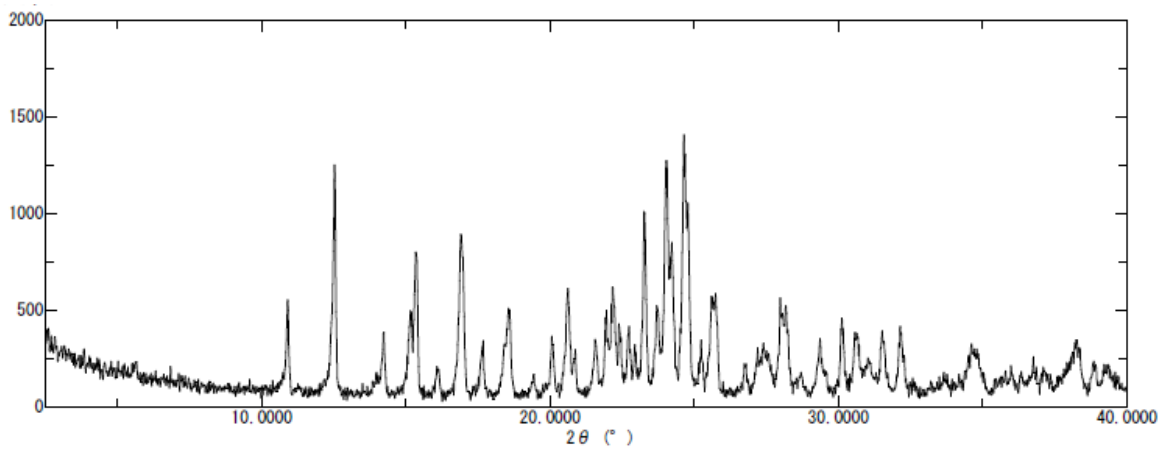

(B)

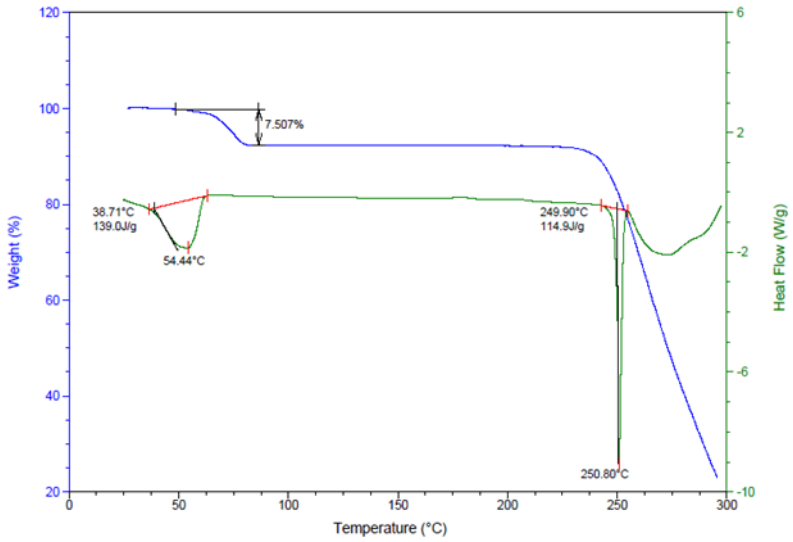

Fig. 5-15 Solid state elucidation of ondansetron HI dihydrate, (A) powder X-ray pattern and (B) thermal behavior. Green line indicates the differential scanning calorimetry (DSC) curve, blue line indicates the thermogravimetric (TG) curve.

The endothermic peak with the decrease of weight was observed at around room temperature. The amount of decrease of weight was equal to the theoretical value of ondansetron HI dihydrate. This result indicated that dehydration of dihydrate occurred at relatively low temperature. The endothermic peak around 250 ºC indicated the melting temperature of an anhydrate appeared after the dehydration.

For the isolation of an anhydrate A, time course data of XRD patterns was obtained after the heating a dihydrate of HI salt at 80 ºC.

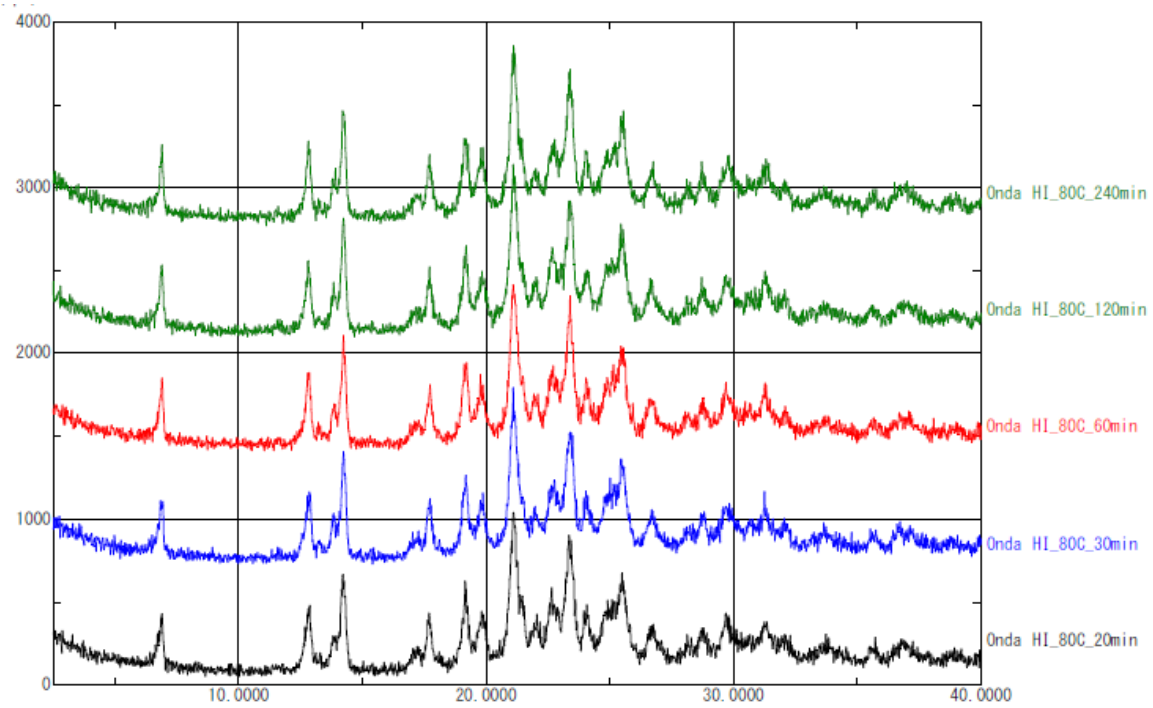

Fig. 5-16 Reversibility after heating confirmed with X-ray diffraction patterns.

As a result, an anhydrate A was kept for 4 hours after heating. The appearance of test materials was slightly changed from white to pale brownish yellow by the heating.

In the next step, the hygroscopicity of a dihydrate was evaluated. Result was shown in Fig. 5-17.

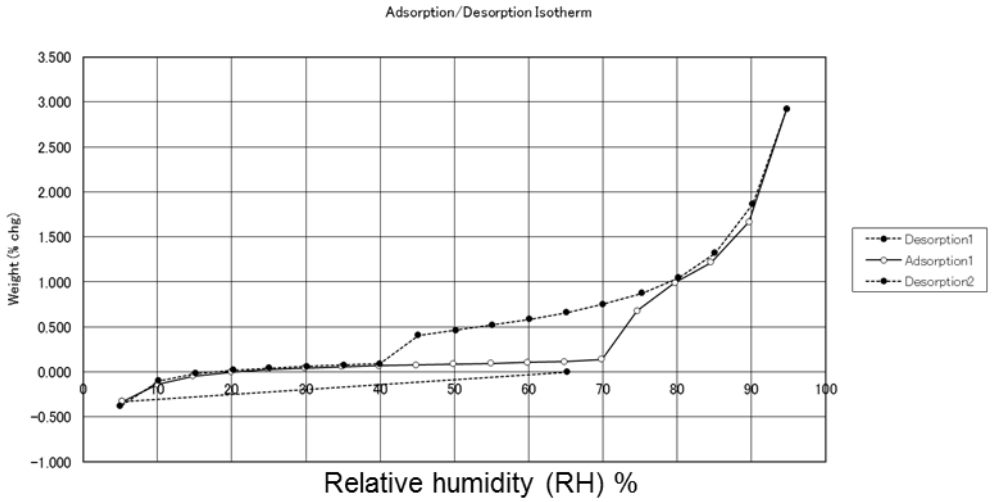

Fig. 5-17 Hygroscopicity of ondansetron hydroiodide dihydrate at 25ºC.

The dihydrate was absorbed at the high relative humidity condition, but the decrease of weight was not observed at low humidity. The dihydrate was stable at the lower relative humidity.

In the next step, the hygroscopicity of an anhydrate A was evaluated. Result was shown.

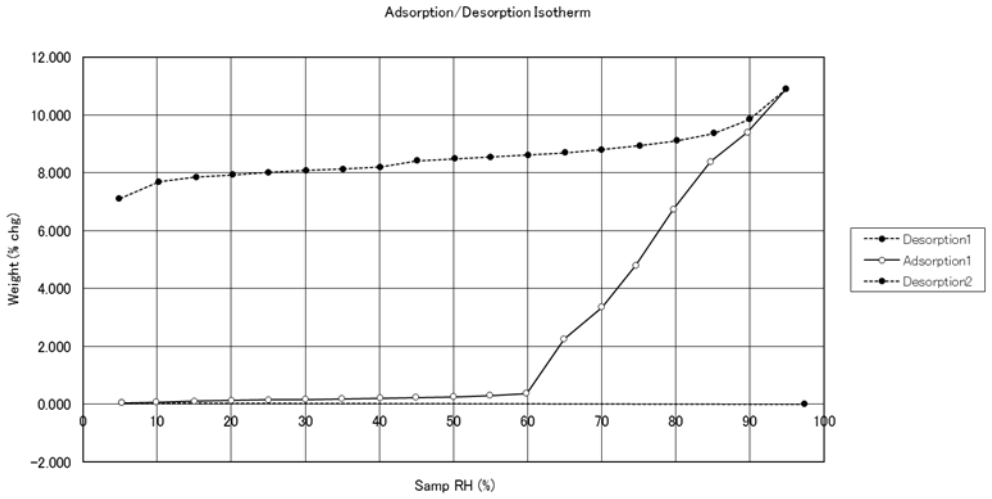

Fig. 5-18 Hygroscopicity of ondansetron hydroiodide anhydrate A at 25 ºC.

An anhydrate A absorbed at around 75% RH, and the increase of weight was almost equal to the amount of two water molecules. The increased weight was not decreased at low RH. By confirming the crystal form with PXRD, an anhydrate transformed back to a dihydrate. In summary, an anhydrate A obtained with heating a dihydrate transformed back to the initial dihydrate at the high

humidity condition.

For deeper understanding the crystal transition profile of a dihydrate with heating, XRD-with heating measurements were carried out. Results were shown below.

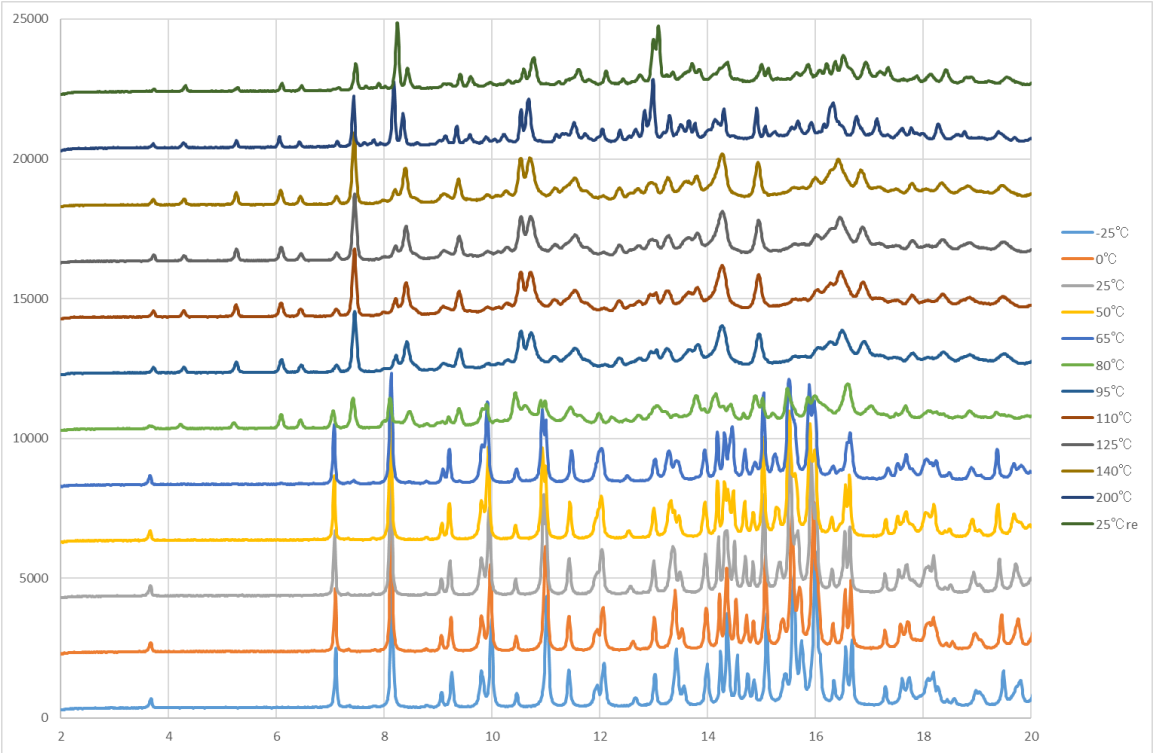

Fig. 5-19 XRD with heating measurement at SPring-8 BL19B2

XRD with heating was carried out at SPring-8 BL19B2. Although the crystal form transition was observed with heating, XRD pattern of an anhydrate A was unclear and it was difficult to solve the crystal structure with PXRD.

5.4.3. Ondansetron HI anhydrate B

The crystal structure of an anhydrate was shown in Fig. 5-20.

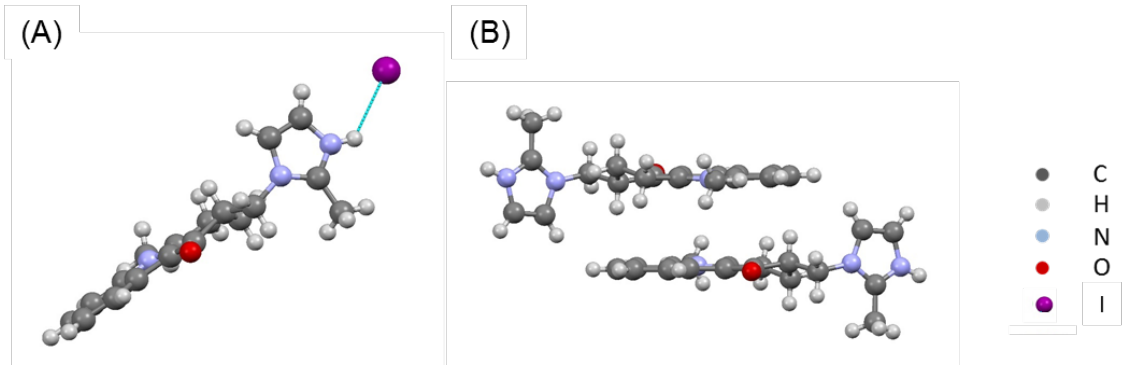

Fig. 5-20 Crystal structure of ondansetron HI anhydrate B. (A) hydrogen bonds network, (B) π-π stacking interaction.

In an anhydrate B structure, an ionic bond was formed between an imidazole cation and an iodide anion. The stacking interaction which was observed in all of crystal phase of ondansetron was also maintained in an anhydrate. The space group was $P2_1/c$.

The result of powder X-ray pattern and thermal analyses were shown to study the solid state of an isolated anhydrate B.

(A)

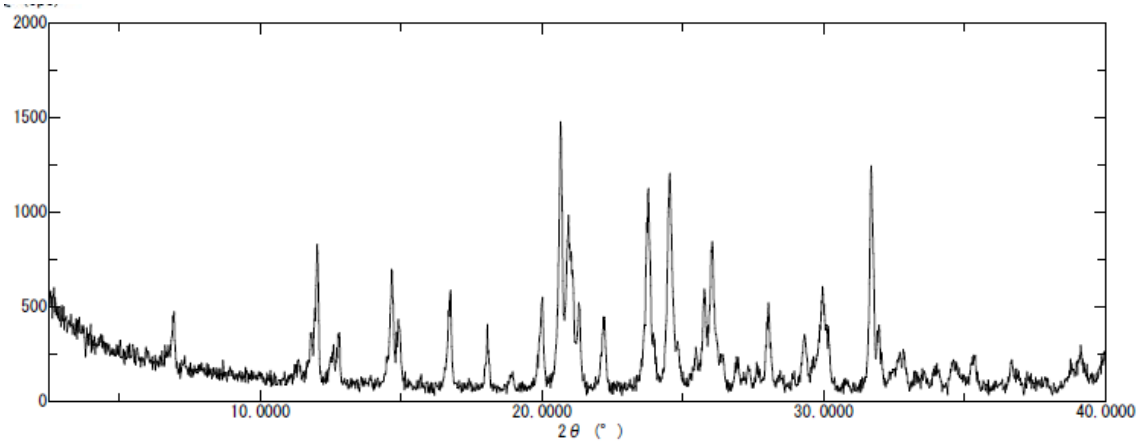

(B)

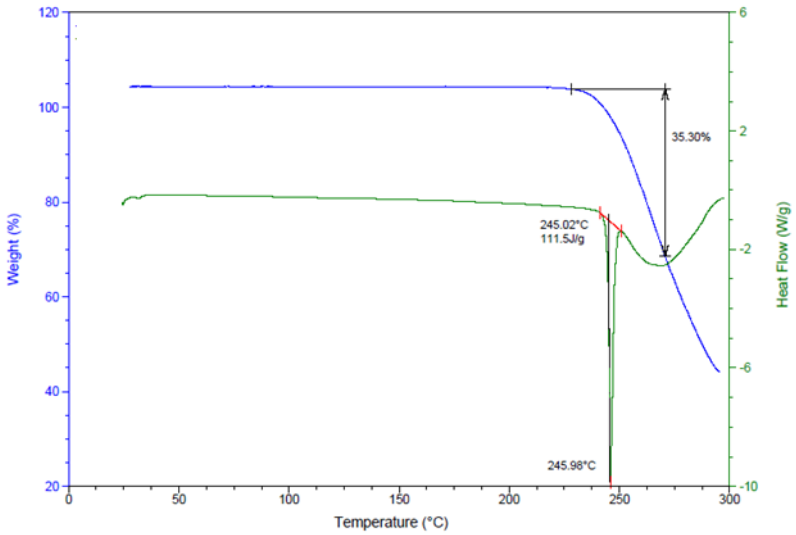

Fig. 5-21 Solid state elucidation of ondansetron HI anhydrate B, (A) powder X-ray pattern and (B) thermal behavior. Green line indicates the differential scanning calorimetry (DSC) curve, blue line indicates the thermogravimetric (TG) curve.

XRD pattern was equivalent to the pattern calculated by the crystal structure. An endothermic peak was observed around 245 ºC, and this peak corresponded to the melting temperature of an anhydrate B. In comparison with the result of thermal analyses, the temperature of endothermic peaks of an anhydrate A and B was slightly different, so anhydrate of HI salt may show the crystal polymorphs. Melting temperature of an anhydrate A (about 250 ºC) was slightly higher than that of B (about 245 ºC)

5.5. Short summary

Synthesis of ondansetron HBr salt and HI salt was succeeded. The landscape of dehydration of ondansetron salts were shown in Fig. 5-22.

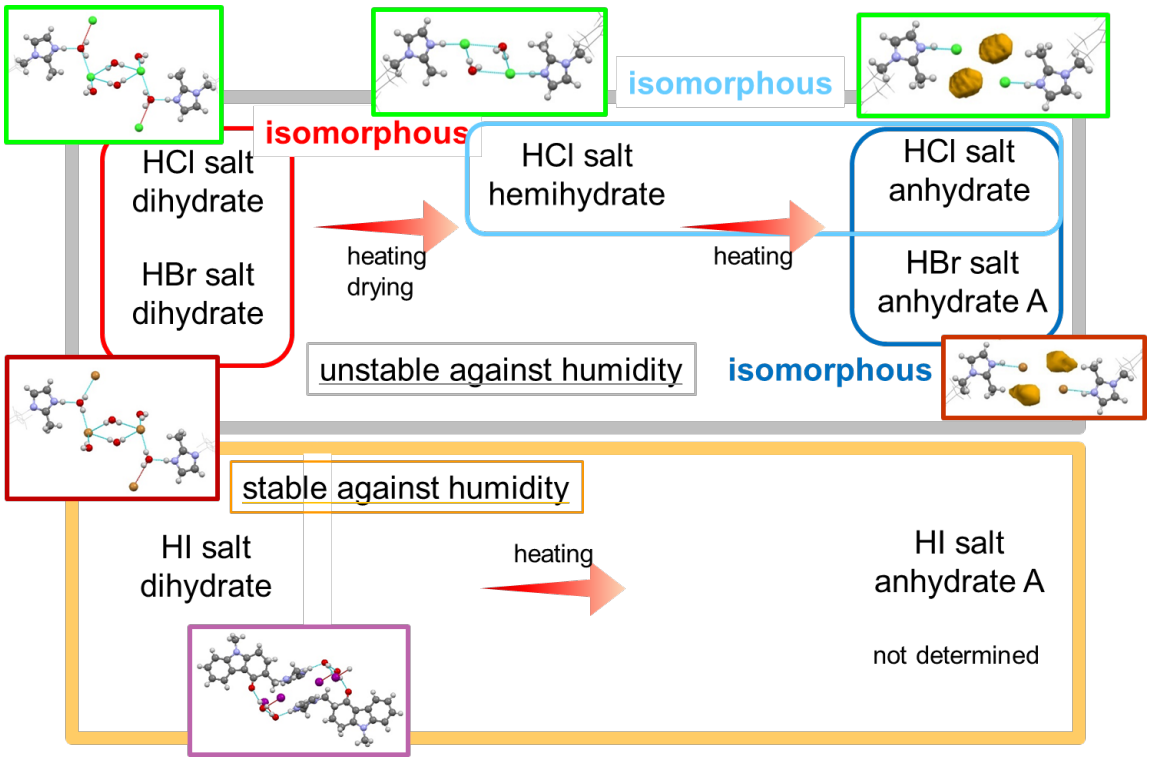

Fig. 5-22 The landscape of dehydration tendency of ondansetron salts

Ondansetron HCl, HBr and HI salts formed the dihydrates. The relationship between ondansetron HCl and HBr dihydrate was isomorphous, but ondansetron HI dihydrate showed the different structure. Ondansetron HBr did not show the two-stage dehydration observed in the reaction of ondansetron HCl dihydrate despite the crystal structure of the dihydrate was isomorphic. Isomorphic polymorphs do not always show the same physicochemical properties. Ondansetron HI salt showed the stability against humidity, the dihydrate was considered to be more stable than those of HCl and HBr salt. Halogen anions would be involved in forming hydrogen bonds with water molecules because of their hydrophilic properties. Exchange of halogen anion contributed to and was effective for the improvement of hygroscopicity.

The anhydrates which were stable at room environment were observed on both ondansetron HBr (form B) and HI salt (form A and B) although an anhydrate of HCl salt was unstable. Unfortunately, both anhydrates were unstable at the high humidity condition, so it is difficult to select their anhydrates as development forms. Crystal structures of both anhydrates were quite different from that of an anhydrate of HCl salt which was unstable at room

environment and was difficult to isolate. These results also indicated that exchange of halogen anion contributed to the changing of the crystal structure. Since it is difficult to predict how crystal structure will be formed and how properties will be observed, a lot of data will be acquired for the rational design of salt optimization.

Chapter 6
Conclusions

The importance of physicochemical properties for drug discovery is well known, and a lot of studies have been conducted in early drug discovery stage. Since the solid state of API represents the physicochemical properties, the changing of the solid state should be carefully handled despite the changing is expected or unexpected. In case of hydrates, the unexpected form change in the manufacture process and under the storage condition was sometimes observed, so the elucidation of dehydration mechanism using the crystal structure is carried out for understanding the solid state of hydrates. In this research, precise elucidation the dehydration mechanism was conducted. The purpose is to prove that the combination of crystal structure analysis and kinetic analysis is effective for understanding the dehydration mechanism by using ondansetron and ozagrel as model compounds.

In chapter 2, ondansetron hydrochloride dihydrate was selected as one of the model compounds for elucidating the dehydration mechanism and evaluating the relationship of between the crystal structure and physicochemical properties. Ondansetron hydcochloride dihydrate transformed into an anhydrate under heating condition. Interestingly, that dihydrate transformed into a hemihydrate under heating conditions as an intermediate before the transformation into an anhydrate. Both the hemihydrate and the anhydrate were unstable at room environment and these forms immediately went back to the initial dihydrate. Crystal structure analysis for two unstable forms succeeded with powder X-ray patterns. Changing of the hydrogen bonds network was observed thought these transformations although the overall structures were similar. The void structure was observed in an anhydrate, so this void structure was considered to be accountable for the root cause of the instability of an anhydrate at room conditions.

In chapter 3, kinetic analysis was carried out about the dehydration reactions of ondansetron HCl dihydrate and consideration of mechanism was discussed. Two kinds of analyses which were the isothermal method and the isoreaction ratio method (Ozawa method) were conducted for the dehydration reaction of ondansetron hydrochloride dihydrate. Both methods estimated the activation energy and these values for the first dehydration reaction (Ea^{1st}) were almost equivalent. Generally speaking, large variability was sometimes observed at the solid state reaction. From the view point of variability, it is important that the

different methods gave us the equivalent values of Ea. Ea values of first dehydration and second dehydration reaction were almost the same, and Ea^{1st} was slightly larger than Ea^{2nd}. The order of the number of cleaved hydrogen bonds and Ea was not controversial, and it was possible to qualitatively explain in comparison with the crystal structures (Fig. 3-6). The Ea^{rev} was calculated as 61 ± 7 kJ/mol and was approximately half of the value of forward reaction (Ea^{1st}: 114 ± 7 kJ/mol). This result supported that a dihydrate is more stable than a hemihydrate at a normal environment.

In chapter 4, the mechanism of dehydration of ozagrel hydrochloride monohydrate was elucidated. Crystal structure analysis of that monohydrate using powder X-ray diffraction was suceeded. The monohydrate transformed into an anhydrate A, and an anhydrate A transformed into an anhydrate B. Transformation reaction into an anhydrate A was evaluated with kinetic analysis, the mechanism of dehydration reaction depended on the temperature. At the lower temperature, the dehydration was dominant. On the other hand, at the higher temperature, the crystal form changing was dominant. These mechanisms have not been supported by the crystal structure because crystal structure of an anhydrate A has not been obtained, yet. Further evaluation will be needed.

Salt exchange is useful and powerful method for controlling the physicochemical properties of APIs. In chapter 5, it was examined that salt exchange affected the forming the hydrate form and physicochemical properties such as hygroscopicity, dehydration mechanism, the activation energy. Ondansetron HCl was used as a model compound. Ondansetron HCl, HBr and HI salts could be synthesized and formed the dihydrates. The relationship between ondansetron HCl and HBr dihydrate was isomorphous, but ondansetron HI dihydrate showed the different structure. Ondansetron HBr did not show the two-stage dehydration observed in the reaction of ondansetron HCl dihydrate despite the crystal structure of the dihydrate was isomorphic. Isomorphic polymorphs do not always show the same physicochemical properties. Ondansetron HI salt showed the stability against humidity, therefore, the dihydrate was considered to be more stable than those of HCl and HBr salt. Halogen anions would be involved in forming hydrogen bonds with water molecules because of their hydrophilic properties. Exchange of halogen anion contributed to and was effective for the improvement of hygroscopicity. The anhydrates which were stable at room environment were observed on both ondansetron HBr and HI salt although an anhydrate of HCl salt was unstable. Crystal structures of both anhydrates were quite different from that of an anhydrate of HCl salt which was unstable at room environment and was difficult to isolate. These results also indicated that exchange of halogen anion contributed to the changing of the crystal structure. Since it is difficult to predict how crystal structure will be formed and how properties will be observed, a lot of data will be acquired for the rational design of salt optimization.

In summary, I proved that the combined usage of kinetic analysis and crystal structure is powerful tool for the mechanistic consideration of dehydration using ondansetron and ozagrel as model compounds. Deep understanding for the dehydration mechanism is expected to adapt the rational design of salt optimization and accelerate drug discovery. Drug discovery becomes more difficult, so precious and promising candidates have to be developed in a careful manner. I believe that deep understanding for the solid state and transition mechanism will help us increasing the probability of drug discovery.

Chapter 7

Reference

(1) Scannell, J. W.; Blanckley, A.; Boldon, H.; Warrington, B., Diagnosing the decline in pharmaceutical R&D efficiency. *Nature reviews. Drug discovery* **2012,** 11, (3), 191-200.
(2) Connelly, P. R.; Vuong, T. M.; Murcko, M. A., Getting physical to fix pharma. *Nat Chem* **2011,** 3, (9), 692-695.
(3) Bayliss, M. K.; Butler, J.; Feldman, P. L.; Green, D. V. S.; Leeson, P. D.; Palovich, M. R.; Taylor, A. J., Quality guidelines for oral drug candidates: dose, solubility and lipophilicity. *Drug discovery today* **2016,** 21, (10), 1719-1727.
(4) DeWitte, R. S., Avoiding physicochemical artefacts in early ADME–Tox experiments. *Drug discovery today* **2006,** 11, (17), 855-859.
(5) Thomas, V. H.; Bhattachar, S.; Hitchingham, L.; Zocharski, P.; Naath, M.; Surendran, N.; Stoner, C. L.; El-Kattan, A., The road map to oral bioavailability: an industrial perspective. *Expert Opinion on Drug Metabolism & Toxicology* **2006,** 2, (4), 591-608.
(6) Bauer, J.; Spanton, S.; Henry, R.; Quick, J.; Dziki, W.; Porter, W.; Morris, J., Ritonavir: An Extraordinary Example of Conformational Polymorphism. *Pharmaceutical Research* **2001,** 18, (6), 859-866.
(7) Jamrogiewicz, M.; Ciesielski, A., Application of vibrational spectroscopy, thermal analyses and X-ray diffraction in the rapid evaluation of the stability in solid-state of ranitidine, famotidine and cimetidine. *Journal of Pharmaceutical and Biomedical Analysis* **2015,** 107, 236-243.
(8) Colgan, S. T.; Timpano, R. J.; Roberts, M.; Weaver, R.; Ryan, K.; Fields, K. W.; Scrivens, G., Opportunities for Lean Stability Strategies. *J Pharm Innov* **2014,** 9, (4), 259-271.
(9) International Conference on Harmonisation (ICH), Guideline http://www.ich.org/products/guidelines.html.
(10) International Conference on Harmonisation (ICH), Guideline on StabilityTesting of New Drug Substances and Products Q1A(R2). **2003**.
(11) Byrn, S. R.; Zografi, G.; Chen, X. M., Accelerating Proof of Concept for Small Molecule Drugs Using Solid-State Chemistry. *Journal of Pharmaceutical Sciences* **2010,** 99, (9), 3665-3675.
(12) Li, Q. C.; Cohen, K.; Tougas, T.; Qiu, F.; Li, J.; McCaffrey, J.; Purdue, T.; Song, J. H. J.; Swanek, F.; Abelaira, S., Best Practices for Drug Substance Stress and Stability Studies During Early-Stage Development Part II-Conducting

Abbreviated Long-Term and Accelerated Stability Testing on the First Clinical Drug Substance Batch to Confirm and Adjust the Drug Substance Retest Period/Powder for Oral Solution Shelf Life. *J Pharm Innov* **2013,** 8, (1), 56-65.
(13) Dyar, S. C.; Notari, R. E., Hydrolysis kinetics and stability predictions for a mixture of R and S temocillin isomers. *International journal of pharmaceutics* **1998,** 173, (1), 221-232.
(14) Yang, C. Q.; Ren, T. K.; Wang, J.; Wang, Y. L.; Tao, X. L., Thermodynamic stability analysis of m-nisoldipine polymorphs. *Journal of Chemical Thermodynamics* **2013,** 58, 300-306.
(15) Bednarchuk, T. J.; Kowalska, D.; Kinzhybalo, V.; Wolcyrz, M., Temperature-induced reversible structural phase transition and X-ray diffuse scattering in 2-amino-3-nitropyridinium hydrogen sulfate. *Acta Crystallographica Section B* **2017,** 73, (3), 337-346.
(16) Pudipeddi, M.; Serajuddin, A. T. M., Trends in solubility of polymorphs. *Journal of Pharmaceutical Sciences* **2005,** 94, (5), 929-939.
(17) Lu, J., & Rohani, S., Polymorphism and crystallization of active pharmaceutical ingredients (APIs). *Current medicinal chemistry* **2009,** 16, (7), 884-905.
(18) Pantola, R. C., & Bahuguna, R., Polymorphism: Quality rationalization, mitigation and authentication strategies with respect to regulatory compliances in pharmaceutical industry. *Research Journal of Pharmacy and Technology* **2012,** 5, (10), 1264-1269.
(19) Fong, S. Y. K., Bauer-Brandl, A., & Brandl, M., Oral bioavailability enhancement through supersaturation: An update and meta-analysis. *Expert Opinion on Drug Delivery* **2017,** 14, (3), 403-426.
(20) Kanaujia, P.; Poovizhi, P.; Ng, W. K.; Tan, R. B. H., Amorphous formulations for dissolution and bioavailability enhancement of poorly soluble APIs. *Powder Technol* **2015,** 285, 2-15.
(21) Balbach, S.; Korn, C., Pharmaceutical evaluation of early development candidates “the 100 mg-approach”. *International journal of pharmaceutics* **2004,** 275, (1), 1-12.
(22) Korn, C.; Balbach, S., Compound selection for development – Is salt formation the ultimate answer? Experiences with an extended concept of the “100mg approach”. *Eur J Pharm Sci* **2014,** 57, 257-263.
(23) Yalkowsky, S. H., Carnelley's Rule and the Prediction of Melting Point. *Journal of Pharmaceutical Sciences* **2014,** 103, (9), 2629-2634.
(24) Jain, A.; Yang, G.; Yalkowsky, S. H., Estimation of Melting Points of Organic Compounds. *Industrial & Engineering Chemistry Research* **2004,** 43, (23), 7618-7621.
(25) Jantratid, E.; Janssen, N.; Reppas, C.; Dressman, J. B., Dissolution Media Simulating Conditions in the Proximal Human Gastrointestinal Tract: An Update. *Pharmaceutical Research* **2008,** 25, (7), 1663.
(26) Vertzoni, M.; Pastelli, E.; Psachoulias, D.; Kalantzi, L.; Reppas, C.,

Estimation of Intragastric Solubility of Drugs: In What Medium? *Pharmaceutical Research* **2007,** 24, (5), 909-917.
(27) Bergström, C. A. S.; Holm, R.; Jørgensen, S. A.; Andersson, S. B. E.; Artursson, P.; Beato, S.; Borde, A.; Box, K.; Brewster, M.; Dressman, J.; Feng, K.-I.; Halbert, G.; Kostewicz, E.; McAllister, M.; Muenster, U.; Thinnes, J.; Taylor, R.; Mullertz, A., Early pharmaceutical profiling to predict oral drug absorption: Current status and unmet needs. *Eur J Pharm Sci* **2014,** 57, 173-199.
(28) Tong, W.-Q. T.; Whitesell, G., In Situ Salt Screening-A Useful Technique for Discovery Support and Preformulation Studies. *Pharm Dev Technol* **1998,** 3, (2), 215-223.
(29) Morissette, S. L.; Almarsson, Ö.; Peterson, M. L.; Remenar, J. F.; Read, M. J.; Lemmo, A. V.; Ellis, S.; Cima, M. J.; Gardner, C. R., High-throughput crystallization: polymorphs, salts, co-crystals and solvates of pharmaceutical solids. *Adv Drug Deliver Rev* **2004,** 56, (3), 275-300.
(30) Diniz, L. F.; Carvalho, P. S.; de Melo, C. C.; Ellena, J., Reducing the Hygroscopicity of the Anti-Tuberculosis Drug (S,S)-Ethambutol Using Multicomponent Crystal Forms. *Crystal Growth & Design* **2017,** 17, (5), 2622-2630.
(31) Morissette, S. L.; Soukasene, S.; Levinson, D.; Cima, M. J.; Almarsson, Ö., Elucidation of crystal form diversity of the HIV protease inhibitor ritonavir by high-throughput crystallization. *Proceedings of the National Academy of Sciences* **2003,** 100, (5), 2180-2184.
(32) Remenar, J. F.; MacPhee, J. M.; Larson, B. K.; Tyagi, V. A.; Ho, J. H.; McIlroy, D. A.; Hickey, M. B.; Shaw, P. B.; Almarsson, Ö., Salt Selection and Simultaneous Polymorphism Assessment via High-Throughput Crystallization: The Case of Sertraline. *Org Process Res Dev* **2003,** 7, (6), 990-996.
(33) Heinrich, S. W., C., Pharmaceutical Salts: Properties, Selection, and Use, 2nd Revised Edition. *Wiley InterScience* **2011**, 388.
(34) Paulekuhn, G. S.; Dressman, J. B.; Saal, C., Trends in Active Pharmaceutical Ingredient Salt Selection based on Analysis of the Orange Book Database. *J Med Chem* **2007,** 50, (26), 6665-6672.
(35) Brittain, H. G., Polymorphism and solvatomorphism 2010. *Journal of Pharmaceutical Sciences* **2012,** 101, (2), 464-484.
(36) Tieger, E.; Kiss, V.; Pokol, G.; Finta, Z.; Dusek, M.; Rohlicek, J.; Skorepova, E.; Brazda, P., Studies on the crystal structure and arrangement of water in sitagliptin L-tartrate hydrates. *Crystengcomm* **2016,** 18, (21), 3819-3831.
(37) Grobelny, P.; Mukherjee, A.; Desiraju, G. R., Polymorphs and hydrates of Etoricoxib, a selective COX-2 inhibitor. *Crystengcomm* **2012,** 14, (18), 5785-5794.
(38) Mimura, H.; Gato, K.; Kitamura, S.; Kitagawa, T.; Kohda, S., Effect of water content on the solid-state stability in two isomorphic clathrates of cephalosporin: Cefazolin sodium pentahydrate (alpha form) and FK041 hydrate.

Chem Pharm Bull **2002,** 50, (6), 766-770.
(39) Fujii, K.; Aoki, M.; Uekusa, H., Solid-State Hydration/Dehydration of Erythromycin A Investigated by ab Initio Powder X-ray Diffraction Analysis: Stoichiometric and Nonstoichiometric Dehydrated Hydrate. *Crystal Growth & Design* **2013,** 13, (5), 2060-2066.
(40) Kons, A.; Berzins, A.; Actins, A., Polymorphs and Hydrates of Sequifenadine Hydrochloride: Crystallographic Explanation of Observed Phase Transitions and Thermodynamic Stability. *Crystal Growth & Design* **2017,** 17, (3), 1146-1158.
(41) Zhang, Q.; Mei, X. F., Two New Polymorphs of Huperzine A Obtained from Different Dehydration Processes of One Monohydrate. *Crystal Growth & Design* **2016,** 16, (6), 3535-3542.
(42) Braun, D. E.; Koztecki, L. H.; McMahon, J. A.; Price, S. L.; Reutzel-Edens, S. M., Navigating the Waters of Unconventional Crystalline Hydrates. *Molecular Pharmaceutics* **2015,** 12, (8), 3069-3088.
(43) Bond, A. D.; Cornett, C.; Larsen, F. H.; Qu, H.; Raijada, D.; Rantanen, J., Structural basis for the transformation pathways of the sodium naproxen anhydrate–hydrate system. *Iucrj* **2014,** 1, (Pt 5), 328-337.
(44) Kobayashi, K.; Fukuhara, H.; Hata, T.; Sekine, A.; Uekusa, H.; Ohashi, Y., Physicochemical and Crystal Structure Analyses of the Antidiabetic Agent Troglitazone. *Chemical and Pharmaceutical Bulletin* **2003,** 51, (7), 807-814.
(45) Seki, T.; Sakurada, K.; Muromoto, M.; Seki, S.; Ito, H., Detailed Investigation of the Structural, Thermal, and Electronic Properties of Gold Isocyanide Complexes with Mechano-Triggered Single-Crystal-to-Single-Crystal Phase Transitions. *Chemistry – A European Journal* **2016,** 22, (6), 1968-1978.
(46) Nauha, E.; Bernstein, J., "Predicting" Polymorphs of Pharmaceuticals Using Hydrogen Bond Propensities: Probenecid and Its Two Single-Crystal-to-Single-Crystal Phase Transitions. *Journal of Pharmaceutical Sciences* **2015,** 104, (6), 2056-2061.
(47) Harris, K. D. M.; Tremayne, M.; Lightfoot, P.; Bruce, P. G., CRYSTAL-STRUCTURE DETERMINATION FROM POWDER DIFFRACTION DATA BY MONTE-CARLO METHODS. *Journal of the American Chemical Society* **1994,** 116, (8), 3543-3547.
(48) Harris, K. D. M., Powder Diffraction Crystallography of Molecular Solids. In *Advanced X-Ray Crystallography*, Rissanen, K., Ed. 2012; Vol. 315, pp 133-177.
(49) Noguchi, S.; Miura, K.; Fujiki, S.; Iwao, Y.; Itai, S., Clarithromycin form I determined by synchrotron X-ray powder diffraction. *Acta Crystallographica Section C* **2012,** 68, (2), o41-o44.
(50) Colombo, V.; Masciocchi, N.; Palmisano, G., Crystal Chemistry of the Antibiotic Doripenem. *Journal of Pharmaceutical Sciences* **2014,** 103, (11), 3641-3647.

(51) David, W. I. F.; Shankland, K., Structure determination from powder diffraction data. *Acta Crystallographica Section A* **2008,** 64, 52-64.
(52) Fujii, K.; Uekusa, H.; Itoda, N.; Yonemochi, E.; Terada, K., Mechanism of Dehydration-Hydration Processes of Lisinopril Dihydrate Investigated by ab Initio Powder X-ray Diffraction Analysis. *Crystal Growth & Design* **2012,** 12, (12), 6165-6172.
(53) Esmaeili, A.; Kamiyama, T.; Oishi-Tomiyasu, R., New functions and graphical user interface attached to powder indexing software CONOGRAPH. *Journal of Applied Crystallography* **2017,** 50, 651-659.
(54) Oishi-Tomiyasu, R., Robust powder auto-indexing using many peaks. *Journal of Applied Crystallography* **2014,** 47, 593-598.
(55) Zong, Z.; Qiu, J.; Tinmanee, R.; Kirsch, L. E., Kinetic model for solid-state degradation of gabapentin. *Journal of Pharmaceutical Sciences* **2012,** 101, (6), 2123-2133.
(56) Masuda, K.; Ishige, T.; Yamada, H.; Fujii, K.; Uekusa, H.; Miura, K.; Yonemochi, E.; Terada, K., Study of the Pseudo-Crystalline Transformation from Form I to Form II of Thiamine Hydrochloride (Vitamin B₁). *Chemical and Pharmaceutical Bulletin* **2011,** 59, (1), 57-62.
(57) Kirsch, B. L.; Richman, E. K.; Riley, A. E.; Tolbert, S. H., In-Situ X-ray Diffraction Study of the Crystallization Kinetics of Mesoporous Titania Films. *The Journal of Physical Chemistry B* **2004,** 108, (34), 12698-12706.
(58) Vyazovkin, S.; Dranca, I., Physical Stability and Relaxation of Amorphous Indomethacin. *The Journal of Physical Chemistry B* **2005,** 109, (39), 18637-18644.
(59) Jones, A. R.; Winter, R.; Florian, P.; Massiot, D., Tracing the Reactive Melting of Glass-Forming Silicate Batches by In Situ 23Na NMR. *The Journal of Physical Chemistry B* **2005,** 109, (10), 4324-4332.
(60) Bertmer, M.; Nieuwendaal, R. C.; Barnes, A. B.; Hayes, S. E., Solid-State Photodimerization Kinetics of α-trans-Cinnamic Acid to α-Truxillic Acid Studied via Solid-State NMR. *The Journal of Physical Chemistry B* **2006,** 110, (12), 6270-6273.
(61) Khawam, A.; Flanagan, D. R., Complementary Use of Model-Free and Modelistic Methods in the Analysis of Solid-State Kinetics. *The Journal of Physical Chemistry B* **2005,** 109, (20), 10073-10080.
(62) Cai, J.; Liu, R., Kinetic Analysis of Solid-State Reactions: A General Empirical Kinetic Model. *Industrial & Engineering Chemistry Research* **2009,** 48, (6), 3249-3253.
(63) Khawam, A.; Flanagan, D. R., Solid-State Kinetic Models: Basics and Mathematical Fundamentals. *The Journal of Physical Chemistry B* **2006,** 110, (35), 17315-17328.
(64) Joseph, A.; Bernardes, C. E. S.; Viana, A. S.; Piedade, M. F. M.; Minas da Piedade, M. E., Kinetics and Mechanism of the Thermal Dehydration of a Robust and Yet Metastable Hemihydrate of 4-Hydroxynicotinic Acid. *Crystal*

Growth & Design **2015,** 15, (7), 3511-3524.
(65) Henriet, T.; Gana, I.; Ghaddar, C.; Barrio, M.; Cartigny, Y.; Yagoubi, N.; Do, B.; Tamarit, J. L.; Rietveld, I. B., Solid state stability and solubility of triethylenetetramine dihydrochloride. *International journal of pharmaceutics* **2016,** 511, (1), 312-21.
(66) Berzins, A.; Actins, A., Dehydration of mildronate dihydrate: a study of structural transformations and kinetics. *Crystengcomm* **2014,** 16, (19), 3926-3934.
(67) Berzins, A.; Actins, A., Effect of experimental and sample factors on dehydration kinetics of mildronate dihydrate: mechanism of dehydration and determination of kinetic parameters. *J Pharm Sci* **2014,** 103, (6), 1747-55.
(68) Brown, G. W.; Paes, D.; Bryson, J.; Freeman, A. J., The effectiveness of a single intravenous dose of ondansetron. *Oncology* **1992,** 49, (4), 273-8.
(69) Collin, S.; Moureau, F.; Quintero, M. G.; Vercauteren, D. P.; Evrard, G.; Durant, F., Stereoelectronic requirements of benzamide 5HT3 antagonists. Comparison with D2 antidopaminergic analogues. *Journal of the Chemical Society, Perkin Transactions 2* **1995**, (1), 77-84.
(70) Llacer, J. M.; Gallardo, V.; Delgado, R.; Parraga, J.; Martin, D.; Ruiz, M. A., X-ray diffraction and electron microscopy in the polymorphism study of ondansetron hydrochloride. *Drug development and industrial pharmacy* **2001,** 27, (9), 899-908.
(71) Llacer, J. M.; Gallardo, V.; Parera, A.; Ruiz, M. A., Formation of ondansetron polymorphs. *International journal of pharmaceutics* **1999,** 177, (2), 221-9.
(72) Osaka, K.; Matsumoto, T.; Miura, K.; Sato, M.; Hirosawa, I.; Watanabe, Y., The Advanced Automation for Powder Diffraction toward Industrial Application. *Sri 2009: The 10th International Conference on Synchrotron Radiation Instrumentation* **2010,** 1234, 9-12.
(73) Neumann, M., X-Cell: a novel indexing algorithm for routine tasks and difficult cases. *Journal of Applied Crystallography* **2003,** 36, (2), 356-365.
(74) Sun, H.; Jin, Z.; Yang, C.; Akkermans, R. L. C.; Robertson, S. H.; Spenley, N. A.; Miller, S.; Todd, S. M., COMPASS II: extended coverage for polymer and drug-like molecule databases. *Journal of molecular modeling* **2016,** 22, (2), 47.
(75) Engel, G. E.; Wilke, S.; Konig, O.; Harris, K. D. M.; Leusen, F. J. J., PowderSolve - a complete package for crystal structure solution from powder diffraction patterns. *Journal of Applied Crystallography* **1999,** 32, (6), 1169-1179.
(76) Veldhuizen, D. A. V.; Lamont, G. B., Multiobjective Evolutionary Algorithms: Analyzing the State-of-the-Art. *Evolutionary Computation* **2000,** 8, (2), 125-147.
(77) Zhang, X.; Yin, Q. X.; Du, W.; Gong, J. B.; Bao, Y.; Zhang, M. J.; Hou, B. H.; Hao, H. X., Phase Transformation between Anhydrate and Monohydrate

of Sodium Dehydroacetate. *Industrial & Engineering Chemistry Research* **2015,** 54, (13), 3438-3444.
(78) Ozawa, T., Kinetic analysis of derivative curves in thermal analysis. *Journal of thermal analysis* **1970,** 2, (3), 301-324.
(79) Kabe, J., (3) A Double-blind Placebo-controlled Study of OKY-046 for the Treatment of Chronic Asthma. *Japanese Journal of Medicine* **1989,** 28, (4), 552-555.
(80) Wang, Y.-T.; Tang, G.-M.; Liu, Z.-M.; Yi, X.-H., Can One-Dimensional Water Be Controlled by Transformation of Substitution Groups Based on Organic Hosts? *Crystal Growth & Design* **2007,** 7, (11), 2272-2275.
(81) Lou, B.; Guo, X.; Lin, Q.; Lin, J.; Chen, Y., Crystal Structure of Ozagrel Fumarate dihydrate
(Ozagrel = (E)-3-[4-(1H-imidiazol-1-ylmethyl)phenyl]-2-propenic acid). *Journal of Chemical Crystallography* **2009,** 39, (11), 831-834.
(82) Lou, B.; Guo, X.; Lin, Q., Crystal Structure of the Dihydrogen Phosphate Salt of Ozagrel (ozagrel=(E)-3-[4-(1H-Imidiazol-1-ylmethyl)phenyl]-2-Propenic Acid). *Journal of Chemical Crystallography* **2009,** 39, (7), 469-473.